INFORMATION TO USERS

This reproduction was made from a copy of a document sent to us for microfilming. While the most advanced technology has been used to photograph and reproduce this document, the quality of the reproduction is heavily dependent upon the quality of the material submitted.

The following explanation of techniques is provided to help clarify markings or notations which may appear on this reproduction.

1. The sign or "target" for pages apparently lacking from the document photographed is "Missing Page(s)". If it was possible to obtain the missing page(s) or section, they are spliced into the film along with adjacent pages. This may have necessitated cutting through an image and duplicating adjacent pages to assure complete continuity.

2. When an image on the film is obliterated with a round black mark, it is an indication of either blurred copy because of movement during exposure, duplicate copy, or copyrighted materials that should not have been filmed. For blurred pages, a good image of the page can be found in the adjacent frame. If copyrighted materials were deleted, a target note will appear listing the pages in the adjacent frame.

3. When a map, drawing or chart, etc., is part of the material being photographed, a definite method of "sectioning" the material has been followed. It is customary to begin filming at the upper left hand corner of a large sheet and to continue from left to right in equal sections with small overlaps. If necessary, sectioning is continued again—beginning below the first row and continuing on until complete.

4. For illustrations that cannot be satisfactorily reproduced by xerographic means, photographic prints can be purchased at additional cost and inserted into your xerographic copy. These prints are available upon request from the Dissertations Customer Services Department.

5. Some pages in any document may have indistinct print. In all cases the best available copy has been filmed.

University
Microfilms
International

300 N. Zeeb Road
Ann Arbor, MI 48106

Yan, Zong-Yi

THREE-DIMENSIONAL HYDRODYNAMIC AND OSMOTIC PORE ENTRANCE PHENOMENA

City University of New York PH.D. 1985

THREE-DIMENSIONAL HYDRODYNAMIC AND OSMOTIC PORE ENTRANCE PHENOMENA

by

Zong-Yi Yan

A dissertation submitted to the Graduate Faculty in Engineering in partial fulfillment of the requirements for the degree of Doctor of Philosophy, The City University of New York.

1985

This manuscript has been read and accepted for the Graduate Faculty in Engineering in satisfaction of the dissertation requirement for the degree of Doctor of Philosophy.

March 4, 1985
date

Sheldon Weinbaum
Chairman of Examining Committee

Feb 21, 1985
date

Paul Karmel
Executive Officer

Professor Sheldon Weinbaum, Chairman

Professor Robert Pfeffer, Co-Chairman

Professor Peter Ganatos

Professor Zeev Dagan

Professor Charles Malderelli

Supervisory Committee

The City University of New York

Abstract

THREE-DIMENSIONAL HYDRODYNAMIC AND
OSMOTIC PORE ENTRANCE PHENOMENA

by

Zong-Yi Yan

Advisor: Professor Sheldon Weinbaum
Co-Advisor: Professor Robert Pfeffer

This thesis studies two important aspects of pore entrance/exit phenomena in biological and synthetic membranes--the three-dimensional osmotic fine structure and the hydrodynamic interaction near the pore entrance.

Chapter 2 presents a detailed quantitative model of osmotic fine structure for both permeable and semi-permeable membranes in dilute bathing solutions. By introducing an approximate description of the hydrodynamic interactions in the entrance/exit regions, the balance between the convective and diffusive fluxes is considered both inside and outside a membrane pore. For permeable membranes, the concentration variations in the entrance/exit regions may have an important influence on the osmotic flow rate, especially for relatively short pores, small solute particles and not very dilute solutions. It is shown for permeable membranes that the three-dimensional entrance region within two to three pore-radii from the pore opening forms a substructure of the much thicker

unstirred layer described by Dainty (1963) and Pedley et al. (1978). When the porosity is low (such as in most biological membranes), the wall concentration in Pedley's solution is the far field concentration for the present entrance/exit solutions.

Chapter 3 proposes a combined multipole series representation and integral equation method for solving the problem of a finite sphere entering a zero-thickness orifice. This method combines the flexibility of the integral equation method for treating complicated geometries and the accuracy and computational efficiency of the multipole technique. Both axisymmetric and three-dimensional solutions are obtained. The present three-dimensional solutions for the force and torque correction factors are the first for a finite sphere and are valid for the difficult case where the sphere intersects the plane of the orifice opening. The behavior in the vicinity of the pore opening is important in many particle - pore entrance phenomena because of the rapid variations in the hydrodynamic force and torque coefficients in this region. The convergence of the present three-dimensional solution deteriorates beyond a few pore-radii from the pore axis or near the plane wall. The practical usefulness of the solution in these regions is limited by excessive computation cost.

ACKNOWLEDGEMENTS

My largest debt is to my co-mentors, Professor Sheldon Weinbaum and Professor Robert Pfeffer, for their valuable guidance and thoughtful assistance in directing this research.

I am also grateful to Professor Peter Ganatos for his continuing help in many aspects of this research and for his useful suggestion about the weighted residual technique, to The City University of New York Computer Center for the use of their facilities, and to the National Science Foundation for their support of this research under Grant No. ENG82-00301.

I wish to thank Miss Hannah Stolar for her four years of English tutoring which has contributed immeasurably to the improvement of my English skills.

I have been on leave from the Chinese Academy of Sciences for almost five years. I'd like to devote this work to my dear Motherland, The People's Republic of China, where I was born, brought up and educated. My past preparations and experiences in China have turned out to be of great value for this research. My special respect is given to my former mentors, the late Professor Y. H. Kuo and Professor H. S. Tan.

Finally, I am very much obliged to my wife, Ms. Hui-Xian Shan, who has shared with me all the hardship and is always a reliable source of encouragement in weathering the difficulties in reaching my goals.

TABLE OF CONTENTS

LIST OF TABLES

LIST OF FIGURES

CHAPTER 1

INTRODUCTION

Pore entrance phenomena relating to biological and synthetic membranes are of great biological and engineering interest. When a suspended particle approaches a pore, the hydrodynamic interaction between the particle and the pore entrance geometry produces a number of significant effects: the velocity of a neutrally buoyant particle will differ from the velocity of the suspending fluid; the particle's trajectory will deviate from the fluid streamline; the particle's diffusivity is no longer a scalar, as it should be in an unbounded fluid, but becomes a second-order tensor; the components of this diffusivity vary with position in a three-dimensional way; to name a few. These effects are important in many problems involving particle-pore entrance phenomena, for example, the plasma-screening of red cells entering small blood vessels or glass tubes; osmotic behavior at the pore opening of permeable or semi-permeable membranes; the molecular sieving of macromolecules in the loading of plasmalemma vesicles; the filtration of particulates in nuclepore filters; air pollution control; purification of lakes and streams; the collection efficiency of synthetic membranes and filters; the entrance of highly deformable particles into pores such as in red blood cell deformability tests.

Among these phenomena, osmosis is of special importance for biological applications. Osmotic flow occurs across the membranes of all living cells and through the intercellular clefts in the organs and tissues of the human body,

animals and plants. While the macroscopic behavior of osmosis has been well described by principles of irreversible thermodynamics (Kedem and Katchalsky 1958), the fine structure of the osmotic mechanism remains one of the most puzzling aspects of membrane transport. Since Mauro (1957) and Ray (1960) first proposed a qualitative hypothesis, many attempts have been made to explore the relationship between the macroscopic osmotic behavior and the microscopic characteristics of the membrane and the solution within the pore (e.g. Anderson and Quinn 1974, Anderson and Malone 1974, Curry 1974, Levitt 1975, Ganatos, Weinbaum, Fischbarg and Liebovitch 1980, Anderson 1981). All these hydrodynamic treatments have focused attention exclusively on the flow within the pore itself and have ignored the "unstirred layer" in the bathing solution adjacent to the membrane and the local pore entrance/exit effects. The "unstirred layer" introduced by Dainty (1963) is a convective-diffusive layer of several hundred microns thickness adjacent to the membrane where the concentration adjusts to its value in the bulk solution. This layer is typically of two or more orders of magnitude thicker than the characteristic length for the pore entrance/exit effects studied herein. Pedley and Fischbarg (1978) proposed a one-dimensional model to estimate the errors due to neglecting this unstirred layer adjacent to a semi-permeable membrane. Assuming that the layer thickness δ is known in advance, they show that the membrane concentration C_m differs from the bulk solution

concentration C_b by a few percent for biological membranes, but the difference can be substantially larger for some very leaky artificial membranes. For the latter case, a significant error may occur in estimating the osmotic flow rate if C_b is used instead of C_m. However, as will be shown in this thesis, for permeable biological membranes with low porosity and discrete pores, the concentration field near each pore entrance forms a substructure in which the membrane concentration C_m in Pedley's one-dimensional model serves as the far field concentration for the local three-dimensional changes that occur in the entrance/exit regions of each pore.

The present study will propose a new detailed quantitative model of osmotic fine structure for both permeable and semi-permeable membranes in dilute bathing solutions. A complete analysis will be developed to take into account the solvent and solute movements both inside and outside the pore, including the entrance/exit regions near the pore opening. This analysis will enable us to determine the relative importance of the pore interior, the entrance/exit regions and Pedley's unstirred layer in estimating osmotic flow. Instead of assuming the layer thickness, as in Pedley's model, the characteristic length of the entrance/exit regions will be determined as part of the solution. Then, on the basis of a comparison between the different length scales, we will be able to discuss how the three-dimensional substructure of the fine scale in the pore

entrance/exit regions can be related to Pedley's much thicker one-dimensional unstirred layer. This study will be presented in Chapter 2.

In solving the problem of osmosis, as well as all other problems involving pore entrance phenomena, a three-dimensional hydrodynamic analysis of the motion of a finite neutrally buoyant particle towards a pore is an essential input. However, this problem is very difficult. Even the simplest problem of a sphere approaching a circular orifice of zero thickness in an infinite plane wall is analytically intractable. The reflections method, which was extensively used to treat weak hydrodynamic interactions of particles with boundaries, is shown to converge very slowly when the sphere-wall-spacing is of the order of five sphere radii or less (Ganatos, Weinbaum and Pfeffer 1980). To attack such problems with strong hydrodynamic interactions, two numerical theories, the multipole series representation technique and the integral equation method, have been developed in recent years (Weinbaum 1981, Ladyzhenskaya 1963).

Using the multipole series representation technique, Dagan, Weinbaum and Pfeffer (1982b) were able to obtain an axisymmetric solution for a finite sphere approaching a zero thickness orifice when the sphere center on the pore axis is located no less than 1.1 times the sphere radius from the orifice plane. The attempts to extend this technique to the three-dimensional case have encounted great

mathematical difficulty and, hence, only an approximate three-dimensional theory was developed (Dagan, Weinbaum and Pfeffer 1983), in which the transverse curvature effect of the pore and the sphere rotation are neglected. This theory is not valid when the sphere center is less than two pore-radii from the pore opening.

On the other hand, solutions for the translation of a stokeslet near the entrance geometry has recently been obtained for the axisymmetric case (Davis, O'Neill and Brenner 1981) and the three-dimensional case (Davis 1983, Miyazaki and Hasimoto 1984). Since the stokeslet in these solutions can be considered as an approximation to a small particle, this singular solution can also be integrated over the surface of a finite particle, in principle, to determine the disturbance produced by the translation of a finite particle at the orifice entrance. However, this approach is beset by major numerical difficulties that arise from the complicated nature of the fundamental solution for this geometry. Solutions for the rotation of the particle or the flow past the particle are also not available.

One promising approach is the integral equation method using the hydrodynamic potential theory (Youngren and Acrivos 1975). This method is very flexible in treating a complicated geometry although it gives lower accuracy and requires longer computation time in comparison with the multipole series representation technique. In this thesis a combined multipole series representation and integral

equation method will be developed so that the advantages of each method can be utilized. This combined method will be used to obtain the three-dimensional solution for a finite sphere. In particular, it is hoped that this solution will be valid in the vicinity of the pore opening, including the case where the sphere intersects the plane of the orifice, which could not be treated by previous methods. This study will be presented in Chapter 3.

During my study of the osmosis problem in Chapter 2, the application of the method developed in Chapter 3 to the three-dimensional hydrodynamic interaction was still in progress. Therefore, at that time, an approximate description of the three-dimensional interaction was proposed, based on the available data and some physically reasonable assumptions. It was later found that this description provided a reasonably good approximation to the accurate solution obtained in Chapter 3. It is believed that the approximate hydrodynamic parameters used in Chapter 2 are adequate in showing the essential features of the osmotic fine structure at the pore entrance/exit and, thus, they will not be recalculated, considering the excessive computation cost for the accurate three-dimensional solution in Chapter 3.

CHAPTER 2

THE FINE STRUCTURE OF OSMOSIS AT THE ENTRANCE AND EXIT OF BIOLOGICAL MEMBRANE PORES

1. INTRODUCTION

When two solutions of different concentrations are separated by a porous barrier (membrane), a net volumetric flux is observed; such transport is called "osmotic flow". Osmotic phenomena are of great biological significance. Osmosis occurs across the plasmalemma membranes of all living cells and through the intercellular clefts of the epithelial and endothelial cell layers lining all the internal body organs such as the kidney tubules, blood capillaries, intestines, gall bladder and cornea, to mention a few. Other biological examples are the synthetic membranes in artificial organs and the water exchange in plant cells and tissues.

Kedem and Katchalsky (1958) have proposed a pair of flux equations describing the osmosis of a dilute solution of a non-electrolyte across a porous membrane based on principles of irreversible thermodynamics:

$$J_s = \omega \Delta\pi + (1-\sigma)\bar{C} J_v \,, \tag{1a}$$

$$J_v = L_p (\Delta p - \sigma \Delta\pi) \,. \tag{1b}$$

These equations relate the solute flow J_s and the total volume flux J_v to the difference of hydrodynamic and osmotic pressures, Δp and $\Delta\pi$, across the membrane through three independent phenomenological coefficients: the

hydraulic permeability L_p, the diffusive permeability ω and the reflection coefficient σ, which represent overall properties of the membrane. Here $\bar{C}$ is some unknown average solute concentration in the pore, $\sigma=1$ for semi-permeable membranes (permeable to the solvent only) and $\sigma=0$ for non-selectively permeable membranes. These equations are valid for any membrane regardless of pore geometry and solute characteristics. Because of this generality, the irreversible thermodynamic description is of considerable value in guiding the design of experiments and in testing more detailed theories related to the membrane microstructure.

For a dilute solution, the osmotic pressure π is related to the solute concentration C by van't Hoff's law (e.g. see Hsieh 1975):

$$\pi = \bar{R} T C . \tag{2}$$

Here $\bar{R}$ is the universal gas constant and T is the absolute temperature. Therefore, for dilute solutions at constant temperature the Kedem-Katchalsky equations can be written in terms of Δp and ΔC as follows:

$$J_s = \omega \bar{R} T \Delta C + (1-\sigma) \bar{C} J_v , \tag{3a}$$

$$J_v = L_p (\Delta p - \sigma \bar{R} T \Delta C). \tag{3b}$$

Equation (3b) shows the equivalence between the pressure difference and the concentration difference in their effect of producing a volume flow across the membrane. This

equivalence can easily be demonstrated by experiments. For example, the transfer of water through a membrane when a hydrostatic pressure is applied can be duplicated in the absence of a pressure difference by contaminating one volume of the water adjacent to the membrane with a solute to which the membrane is absolutely impermeable.

However, it is not clear from the irreversible thermodynamics why a concentration difference across a membrane should have the same effect as a pressure difference and whether it should lead to a bulk flow of solvent or the diffusion of solvent through pores in the membrane. Mauro (1957) and Ray (1960) analyzed a large body of experimental data and concluded that the observed osmotic flow rates were several times to several hundred times higher than would have been expected on the basis of a diffusional concentration gradient for the solvent using estimated pore lengths as the characteristic length scale. These differences cannot be explained by experimental errors. To explain why osmosis is dominated by bulk flow of the solvent through pores of the membrane rather than by diffusion across the membrane, Mauro (1957) and Ray (1960) hypothesized that for a semi-permeable membrane the distance over which the concentration changes from the value on one side of the membrane to that on the other side should be about the same as the pore radius, since solute particles larger than the pore radius would not be able to penetrate further. Then, for a given concentration difference, they argued, the

concentration gradient in this narrow region within the pore near its opening should be much steeper than calculated using the whole pore length. Thus the water in this region should diffuse out of the pore much more rapidly than expected based on the average gradient across the membrane and it should be supplemented by the passive water flux through the pore from the other side. This passive water movement should set up a pressure drop along the pore length just equal to the osmotic pressure. Anderson and Malone (1974), while accepting the basic tenets of the Mauro-Ray hypothesis, pointed out that a simple one-dimensional treatment is inadequate in explaining osmotic flows. They showed that in the pore of a permeable membrane the steric exclusion of the solute near the pore wall creates an abrupt radial pressure change proportional to the radial solute concentration difference between the core and this exclusion layer. They then argued that an axial concentration gradient in the core establishes an axial pressure gradient in the exclusion layer which pushes the fluid through the pore. Therefore, they emphasized the three-dimensional variations of solute concentration within the pore as having the dominant influence on transport rates in a permeable membrane.

The above descriptions were the first qualitative models to explore the fine structure of osmosis. Since then many hydrodynamic analysis have been devoted to the relationship

between the macroscopic osmotic behavior and the microscopic characteristics of the membrane and solution within the pore itself. Katchalsky (1961) and Dainty and Ginzburg (1963) proposed to express the phenomenological coefficients in terms of molar friction coefficients f_{ij}, describing the friction between solvent, solute and wall molecules. Bean (1972), Curry (1974) and Levitt (1975) studied the motion of a neutrally buoyant particle driven by a gradient of chemical potential in a Poiseuille flow. Anderson and Quinn (1974) extended the hydrodynamic formalism to pores and slits where the wall creates a radial potential with an exclusion layer due to electrical, steric or other forces. Anderson and Malone (1974), Brenner and Gaydos (1977) and Anderson (1981) discussed osmotically driven flows, using different hydrodynamic and statistical-mechnical models with non-interacting or interacting particles of spherical or non-spherical shapes, cylindrical or non-cylindrical pore boundaries and steric or long-range wall effects. All the above calculations have described the hydrodynamic interaction using the reflections method of weak interaction theory or ad hoc methods, Curry(1974). These solutions can yield significant errors in the hydrodynamic coefficients when the particle is more than one fifth the pore diameter. To overcome this difficulty, the boundary collocation technique of strong interaction theory was developed by Ganatos, Weinbaum and Pfeffer (1980) and Ganatos, Pfeffer and Weinbaum (1980) to obtain exact analytical-numerical solutions for the

general motion of a sphere of arbitrary size and position between two parallel plane walls. Using these hydrodynamic results, Ganatos, Weinbaum, Fischbarg and Liebovitch (1980) determined the phenomenological coefficients for the passage of spherical molecules through an intercellular cleft.

All these hydrodynamic treatments, especially Mauro and Ray's hypothesis, are enlightening. However, they have focused attention exclusively on the flow within the pore or slit and have ignored the "unstirred layer" in the bulk solution adjacent to the membrane and all pore entrance/exit effects. The "unstirred layer" introduced by Dainty (1963) is a convective-diffusive layer near the plane of the membrane where the concentration adjusts to its value in the bulk solution at a distance of several hundred microns. Pedley and Fischbarg (1978) has attempted to estimate the errors due to neglecting this unstirred layer adjacent to a semi-permeable membrane. In their one-dimensional analysis, the layer thickness δ is taken as known from measurements and then the solute concentration C_m at the membrane surface is established from the balance between the diffusive flux and the convective flux. The dependence of the water flow on C_m makes this problem nonlinear. Their numerical results show that while C_m differs from the bulk solution concentration C_b by only a small percentage for most biological membranes, C_m/C_b may be as low as 0.0042 for some very leaky artificial membrane under extreme conditions. For the latter case, if the ΔC in the Kedem-Katchalsky equation (3b)

were based on C_b, rather than on C_m as it should be, a significant error would result in predicting the volume flow rate J_v.

Pedley and Fischbarg (1978) did not explain how to estimate δ in advance, how the value of δ itself depends on the osmotic flow or how a substructure consisting of an array of discrete pores is related to a simple one-dimensional model. In Pedley's following papers (1980, 1981), the values of δ are estimated for two special types of stirring motion in the bulk solution, i.e., the stirring is represented as a two-dimensional stagnation point flow or a shearing flow parallel to the wall. Pedley's assumption of an unstirred layer of constant thickness, at whose outside edge ($z= \delta$) the concentration C_b is given, is a considerable simplification. In practice, the concentration will approach asymptotically to the bulk value C_b and δ should be defined as the distance z at which the concentration differs from C_b by some given fraction. However, if there were no stirring motion in the bulk solution and if the fluid region could be regarded as semi-infinite, there would be no steady-state solution according to Pedley's model since the concentration would grow exponentially with the distance from the wall and thus no δ could be defined. Near the plane of the membrane, an equally important difficulty is how the membrane concentration C_m should be defined.

As can be seen from the foregoing, although the

macroscopic thermodynamic behavior of osmotic flow is well understood, the fine structure of the osmotic mechanism within the pore, near its openings and its relationship to the larger scale structure of the unstirred layer are puzzling aspects of membrane transport that are still not well understood. The situation is somewhat akin to an adiabatic shockwave where the Rankine-Hugoniot relations between the equilibrium end states are easily derived, but a detailed description of the dissipative processes in the interior of the shock is required to describe the transition between the end states.

A complete analysis of the osmotic mechanism should take into account the entire domain of flow, including the entrance/exit regions. To clarify this point, let us consider a semi-permeable membrane. It is a convention in defining concentration that a solute particle should be conceptually treated like a single point so that only the motion of the particle center should be traced and the concentration should be defined on the basis of the particle center (Brenner and Gaydos 1977). When the membrane is absolutely impermeable to the solute, no particle center can be located within the pore. This means that within the whole pore length the solute concentration should be identically zero and thus make no contribution to the driving force of osmosis. On the other hand, the strong hydrodynamic interactions between the solute particle and the pore entrance geometry should tend to retard the diffusion of the solute towards the pore

in some, as yet, undefined region outside the pore. The solute particles, not being able to enter the pore, would reside in the vicinity of the pore opening and thus set up a region of steep concentration gradient outside the pore, instead of within the pore. For the case of a partially permeable membrane, one should consider the balance between the convective and diffusive fluxes both inside and outside the pore, which establish a standing gradient of concentration both along the pore length and near the entrance and exit. In such an analysis the thickness of the unstirred layer should be determined as part of the solution rather than as a prescribed quantity.

Pedley's one-dimensional model was presented for a semi-permeable membrane. As we shall show in the present study, for a permeable membrane the changes in concentration near the entrance or exit of the pore demonstrate a clear three-dimensional nature with a fine scale structure whose characteristic length is several pore-radii. Only beyond this fine-length-scale can the flows through different pores become well mixed and Pedley's one-dimensional model applied. When the porosity is low (such as in biological membranes), we shall show that the spacing between pores is large compared to the entrance and exit mixing regions, with the result that the membrane concentration C_m in Pedley's model can be treated as the far field solution for the inner structure described in this investigation. High porosity membranes have an intermediate layer whose

thickness is characterized by the spacing between pores. This intermediate layer describing the interactions between pores and the transition to Pedley's one-dimensional model still needs to be developed.

To treat the near field three-dimensional nature of the entrance/exit effects, one has to consider the hydrodynamic interaction of the particle with the entrance/exit geometry. The neutrally buoyant velocity of the particle differs from the solvent phase velocity and the particle diffusivity is no longer a scaler, as it would be in an unbounded fluid; rather, it is a second-order tensor. This tensorial property is a direct consequence of the fact that a solute particle experiences different hydrodynamic resistances when it moves in different directions. Moreover, the axial and radial diffusivities are not constants, but are functions of the position of the particle center. All these observations indicate that a three-dimensional hydrodynamic analysis of the motion of a finite neutrally buoyant particle towards a pore is essential input in the larger problem.

Unfortunately, the hydrodynamic problem just described is very difficult. It is because of this difficulty that no detailed analysis has previously appeared for the fine scale structure of the region of steep concentration gradient near the pore entrance and exit in the more than twenty years that has elapsed since Mauro and Ray first proposed their hypothesis. Even the simplest case of the axisymmetric

motion of a finite spherical particle towards a pore of infinitesimal length is analytically intractable. The method of reflections, which was extensively used in the past to treat weak hydrodynamic interactions of particles with boundaries, breaks down when the sphere-wall-spacing is of order of five sphere radii or less (Ganatos, Weinbaum and Pfeffer 1980; Ganatos, Pfeffer and Weinbaum 1980). It is only two years ago that a theoretical solution was obtained by Dagan, Weinbaum and Pfeffer (1982b) for the axisymmetric approach of a finite sphere to a circular pore in a plane wall of zero thickness. Using the multipole series representation and boundary collocation technique, these authors were able to obtain accurate results for the hydrodynamic resistance when the sphere center was located no less than 1.1 times the sphere radius from the plane wall. Wu and Skalak (1984) solved, by a similar method, the axisymmetric problem of a sphere moving from a half-space towards a semi-infinite circular cylindrical pore. In a separate paper, Dagan, Weinbaum and Pfeffer (1982a) developed an infinite series solution for the axisymmetric creeping motion of pure fluid through an orifice of finite length. Their results show that the velocity profile approaches to within 1.5 percent of a Poisuille profile after a short entrance distance of half the pore radius. In the far field the solution matches exactly the streamline pattern for a flow through an orifice of zero thickness obtained by Sampson (1891), see

Happel and Brenner (1973), p.153. The attempts to extend the above methods to three-dimensional cases have encounted considerable difficulty. As of the present time, the only three-dimensional theory for the entrance problem of a finite particle is the approximate solution by Dagan, Weinbaum and Pfeffer (1983). These authors were able to obtain an approximate solution for the deviation of the sphere trajectory from the fluid streamlines when the particle is roughly more than two pore-radii from the entrance. However, their data for particle resistances neglect the transverse curvature effect of the pore, the sphere rotation and the near field entrance interaction. More recently, Miyazaki and Hasimoto (1984) have obtained a closed-form solution for the three-dimensional translation of a stokeslet near a circular pore in a plane wall, using Green and Neumann functions supplemented by an edge function to remove the singularity at the rim of the pore. Their solutions are a useful approximation for the case of a small translating particle. However, no solutions are presented for a rotating particle or the flow past a stationary particle near the pore entrance.

In a study concurrent with this investigation (see Chapter 3), the author has applied the integral equation method (see Ladyzhenskaya 1963, and Youngren and Acrivos 1975) to the hydrodynamic interaction problem of a sphere near a pore of zero length. This axisymmetric theory has turned out to be valid for an arbitrary position of the sphere center along

the pore axis (including the cases where the sphere partly or wholly enters the pore, which could not be treated by other methods). Although the full extension of this analysis to three-dimensional cases is still in progress, the available hydrodynamic data when combined with physically reasonable assumptions, is sufficient to provide a realistic, if not quantitatively accurate, description of the three-dimensional hydrodynamic interaction with the pore entrance geometry. This approximate hydrodynamic description will enable us to obtain approximate solutions for the deterministic motion of a neutrally buoyant sphere and for the diffusivity tensor in the near fluid entrance region where the earlier approximations of Dagan, Weinbaum and Pfeffer (1983) were not valid.

The general outline of Chapter 2 is as follows. The complex coupling between the solvent and solute phases is mathematically formulated in Section 2. A detailed discussion of the three-dimensional hydrodynamic interaction is given in Section 3 together with solutions for the neutrally buoyant sphere motion and its diffusivity tensor. The numerical solution procedures and results are presented in Section 4 and Section 5, respectively.

2. FORMULATION

In this study, we consider a membrane with a single circular pore of length ℓ and radius R_0 (Fig. 1). The half-space ($z>0$) on the right side contains a dilute solution of identical spherical particles of radius a. It is assumed that both R_0 and a are much larger than the size of the solvent (e.g. water) molecules so that the continuum theory of fluid dynamics can be applied. Fig. 1(a) shows the case of a permeable membrane in which R_0 is larger than a and the left half-space ($z<-\ell$) contains a dilute solution of different concentration. Fig. 1(b) shows the case of a semi-permeable membrane in which R_0 is smaller than a and the left half-space ($z<-\ell$) contains pure solvent. In either case, the solution is assumed to be so dilute that the hydrodynamic interactions between the particles are negligible, although the interactions between the individual particles and the pore entrance/exit geometry must be considered. The broken lines in Figs. 1(a) and 1(b) define the limiting positions at which the particle centers can get closest to the wall. Between these lines and the wall are the exclusion layers where no solute is present. Far away from the pore openings, the hydrostatic pressures on the two sides of the membrane are assumed to be the same, i.e. $p_{-\infty}=p_{\infty}$, in order to isolate the osmotic effect.

Now, given the concentration C_{∞} in the bulk solution on the right side (for a permeable membrane, also $C_{-\infty}$ on the

left), the viscosity μ and the radius a of the solute and the pore dimensions (R_o, ℓ), we shall try to find the profiles of concentration and pressure, including the entrance and exit regions. We will start with a discussion of the constitutive equation of binary diffusion and then apply the continuity equation for the solute phase to the pore interior and both the half-spaces in sequence. Finally, with the help of the Kedem-Katchalsky equation we will determine the osmotic flow rate through the pore and complete the formulation of the problem.

2.1 THE CONSTITUTIVE EQUATION OF BINARY DIFFUSION

The steady-state continuity equation for the solute phase is

$$\nabla \cdot (C \vec{U}) = 0 , \qquad (4)$$

where $\vec{U}$ is the particle velocity. It has been costomary in applying Fick's law for diffusion in a binary system to express the particle motion in terms of its diffusion relative to the local mass average velocity of the system (see Bird, Stewart and Lightfoot 1960), which for a dilute solution is essentially the same as the velocity $\vec{V}$ of the solvent phase:

$$\vec{U} = \vec{V} - \vec{\vec{D}} \cdot \frac{1}{C} \nabla C .$$

The hydrodynamic interaction is only accounted for in the

matrix for the diffusivity tensor $\vec{\vec{D}}$. According to this expression, if there were no concentration gradient, the particle velocity $\vec{U}$ would be equal to $\vec{V}$, the solvent velocity. This is certainly not true in the presence of hydrodynamic interaction (e.g. Weinbaum 1981). As Brenner and Gaydos (1977) pointed out, the correct application of Fick's law with hydrodynamic interaction requires that the diffusion be measured relative not to the mass average velocity but to the deterministic velocity $\vec{U}^o$ of a neutrally buoyant particle:

$$\vec{U} = \vec{U}^o - \vec{\vec{D}} \cdot \frac{1}{C} \nabla C \ , \tag{5}$$

or in component form:

$$U_R = U_R^o - D_{RR} \frac{1}{C} \frac{\partial C}{\partial R} - D_{Rz} \frac{1}{C} \frac{\partial C}{\partial z} \ , \tag{6a}$$

$$U_z = U_z^o - D_{zR} \frac{1}{C} \frac{\partial C}{\partial R} - D_{zz} \frac{1}{C} \frac{\partial C}{\partial z} \ . \tag{6b}$$

If there were no hydrodynamic interaction, $\vec{U}^o$ would become the same as $\vec{V}$ and then (5) would reduce to the ordinary Fick's law.

To obtain the expression for the deterministic particle velocity and the diffusivity, we have to consider the balance between the hydrodynamic and thermodynamic forces acting on a particle. Due to the linearity of creeping flow problems, the general motion of a sphere in a plane (x,z) containing the pore axis can be constructed as a

superposition of (i) a pure translation of the sphere with velocities U_x and U_z perpendicular and parallel to the pore axis in a quiescent fluid, (ii) a pure rotation of the sphere with angular velocity Ω perpendicular to the (x,z) plane in a quiescent fluid, and (iii) the flow past a stationary sphere with undisturbed velocity components V_x and V_z, which obey Sampson's solution (see Eqns. (32a) and (32b)), at the sphere center (x,z). The hydrodynamic forces and torque then can be written as in Dagan, Weinbaum and Pfeffer (1983):

$$F_x = 6\pi\mu a \left(U_x F_x^t + a\Omega F_x^r + V_x F_x^s \right),$$

$$F_z = 6\pi\mu a \left(U_z F_z^t + a\Omega F_z^r + V_z F_z^s \right), \qquad (7)$$

$$T_y = 8\pi\mu a^2 \left(U_x T_y^{t,x} + U_z T_y^{t,z} + a\Omega T_y^r + \frac{a}{2z} V_x T_y^{s,x} + \frac{a}{2x} V_z T_y^{s,z} \right),$$

where F_x^t, F_x^r, ..., $T_y^{s,z}$ are the force and torque correction factors obtained from the solutions of the three separate problems mentioned above, with the superscripts t, r, s denoting the three problems in sequence. These correction factors account for the strong hydrodynamic interactions between the sphere and the wall.

As Batchelor (1976) pointed out, the diffusion of particles in a dilute solution can be considered as Brownian motion, provided that the particle configuration does not change significantly during the characteristic viscous relaxation time for the solute particles. The particle flux due to Brownian motion is the same as the flux that would be produced by the application of a certain "thermodynamic"

force to each particle, equal to the gradient of the solute chemical potential with a minus sign. For an ideal solution at constant temperature T, the thermodynamic force per particle is

$$\vec{F}_p = -\frac{1}{N_A}\left(\frac{\bar{R}T}{C}\nabla C + \bar{V}_s \nabla p\right),$$

where N_A is Avogadro constant, $\bar{V}_s$ is the molar volume of the solute, $\bar{R}$ is the universal gas constant and C is the molar concentration per unit volume. For our case of a very dilute solution, $C\bar{V}_s$ is always very small and so the second term in the parenthesis is always negligible compared with the first. Then the above formula reduces to

$$\vec{F}_p = -\frac{1}{N_A}\frac{\bar{R}T}{C}\nabla C \quad . \tag{8}$$

For a neutrally buoyant particle the balance between the hydrodynamic forces (7) and the thermodynamic force (8), along with the condition of vanishing torque, gives

$$6\pi\mu a\left(U_x F_x^t + a\Omega F_x^r + V_x F_x^s\right) = \frac{1}{N_A}\frac{\bar{R}T}{C}\frac{\partial C}{\partial x},$$

$$6\pi\mu a\left(U_z F_z^t + a\Omega F_z^r + V_z F_z^s\right) = \frac{1}{N_A}\frac{\bar{R}T}{C}\frac{\partial C}{\partial z},$$

$$8\pi\mu a^2\left(U_x T_y^{t,x} + U_z T_y^{t,z} + a\Omega T_y^r + \frac{a}{2z}V_x T_y^{s,x} + \frac{a}{2x}V_z T_y^{s,z}\right) = 0.$$

Solving the last equation for Ω and substituting it into the first two, we have

$$U_x \lambda_{xx}^{(U)} + U_z \lambda_{xz}^{(U)} = \frac{\bar{R}T}{6\pi\mu a N_A} \frac{1}{C} \frac{\partial C}{\partial x} - V_x \lambda_{xx}^{(V)} - V_z \lambda_{xz}^{(V)} ,$$

$$U_x \lambda_{zx}^{(U)} + U_z \lambda_{zz}^{(U)} = \frac{\bar{R}T}{6\pi\mu a N_A} \frac{1}{C} \frac{\partial C}{\partial z} - V_x \lambda_{zx}^{(V)} - V_z \lambda_{zz}^{(V)} . \qquad (9)$$

where

$$\lambda_{xx}^{(U)} = F_x^t - F_x^r T_y^{t,x}/T_y^r , \qquad \lambda_{xx}^{(V)} = F_x^s - \frac{a}{2z} F_x^r T_y^{s,x}/T_y^r ,$$

$$\lambda_{xz}^{(U)} = -F_x^r T_y^{t,z}/T_y^r , \qquad \lambda_{xz}^{(V)} = -\frac{a}{2x} F_x^r T_y^{s,z}/T_y^r ,$$

$$\lambda_{zx}^{(U)} = -F_z^r T_y^{t,x}/T_y^r , \qquad \lambda_{zx}^{(V)} = -\frac{a}{2z} F_z^r T_y^{s,x}/T_y^r , \qquad (10)$$

$$\lambda_{zz}^{(U)} = F_z^t - F_z^r T_y^{t,z}/T_y^r , \qquad \lambda_{zz}^{(V)} = F_z^s - \frac{a}{2x} F_z^r T_y^{s,z}/T_y^r .$$

Noting that the x-direction used above is coincident with the R-direction in Fig. 1, we can rewrite U_x, V_x and $\partial C/\partial x$ in (9) as U_R, V_R and $\partial C/\partial R$. When the concentration gradient is absent, the solution of (9) gives the deterministic velocity $\vec{U}^o$:

$$U_R^o = \frac{-1}{\lambda^{(U)}} \left[(\lambda_{xx}^{(V)} \lambda_{zz}^{(U)} - \lambda_{zx}^{(V)} \lambda_{xz}^{(U)}) V_x + (\lambda_{xz}^{(V)} \lambda_{zz}^{(U)} - \lambda_{zz}^{(V)} \lambda_{xz}^{(U)}) V_z \right] ,$$

$$U_z^o = \frac{-1}{\lambda^{(U)}} \left[(\lambda_{zx}^{(V)} \lambda_{xx}^{(U)} - \lambda_{xx}^{(V)} \lambda_{zx}^{(U)}) V_x + (\lambda_{zz}^{(V)} \lambda_{xx}^{(U)} - \lambda_{xz}^{(V)} \lambda_{zx}^{(U)}) V_z \right] , \qquad (11)$$

where

$$\lambda^{(U)} = \lambda_{xx}^{(U)} \lambda_{zz}^{(U)} - \lambda_{xz}^{(U)} \lambda_{zx}^{(U)} . \qquad (11a)$$

Note that when $\vec{V}=0$, we also have $\vec{U}^{o}=0$. For this case (5) reduces to pure diffusion in a stationary medium. Solving (9) for U_R, U_Z and comparing the results with (6), we obtained the expressions for the components of the diffusivity tensor:

$$D_{RR} = D_\infty\left(\frac{-\lambda_{zz}^{(U)}}{\lambda^{(U)}}\right), \qquad D_{Rz} = D_\infty\left(\frac{\lambda_{xz}^{(U)}}{\lambda^{(U)}}\right),$$
$$D_{zR} = D_\infty\left(\frac{\lambda_{zx}^{(U)}}{\lambda^{(U)}}\right), \qquad D_{zz} = D_\infty\left(\frac{-\lambda_{xx}^{(U)}}{\lambda^{(U)}}\right), \tag{12}$$

where

$$D_\infty = \frac{\bar{R}\,T}{6\pi\mu a N_A} \tag{13}$$

is the diffusivity of a spherical solute particle in an unbounded medium.

2.2 THE INTERIOR OF THE PORE

Substituting the constitutive equation (5) into the continuity equation of the solute phase (4), we have

$$\nabla\cdot(C\vec{U}^{o}) = \nabla\cdot(\vec{\vec{D}}\cdot\nabla C)\,. \tag{14}$$

Here the deterministic velocity $\vec{U}^{o}$ and the diffusivity tensor $\vec{\vec{D}}$ are given by (11) and (12) respectively.

There is presently no hydrodynamic theory for determining the hydrodynamic interaction coefficients that would appear in the expressions for U_R^o or D_{RR} for the flow inside the pore. Fortunately, for most membranes of practical

interest the pore length ℓ is much larger than the pore radius R_o so that a one-dimensional approximation can be used (Anderson and Quinn 1974). With $U_z^o(z)$ and $C(z)$ defined as average values over the cross section, the continuity equation (14) reduces to

$$\frac{d}{dz}\left(C U_z^o\right) = \frac{d}{dz}\left(D_{zz}\frac{dC}{dz}\right) . \tag{15}$$

For this approximation, (11) and (12) give

$$U_z^o = -\frac{F_{zo}^s}{F_{zo}^t}\bar{V}_z , \tag{16}$$

$$D_{zz} = D_\infty\left(-\frac{1}{F_{zo}^t}\right) . \tag{17}$$

Here $\bar{V}_z$ is the average velocity of the solvent in the pore and F_{zo}^s and F_{zo}^t should be hydrodynamic parameters averaged over the pore cross section. We shall approximate these hydrodynamic coefficients by their values at the centerline because of the unavailability of other data. Wu and Skalak (1984) have shown with their numerical results that the centerline values F_{zo}^s and F_{zo}^t change very little along the pore axis up to the immediate vicinity of the entrance or exit. Hence U_z^o and D_{zz} can be taken as constants throughout the pore itself. Then, integrating (15) twice we can express $C(z)$ in terms of its values on the two ends of the pore $C_o=C(0)$ and $C_\ell=C(-\ell)$ as follows:

$$C(z) = \left[(C_0 - C_\ell) e^{\frac{U_z^0 z}{D_{zz}}} + C_\ell - C_0 e^{-\frac{U_z^0 \ell}{D_{zz}}} \right] \Big/ \left(1 - e^{-\frac{U_z^0 \ell}{D_{zz}}} \right), \qquad (18)$$

where U_z^0 and D_{zz} are given by (16) and (17). To find the average solvent velocity $\bar{V}_z$ in (16), we return to Kedem-Katchalsky's equations (3a) and (3b), or more conveniently, their equivalent differential forms (e.g. see Anderson and Adamski 1983):

$$J_s = \omega' \bar{R} T \frac{dC}{dz} + (1-\sigma) C J_v , \qquad (19a)$$

$$J_v = L_p \left(\frac{dP}{dz} - \sigma \bar{R} T \frac{dC}{dz} \right) , \qquad (19b)$$

where ω' and L_p are two local coefficients in place of the overall coefficients ω and L_p. When ω' and L_p are constants along the pore length, we simply have (Ogston and Michel 1978)

$$\omega = \frac{\omega'}{\ell} , \quad L_p = \frac{L_p}{\ell} . \qquad (20)$$

With the porosity η of the membrane defined as the ratio of the pore cross section to membrane areas, J_s and J_v can be expressed as

$$J_s = \eta C U_z (1-\tilde{a})^2 , \qquad (21a)$$

$$J_v = \eta \bar{V}_z , \qquad (21b)$$

where

$$\tilde{a} = \frac{a}{R_0} . \qquad (21c)$$

Using (16) and (17), we can rewrite (6b) as

$$CU_z = C\left(-\frac{F^s_{z0}}{F^t_{z0}}\right)\bar{V}_z - D_\infty\left(-\frac{1}{F^t_{z0}}\right)\frac{dC}{dz} \quad .$$

With the help of (21a), (21b) and (13), comparison of this expression with (19a) leads to

$$\sigma = \sigma_o \equiv 1 + \frac{F^s_{z0}}{F^t_{z0}}(1-\tilde{\alpha})^2 \quad , \tag{22a}$$

$$\omega' = \omega'_o \equiv \frac{\eta\,(1-\tilde{\alpha})^2}{6\pi\mu\, a\, N_A\,(-F^t_{z0})} \quad . \tag{22b}$$

Using the Poiseuille formula, we can derive Λ_p from (19b):

$$\Lambda_p = \left(\frac{J_v}{\frac{dp}{dz}}\right)_{\frac{dC}{dz}=0} = \eta\left(\frac{\bar{V}_z}{\frac{dp}{dz}}\right)_{\frac{dC}{dz}=0} = \frac{\eta R_o^2}{8\mu} \quad . \tag{23}$$

Here the dependence of Λ_p on C is neglected for our dilute solution. Equation (22a) indicates that the reflection of the solute in the pore comes from two sources: the slip between the particle and solvent velocities ($-F^s_{z0}/F^t_{z0}$) and the steric exclusion $(1-\tilde{\alpha})^2$. Attempts have been made to devise more refined models for the estimation of the reflection coefficient σ (Bean 1972, Anderson and Quinn 1974, Anderson and Malone 1974, Curry 1974). However, all these models are of approximate nature because of the unavailability of F^s_z and F^t_z for general off-axis positions. Levitt (1975) has proven without referring to any specific

hydrodynamic model, that the σ's in the Kedem-Katchalsky equations (1a) and (1b) are equal to each other. Thus we may substitute (22a) into (19b) to obtain

$$\eta \bar{V}_z = \frac{\eta R_o^2}{8\mu}\left(\frac{dp}{dz} - \sigma_o \bar{R}T \frac{dC}{dz}\right).$$

In terms of the volumetric flow rate q through the pore, defined as

$$q = \bar{V}_z \pi R_o^2 , \tag{24}$$

we have

$$\frac{dp}{dz} = \sigma_o \bar{R}T \frac{dC}{dz} - \frac{8\mu q}{\pi R_o^4} . \tag{25}$$

Integration of (25) gives

$$p(z) - p(0) = \sigma_o \bar{R}T\,(C(z) - C_o) - \frac{8\mu q}{\pi R_o^4} z . \tag{26}$$

The total pressure drop along the pore is

$$p(-l) - p(0) = \sigma_o \bar{R}T\,(C_l - C_o) + \frac{8\mu q l}{\pi R_o^4} , \tag{27}$$

where σ_o is given by (22a).

2.3 THE HALF-SPACES OUTSIDE THE PORE OF A PERMEABLE MEMBRANE

Outside the pore we have to solve the three-dimensional continuity equation (14), or in component form:

$$\frac{1}{R}\frac{\partial}{\partial R}\left(CU_R^\circ R\right) + \frac{\partial}{\partial z}\left(CU_z^\circ\right) = \frac{1}{R}\frac{\partial}{\partial R}\left(D_{RR} R \frac{\partial C}{\partial R} + D_{Rz} R \frac{\partial C}{\partial z}\right) + \frac{\partial}{\partial z}\left(D_{zR}\frac{\partial C}{\partial R} + D_{zz}\frac{\partial C}{\partial z}\right), \tag{28}$$

subject to the following boundary conditions:

In the right half-space ($z>0$):

$$C = C_{\infty} \qquad \text{when } \sqrt{R^2+z^2} \to \infty \text{ and } z>a \quad ; \tag{29a}$$

$$\frac{\partial C}{\partial R} = 0 \qquad \text{when } R=0 \quad ; \tag{29b}$$

$$C U_z = C U_z^0 - D_{zR}\frac{\partial C}{\partial R} - D_{zz}\frac{\partial C}{\partial z} = 0$$

$$\text{when } z=a \text{ and } R \geq R_0$$

$$\text{or } z=\sqrt{a^2-(R_0-R)^2} \text{ and } R_0-a \leq R < R_0 \quad ; \tag{29c}$$

$$\left(\frac{\partial C}{\partial z}\right)_{z=0^+} = \left(\frac{dC}{dz}\right)_{z=0^-} \qquad \text{when } z=0 \text{ and } R<R_0-a \quad . \tag{29d}$$

In the left half-space ($z<-\ell$):

$$C = C_{-\infty} \qquad \text{when } \sqrt{R^2+z^2} \to \infty \text{ and } z<-\ell-a \quad ; \tag{30a}$$

$$\frac{\partial C}{\partial R} = 0 \qquad \text{when } R=0 \quad ; \tag{30b}$$

$$C U_z = C U_z^0 - D_{zR}\frac{\partial C}{\partial R} - D_{zz}\frac{\partial C}{\partial z} = 0$$

$$\text{when } z=-\ell-a \text{ and } R \geq R_0$$

$$\text{or } z=-\ell-\sqrt{a^2-(R_0-R)^2} \text{ and } R_0-a \leq R < R_0 \quad ; \tag{30c}$$

$$\left(\frac{\partial C}{\partial z}\right)_{z=-\ell^-} = \left(\frac{dC}{dz}\right)_{z=-\ell^+} \qquad \text{when } z=-\ell \text{ and } R<R_0-a \quad . \tag{30d}$$

Here the $(dC/dz)_{z=0^-}$ and $(dC/dz)_{z=-\ell^+}$ in (29d) and (30d) are evaluated from the concentration profile (18) inside the pore:

$$\left(\frac{dC}{dz}\right)_{z=0^-} = \frac{U_z^0 (C_0 - C_l)}{D_{zz}\left(1 - e^{-(U_z^0/D_{zz})l}\right)} , \tag{31a}$$

$$\left(\frac{dC}{dz}\right)_{z=-l^+} = \left(\frac{dC}{dz}\right)_{z=0^-} e^{-\frac{U_z^0 l}{D_{zz}}} . \tag{31b}$$

In equations (28)--(30), $\vec{U}^0$ and $\vec{\vec{D}}$ are evaluated by (11) and (12) and the V_x, V_z in (11) are the solvent velocity components. When the solution is dilute, the probability for a particle to appear at a given position is low so that the solvent velocity for our case should differ very little from that of a pure solvent flow. An exact solution for the flow through a finite length pore in the absence of particles has recently been presented in Dagan, Weinbaum and Pfeffer (1982a). The exact infinite series solution is too complicated to use here; however, this exact solution shows that the velocity of pure water for the geometry of our model (Fig. 1) can be closely approximated by Poiseuille profile inside the pore or Sampson's solution outside the pore. The neglect of entrance and exit effects incurs a less than one percent error in the pressure distribution, according to Dagan, Weinbaum and Pfeffer (1982a). In the right half-space Sampson's solution for the solvent velocity can be written as

$$V_R = \frac{3q}{8\pi R_0^2} \frac{\zeta}{R}(R_2 - R_1)\left(\frac{1}{R_1} - \frac{1}{R_2}\right), \tag{32a}$$

$$V_z = \frac{3q}{8\pi R_0^2} \frac{\zeta}{R}(R_1 - R_2)\left(\frac{R-R_0}{R_1} - \frac{R+R_0}{R_2}\right), \tag{32b}$$

where q is the volumetric flow rate of the solvent through the pore, (R,z) are cylindrical coordinates as shown in Fig. 1, ζ is related to the cylindrical coordinates as follows:

$$\zeta = \sqrt{1 - \frac{(R_1 - R_2)^2}{4R_0^2}}, \tag{32c}$$

and

$$R_1 = \sqrt{z^2 + (R-R_0)^2}, \quad R_2 = \sqrt{z^2 + (R+R_0)^2}. \tag{32d}$$

The solvent velocity in the left half-space can be evaluated from the same formulas but with $z+\ell$ in place of z in (32a) and (32d).

To find the pressure variation, we apply the Kedem-Katchalsky equations along the centerline (R=0). The differential form looks like (19a) and (19b), only with partial derivatives in place of the total derivatives in (19a) and (19b). Similar reasoning as in (22) shows that the local reflection coefficient is

$$\sigma(z) = 1 + \left(\frac{F_z^s}{F_z^t}\right)_{R=0}. \tag{33}$$

Note that when z is large, $F_z^s/F_z^t \to -1$ and thus $\sigma(z) \to 0$. Using Sampson's velocity profile, the analogue to (25) is

$$\frac{\partial p}{\partial z} = \sigma(z)\bar{R}T\frac{\partial C}{\partial z} - \frac{3\mu q}{\pi R_0^3}\frac{d}{dz}\left(\frac{zR_0}{R_0^2+z^2} + \tan^{-1}\left(\frac{z}{R_0}\right)\right), \quad (R=0). \tag{34}$$

The integration of (34) gives

$$p(z) - p(0) = \int_0^z \sigma(z)\bar{R}T\frac{\partial C}{\partial z}dz - \frac{3\mu q}{\pi R_0^3}\left[\frac{zR_0}{R_0^2+z^2} + \tan^{-1}\left(\frac{z}{R_0}\right)\right], \quad (R=0), \tag{35}$$

and

$$p_\infty - p(0) = \int_0^\infty \sigma(z)\bar{R}T\frac{\partial C}{\partial z}dz - \frac{3\mu q}{2R_0^3}. \tag{36}$$

Similarly, in the left half-space we have

$$p(z) - p(-\ell) = \int_{-\ell}^z \sigma(z)\bar{R}T\frac{\partial C}{\partial z}dz - \frac{3\mu q}{\pi R_0^3}\left[\frac{(z+\ell)R_0}{(z+\ell)^2+R_0^2} + \tan^{-1}\left(\frac{z+\ell}{R_0}\right)\right], \quad (R=0), \tag{37}$$

and

$$p_{-\infty} - p(-\ell) = \int_{-\ell}^{-\infty} \sigma(z)\bar{R}T\frac{\partial C}{\partial z}dz + \frac{3\mu q}{2R_0^3}. \tag{38}$$

2.4 THE RIGHT HALF-SPACE OUTSIDE THE PORE OF A SEMI-PERMEABLE MEMBRANE

For a semi-permeable membrane where $R_0 < a$, we have to solve the continuity equation (28) subject to the following

boundary conditons in the right half-space ($z>0$):

$$C = C_\infty \qquad \text{when } \sqrt{R^2+z^2}\to\infty \text{ and } z>a \quad ; \tag{39a}$$

$$\frac{\partial C}{\partial R} = 0 \qquad \text{when } R=0 \quad ; \tag{39b}$$

$$CU_z = CU_z^0 - D_{zR}\frac{\partial C}{\partial R} - D_{zz}\frac{\partial C}{\partial z} = 0$$

$$\text{when } z=a \text{ and } R\geq R_0$$

$$\text{or } z=\sqrt{a^2-(R_0-R)^2} \text{ and } R<R_0 \quad . \tag{39c}$$

Because $R_0<a$, the steric exclusion prevents the particles from getting closer to the wall than the broken curve in Fig. 1(b) and thus the particles accumulate there. Across this curve, there is an abrupt change in the solute concentration, which produces a finite difference of osmotic pressure, according to (2). This difference should be balanced by a difference of hydrodynamic pressure across this curve. In particular, along the centerline (R=0) we have

$$p(z_a^+) - \bar{R}TC(z_a^+) = p(z_a^-) \ , \quad (R=0) \ , \tag{40}$$

where

$$z_a = \sqrt{a^2 - R_0^2} \tag{41}$$

is the distance of the broken curve in Fig. 1(b) from the pore opening along the centerline.

To the left of $z=z_a$, the concentration is identically zero and the pressure drop is due to Sampson's solution

alone:

$$p(z) - p(0) = -\frac{3\mu q}{\pi R_o^3}\left[\frac{z R_o}{z^2 + R_o^2} + \tan^{-1}\left(\frac{z}{R_o}\right)\right], \quad (R=0). \qquad (42)$$

The pressure to the right of $z=z_a$ can be evaluated in a way similar to (35):

$$p(z) - p(z_a^+) = \int_{z_a}^{z} \sigma(z)\bar{R}T\frac{\partial C}{\partial z}dz - \frac{3\mu q}{\pi R_o^3}\left[\frac{z R_o}{z^2+R_o^2} + \tan^{-1}\left(\frac{z}{R_o}\right) - \frac{z_a R_o}{z_a^2+R_o^2} - \tan^{-1}\left(\frac{z_a}{R_o}\right)\right], \quad (R=o), \qquad (43)$$

Combining (40), (42) and (43), we have

$$p(z) - p(0) = \int_{z_a}^{z} \sigma(z)\bar{R}T\frac{\partial C}{\partial z}dz + RTC(z_a^+) - \frac{3\mu q}{\pi R_o^3}\left[\frac{z R_o}{z^2+R_o^2} + \tan^{-1}\left(\frac{z}{R_o}\right)\right], \quad (R=0,\ z>z_a), \qquad (44)$$

and

$$p_\infty - p(0) = \int_{z_a}^{\infty} \sigma(z)\bar{R}T\frac{\partial C}{\partial z}dz + \bar{R}TC(z_a^+) - \frac{3\mu q}{2R_o^3}. \qquad (45)$$

2.5 THE OSMOTIC FLOW RATE

For a permeable membrane, the total pressure drop is obtained by combining (27), (36) and (38):

$$p_{-\infty} - p_\infty = \int_{-l}^{-\infty} \sigma(z)\bar{R}T\frac{\partial C}{\partial z}dz - \int_{0}^{\infty} \sigma(z)\bar{R}T\frac{\partial C}{\partial z}dz + \sigma_o RT(C_l - C_o) + \frac{3\mu q}{R_o^3} + \frac{8\mu q l}{\pi R_o^4}.$$

The first three terms of the right hand side of the above equation describe the pressure drop due to the presence of the particles, whereas the last two terms are due to the motion of the solvent phase in the entrance/exit regions and within the pore. The equality of $p_{-\infty}$ and p_∞, as assumed at the beginning of Section 2, requires that the volumetric

flux q should have the following value:

$$q = \frac{R_o^3}{\mu} \frac{\sigma_o \bar{R}T(C_o - C_\ell) + \int_o^\infty \sigma(z)\bar{R}T\frac{\partial C}{\partial z}dz - \int_\ell^\infty \sigma(z)\bar{R}T\frac{\partial C}{\partial z}dz}{3 + \frac{8\ell}{\pi R_o}} \quad . \tag{46}$$

For a semi-permeable membrane, (27), (38) and (45) with $C \equiv 0$ for $z \leq z_a$ give

$$P_{-\infty} - P_\infty = -\int_{z_a}^\infty \sigma(z)\bar{R}T\frac{\partial C}{\partial z}dz - \bar{R}T\,C(z_a^+) + \frac{3\mu q}{R_o^3} + \frac{8\mu q \ell}{\pi R_o^4} \quad .$$

Therefore, for $p_{-\infty}$ equal to p_∞

$$q = \frac{R_o^3}{\mu} \frac{\bar{R}T\,C(z_a^+) + \int_{z_a}^\infty \sigma(z)\bar{R}T\frac{\partial C}{\partial z}dz}{3 + \frac{8\ell}{\pi R_o}} \quad . \tag{47}$$

Equations (46) and (47) show that the osmotic flow rate depends not only on the concentration difference across the membrane, but also on the concentration profile and the local reflection coefficient in the entrance/exit regions. This makes the problem nonlinear. Since the concentration profile is unknown in advance, one has to solve this problem by an iterative procedure. To start, an initial profile of concentration has to be guessed, which will then be used to calculate q from (46) or (47). With this q, one will be able to evaluate the solvent velocity from (32) and (24), and then $\vec{U}^o$ and $\vec{\vec{D}}$ from (11), (12), (16) and (17). With these values, the two sets of boundary value problems (28) with (29) and (28) with (30) can then be numerically solved (for a semi-permeable membrane only one set, i.e. (28) with

(39), is required) to yield the concentration profile. This profile may be used to recalculate q from (46) or (47). The above procedures are then repeated until the concentration profile is determined to within the required accuracy. Finally one can find the pressure profile from (26), (38), (35) or (44).

To estimate the effect of the pore entrance and exit regions on the Kedem-Katchalsky coefficients, we list their expressions (based on (20), (22) and (23)) as follows:

Without the entrance/exit effect :

$$(L_p)_0 = \frac{\eta R_0^2}{8\mu l} \quad , \tag{48}$$

$$\left(\frac{\omega \tilde{V}_s}{L_p}\right)_0 = \frac{16}{9}\hat{a}^2(1-\hat{a})^2\left(\frac{-1}{F^t_{\pi 0}}\right) ; \tag{49}$$

With the entrance/exit effect included:

$$L_p = (L_p)_0 \frac{1}{1+\frac{3\pi}{8}\frac{R_0}{l}} \quad , \tag{50}$$

$$\frac{\omega \tilde{V}_s}{L_p} = \left(\frac{\omega \tilde{V}_s}{L_p}\right)_0 \frac{C_0 - C_l}{C_\infty - C_{-\infty}}\left(1+\frac{3\pi}{8}\frac{R_0}{l}\right) \quad . \tag{51}$$

In this section we have introduced many hydrodynamic force and torque correction factors, whose calculation will be discussed in the next section.

3. CONSIDERATION OF HYDRODYNAMIC INTERACTIONS

Although the spatially varying hydrodynamic data for the force and torque correction factors are not yet available for the general three-dimensional motion of a sphere near a plane with a pore in it, we do know their asymptotic behaviors for the important limiting cases. The values of F_z^t and F_z^s for the axisymmetric flow when the sphere center is located on the pore axis have been obtained by Dagan, Weinbaum and Pfeffer (1982b) and the author of this thesis to high accuracy. When the sphere is far away from the pore opening, the effect of the pore becomes negligible so that the plane wall with a pore may be conceptually replaced by either an infinite solid wall without a pore or a large disc (the infinite solid wall is equivalent to a disc of infinite size). The x-component of the flow past a fixed sphere near a plane wall with a pore is reasonably approximated by a linear shear flow past a sphere in the presence of an infinite wall. The coefficients for all the infinite wall cases except F_z^s are obtained from the infinite bispherical coordinate expansions of Brenner and co-workers. Values for F_z^t are found in Brenner (1961) and values for F_x^s and $T_y^{s,x}$ in Cox and Brenner (1967), and values for F_x^t, $T_y^{t,x}$, F_x^r and T_y^r in Goldman, Cox and Brenner (1967). The coefficient F_z^s is well approximated by the stagnation point flow past a sphere in the presence of a large but finite disc and is given in Dagan, Pfeffer and Weinbaum (1982). This case requires

special treatment since the infinite plane wall solutions do not permit a finite flow normal to the plane of the membrane.

One anticipates that the presence of the pore opening will have the greatest influence on F_z^t and F_z^s since these motions involve a large flow through the pore opening. Significant departures in these coefficients from the infinite wall case can be expected and special treatment is required. In contrast, the rotation or translation of the sphere parallel to the wall induces a much smaller flow through the pore and then can be reasonably approximated by an appropriate infinite wall solution. In addition several of the coefficients are identically zero for the infinite plane wall and should be small compared to unity when the pore is present. In view of these observations we shall make the following assumptions:

1) $F_z^r = T_y^{t,z} = T_y^{s,z} = 0$;
2) F_x^t, F_x^r, F_x^s, T_y^r, $T_y^{t,x}$ and $T_y^{s,x}$ are relatively insensitive to the radial position R and, thus, can be approximated by the results for a sphere near an infinite solid wall, as summarized in Table 1;
3) F_z^t and F_z^s are interpolated between the axisymmetric values (denoted by F_{zo}^t, F_{zo}^s and summarized in Tables 2 and 3) and the results for a sphere near a disc (denoted by F_{zc}^t, F_{zc}^s and summarized in Tables 4 and 5). The technique of interpolation are explained in the following paragraphs for

three different cases according to the relative positions of the projection of the sphere center (point S) and the pore center (point O) as seen in Fig. 2, where the sphere is shown larger than the pore.

Case 1 (Point S is inside the pore) To an observer at point S, the distance ρ of the pore edge to point S looks like an apparent pore radius. ρ changes with the polar angle ϕ around point S. As we can see from Tables 2 and 3, the axisymmetric results for F_{zo}^{t} and F_{zo}^{s} vary with the ratio of radii of the sphere to the pore (a/R_o) when the axial position (z/a) is given. The local velue of a/ρ looks like the apparent ratio of radii of the sphere to the pore and it varies with ϕ. We shall assume that F_z^t is equal to the average value of F_{zo}^{t} corresponding to all the possible values of a/ρ when ϕ takes on the values from 0 to π and z/a is fixed. A similar approximation applies to F_z^s. That is

$$F_z^t = \frac{1}{\pi}\int_0^{\pi} F_{zo}^{t}\left(\frac{a}{\rho}\right) d\phi \quad , \qquad F_z^s = \frac{1}{\pi}\int_0^{\pi} F_{zo}^{s}\left(\frac{a}{\rho}\right) d\phi \quad , \tag{52}$$

where

$$\rho = \begin{cases} R_o - x & \text{when } \phi = o \ ; \\ R_o \dfrac{\sin(\phi-\theta)}{\sin\phi} & \text{when } o<\phi<\pi \ ; \\ R_o + x & \text{when } \phi = \pi \ . \end{cases}$$

and

$$\theta = \sin^{-1}\left(\frac{x}{R_o}\sin\phi\right) \quad \text{when} \quad o<\phi<\pi .$$

Here x is the distance between point S and point 0 (Fig. 2).

Case 2 (Point S is right on the edge of the pore) We can use the same arguments for $\pi/2 \leq \phi \leq \pi$ as in case 1 and find a value F^t_{z2} by averaging F^t_{zo} corresponding to the values of a/ρ for this range of ϕ. But for $0 \leq \phi < \pi/2$ the sphere sees a disc of infinite size rather than a pore. Therefore, the contribution of the part with $0 \leq \phi < \pi/2$ is F^t_{zc} corresponding to $a/R_c=0$, and the value of F^t_z for the whole sphere is the average of F^t_{z2} and F^t_{zc}. Similar arguments hold for F^s_z. Thus we have

$$\begin{aligned} F^t_z &= \tfrac{1}{2}\left[F^t_{z2} + F^t_{zc}(a/R_c=0)\right], \\ F^s_z &= \tfrac{1}{2}\left[F^s_{z2} + F^s_{zc}(a/R_c=0)\right], \end{aligned} \tag{53}$$

where

$$\begin{aligned} F^t_{z2} &= \frac{2}{\pi}\int_{\pi/2}^{\pi} F^t_{zo}(a/\rho)\,d\phi , \\ F^s_{z2} &= \frac{2}{\pi}\int_{\pi/2}^{\pi} F^s_{zo}(a/\rho)\,d\phi , \end{aligned} \tag{54}$$

and

$$\rho = 2R_o\cos(\pi-\phi), \quad \text{when} \quad \frac{\pi}{2} \leq \phi \leq \pi .$$

Case 3 (Point S is outside the pore) Suppose the ray $\phi=\beta$ is tangent to the pore edge. Then for $0 \leq \phi \leq \beta$ the sphere sees a disc of infinite size and for $\beta < \phi \leq \pi$ the observer

at the sphere center sees a disc of radius ρ (the distance from point S to the near edge of the pore). However, for $\beta < \phi \leq \pi$, the solid wall beyond the far edge of the pore cannot be ignored, especially when the sphere is bigger than the pore. One way to take this into consideration is to give the pore effect, F_{z2}^t or F_{z2}^s as evaluated in (54), a weight of R_o/x and the disc effect, as averaged over ϕ from β to π, a weight of $(1-R_o/x)$. Here x is the distance between point S and the pore center O (Fig. 2). It is noted that when $x=R_o$, only the pore effect is retained, exactly as in case 2, and that when $x \to \infty$, only the disc effect is retained as should be expected. The values of F_z^t and F_z^s for the whole sphere are then

$$F_z^t = \frac{1}{\pi}\left[\beta F_{zc}^t\left(\frac{a}{R_c}=0\right) + (\pi-\beta)\frac{R_o}{x}F_{z2}^t + \left(1-\frac{R_o}{x}\right)\int_\beta^\pi F_{zc}^t\left(\frac{a}{\rho}\right)d\phi\right],$$

$$F_z^s = \frac{1}{\pi}\left[\beta F_{zc}^s\left(\frac{a}{R_c}=0\right) + (\pi-\beta)\frac{R_o}{x}F_{z2}^s + \left(1-\frac{R_o}{x}\right)\int_\beta^\pi F_{zc}^s\left(\frac{a}{\rho}\right)d\phi\right], \tag{55}$$

where

$$\rho = \begin{cases} R_o\dfrac{\sin(\phi-\theta)}{\sin\phi} & \text{when } \beta \leq \phi < \pi, \\ x - R_o & \text{when } \phi = \pi, \end{cases}$$

and

$$\beta = \pi - \sin^{-1}\left(\frac{R_o}{x}\right),$$

$$\theta = \pi - \sin^{-1}\left(\frac{x}{R_o}\sin\phi\right), \quad \text{when } \beta \leq \phi < \pi.$$

Using the simplifying assumptions outlined herein and the force and torque correction factors just described, we can simplify (11) and (12) to

$$U_R^0 = -\frac{F_x^s - \frac{a}{2z} F_x^r T_y^{s,x}/T_y^r}{F_x^t - F_x^r T_y^{t,x}/T_y^r} V_R \,, \qquad U_z^0 = -\frac{F_z^s}{F_z^t} V_z \,, \tag{56}$$

and

$$\mathcal{D}_{RR} = D_\infty \left(\frac{-1}{F_x^t - F_x^r T_y^{t,x}/T_y^r} \right) \,, \qquad \mathcal{D}_{Rz} = 0 \,,$$

$$\mathcal{D}_{zR} = 0 \,, \qquad \mathcal{D}_{zz} = D_\infty \left(\frac{-1}{F_z^t} \right) \,, \tag{57}$$

where D_∞ is given by (13).

Typical values of D_{RR}/D_∞ for a/R_o=0.1--1.5 are plotted in Fig. 3. If it were not for the hydrodynamic interaction of the particle with the entrance geometry, these values would have been unity. The very rapid changes near z=a and the slow approach to unity as z increases show the profound influence of the wall interaction. Because of our simplifying assumptions D_{RR} is independent of R.

Fig. 4 gives the changes in D_{zz}/D_∞ with R/R_o for a/R_o= 0.1. When $z > R_o$, the dependence on R is very weak. But as the plane wall is approached, D_{zz} decays rapidly to zero. Even at a distance z/R_o=10, i.e. a hundred times the sphere radius from the pore opening, the value of D_{zz} still

differs from that in an unbounded flow (D_∞) by more than one percent.

Fig. 5 shows the ratios of the solvent velocity V_z and the particle deterministic velocity U_z^o to the average velocity $\overline{V}_z$ in the pore (see (24)) for a/R_o=0.1--1.5. It is seen that without diffusion the neutrally buoyant particle moves with the solvent when it is more than a few diameters from the pore entrance, but that a substantial slip velocity between the two phases is generated when the particle is close to the pore entrance for $a/R_o > 0.5$.

Fig. 6 shows the ratios of the radial solvent velocity V_R and the particle's deterministic velocity U_R^o to the average velocity $\overline{V}_z$ in the pore for a/R_o=0.1. The particle velocity U_R^o vanishes when it approaches the wall ($z \to a$), but within an axial distance of one sphere diameter ($z=3a=0.30R_o$), the particle adapts its radial velocity U_R^o to within a few percent of the solvent velocity V_R. As can be seen from Fig. 5 and Fig. 6, the maximum magnitude of U_R^o is small but not negligible as compared with that of U_z^o. This indicates the necessity of a three-dimensional analysis outside the pore.

Table 6 summarizes the data for F_{zo}^t and F_{zo}^s inside the pore, taken from Happel and Brenner (1973) for a/R_o=0--0.01, from Leichtberg, Pfeffer and Weinbaum (1976) for a/R_o=0.1--0.7 and from Wu and Skalak (1964) for a/R_o=0.8--0.9.

Fig. 7 presents some typical values for the local reflection coefficient $\sigma(z)$ along the pore axis (R=0). The

values of σ inside the pore (σ_o) are calculated from (22a) and those for $z \geqslant a$ from (33). The intermediate values are described by a third order polynomial which smoothly connects the two regions. It can be seen that within a few particle radii $\sigma(z)$ changes from σ_o to almost zero.

4. NUMERICAL PROCEDURES

Let us non-dimensionize length, concentration, diffusivity, velocity, volumetric flow rate and pressure in terms of R_o, C_∞, D_∞ and μ such that

$$\hat{R} = \frac{R}{R_o} , \quad \hat{Z} = \frac{Z}{R_o} , \quad \hat{a} = \frac{a}{R_o} , \quad \hat{\ell} = \frac{\ell}{R_o} ,$$

$$\tilde{D}_{RR} = \frac{D_{RR}}{D_\infty} , \quad \tilde{D}_{ZZ} = \frac{D_{ZZ}}{D_\infty} , \quad \tilde{V}_R = \frac{V_R R_o}{D_\infty} , \quad \tilde{V}_Z = \frac{V_Z R_o}{D_\infty} , \tag{58}$$

$$\tilde{U}_R = \frac{U_R R_o}{D_\infty} , \quad \tilde{U}_Z = \frac{U_Z R_o}{D_\infty} , \quad \tilde{U}_R^o = \frac{U_R^o R_o}{D_\infty} , \quad \tilde{U}_Z^o = \frac{U_Z^o R_o}{D_\infty} ,$$

$$\tilde{q} = \frac{q}{\pi R_o D_\infty} , \quad \tilde{C} = \frac{C}{C_\infty} , \quad \tilde{p} = \frac{p R_o^2}{\mu D_\infty} ,$$

where tilda quantities are dimensionless. D_∞ is given by (13). The dimensionless form of (28), with $D_{RZ}=D_{ZR}=0$ by (57), is

$$\frac{1}{\tilde{R}} \frac{\partial}{\partial \tilde{R}} \left(\tilde{C} \tilde{U}_R^o \tilde{R} \right) + \frac{\partial}{\partial \tilde{Z}} \left(\tilde{C} \tilde{U}_Z^o \right) = \frac{1}{\tilde{R}} \frac{\partial}{\partial \tilde{R}} \left(\tilde{D}_{RR} \tilde{R} \frac{\partial \tilde{C}}{\partial \tilde{R}} \right) + \frac{\partial}{\partial \tilde{Z}} \left(\tilde{D}_{ZZ} \frac{\partial \tilde{C}}{\partial \tilde{Z}} \right) , \tag{59}$$

where

$$\tilde{D}_{RR} = \frac{-1}{F_x^t - F_x^r T_y^{t,x} / T_y^r} , \qquad \tilde{D}_{ZZ} = \frac{-1}{F_z^t} , \tag{60}$$

$$\tilde{U}_R^o = \frac{-\left(F_x^s - \frac{\hat{a}}{2\hat{z}} F_x^r T_y^{s,x} / T_y^r \right)}{F_x^t - F_x^r T_y^{t,x} / T_y^r} \tilde{V}_R , \qquad \tilde{U}_Z^o = - \frac{F_z^s}{F_z^t} \tilde{V}_Z , \tag{61}$$

by (56) and (57). By (32), $\tilde{V}_R$ and $\tilde{V}_Z$ in the right half-space are

$$\tilde{V}_R = \frac{3}{8}\,\tilde{q}\,\tilde{z}\,\frac{\zeta}{\tilde{R}}\,(\tilde{R}_2-\tilde{R}_1)\left(\frac{1}{\tilde{R}_1}-\frac{1}{\tilde{R}_2}\right),$$

$$\tilde{V}_z = \frac{3}{8}\,\tilde{q}\,\frac{\zeta}{\tilde{R}}\,(\tilde{R}_1-\tilde{R}_2)\left(\frac{\tilde{R}-1}{\tilde{R}_1}-\frac{\tilde{R}+1}{\tilde{R}_2}\right), \qquad (62)$$

where

$$\zeta = \sqrt{1-\left(\frac{\tilde{R}_2-\tilde{R}_1}{2}\right)^2},$$

$$\tilde{R}_1 = \sqrt{\tilde{z}^2+(\tilde{R}-1)^2}, \quad \tilde{R}_2 = \sqrt{\tilde{z}^2+(\tilde{R}+1)^2}.$$

In the left half-space, $\tilde{z}+\tilde{\ell}$ should be used in place of $\tilde{z}$ in these formulas.

For a permeable membrane, the boundary conditions (29) and (30) become:

In the right half-space ($\tilde{z}>0$):

$$\begin{aligned}
&\tilde{C} = 1 && \text{when } \sqrt{\tilde{R}^2+\tilde{z}^2}\to\infty \text{ and } \tilde{z}>\tilde{a} \quad ; \\
&\frac{\partial\tilde{C}}{\partial\tilde{R}} = 0 && \text{when } \tilde{R}=0 \quad ; \\
&\frac{\partial\tilde{C}}{\partial\tilde{z}} = F_z^s\,\tilde{C}\,\tilde{V}_z && \text{when } \tilde{z}=\tilde{a} \text{ and } \tilde{R}\geq 1 \\
& && \text{or } \tilde{z}=\sqrt{\tilde{a}^2-(1-\tilde{R})^2} \text{ and } 1-\tilde{a}\leq\tilde{R}<1 \quad ; \\
&\frac{\partial\tilde{C}}{\partial\tilde{z}} = \frac{F_{z0}^s\,\tilde{q}\,(\tilde{C}_0-\tilde{C}_\ell)}{1-e^{-F_{z0}^s\tilde{q}\,\tilde{\ell}}} && \text{when } \tilde{z}=0 \text{ and } \tilde{R}<1-\tilde{a} \quad .
\end{aligned} \qquad (63)$$

In the left half-space ($\tilde{z} < -\tilde{\ell}$):

$$\tilde{C} = \tilde{C}_{-\infty} \qquad \text{when } \sqrt{\tilde{R}^2+\tilde{z}^2} \to \infty \text{ and } \tilde{z} < -\tilde{\ell}-\tilde{a} \ ;$$

$$\frac{\partial \tilde{C}}{\partial \tilde{R}} = 0 \qquad \text{when } \tilde{R} = 0 \ ;$$

$$\frac{\partial \tilde{C}}{\partial \tilde{z}} = F_z^s \tilde{C} \tilde{V}_z \qquad \text{when } \tilde{z} = -\tilde{\ell}-\tilde{a} \text{ and } \tilde{R} \geq 1$$

$$\text{or } \tilde{z} = -\tilde{\ell} - \sqrt{\tilde{a}^2-(1-\tilde{R})^2} \text{ and } 1-\tilde{a} \leq \tilde{R} < 1 \ ; \tag{64}$$

$$\frac{\partial \tilde{C}}{\partial \tilde{z}} = \frac{F_{z0}^s \tilde{q}(\tilde{C}_0-\tilde{C}_\ell)e^{-F_{z0}^s \tilde{q}\tilde{\ell}}}{1-e^{-F_{z0}^s \tilde{q}\tilde{\ell}}} \qquad \text{when } \tilde{z} = -\tilde{\ell} \text{ and } \tilde{R} < 1-\tilde{a} \ .$$

In deriving (63) and (64), we have used (16), (17), (56) and (57). The dimensionless flow rate $\tilde{q}$, which is essentially the Peclet number, as can be seen from the definition (58), is given from (46) by

$$\tilde{q} = \frac{N_q}{3+\frac{8}{\pi}\tilde{\ell}}\left[\sigma_0(\tilde{C}_0-\tilde{C}_\ell)+\int_0^\infty \sigma(\tilde{z})\frac{\partial \tilde{C}}{\partial \tilde{z}}d\tilde{z} - \int_{-\tilde{\ell}}^{-\infty}\sigma(\tilde{z})\frac{\partial \tilde{C}}{\partial \tilde{z}}d\tilde{z}\right] , \tag{65}$$

where σ_0 and $\sigma(\tilde{z})$ are given by (22a) and (33), N_q is a dimensionless parameter defined as

$$N_q = 6\, a\, R_0^2\, N_A\, C_\infty = \frac{q}{2\pi}\frac{\phi}{\tilde{a}^2} \ , \tag{66}$$

and ϕ is the volume fraction of the solute in the right bulk solution:

$$\phi = \frac{4\pi}{3} a^3 N_A C_\infty \ . \tag{67}$$

Equation (18) for the concentration inside the pore becomes

$$\tilde{C}(\tilde{z}) = \frac{(\tilde{C}_0 - \tilde{C}_\ell)\, e^{F^s_{z0}\hat{q}\tilde{z}} + \tilde{C}_\ell - \tilde{C}_0 e^{-F^s_{z0}\hat{q}\tilde{\ell}}}{1 - e^{-F^s_{z0}\hat{q}\hat{\ell}}} \,. \tag{68}$$

The pressure distribution along the pore axis ($\tilde{R}=0$), from (37), (26) and (35), is given by

$$\hat{p}(\hat{z}) - \hat{p}(0) = \pi N_q \Big[\int_{-\ell}^{\hat{z}} \sigma(\hat{z}) \frac{\partial \hat{C}}{\partial \hat{z}} d\hat{z} + \sigma_\ell (\tilde{C}_\ell - \tilde{C}_0) \Big] + 8\hat{q}\hat{\ell} - 3\hat{q}\Big[\frac{\hat{z}+\hat{\ell}}{(\hat{z}+\hat{\ell})^2+1} + \tan^{-1}(\hat{z}+\hat{\ell}) \Big], \quad (\hat{z} \le -\hat{\ell}), \tag{69}$$

$$\hat{p}(\hat{z}) - \hat{p}(0) = \sigma_0 \pi N_q (\tilde{C}_\ell - \tilde{C}_0) \Big(\frac{1 - e^{F^s_{z0}\hat{q}\tilde{z}}}{1 - e^{-F^s_{z0}\hat{q}\hat{\ell}}} \Big) - 8\hat{q}\tilde{z}, \quad (-\hat{\ell} < \hat{z} < 0), \tag{70}$$

$$\hat{p}(\hat{z}) - \hat{p}(0) = \pi N_q \int_0^{\hat{z}} \sigma(\hat{z}) \frac{\partial \hat{C}}{\partial \hat{z}} d\hat{z} - 3\hat{q}\Big[\frac{\hat{z}}{\hat{z}^2+1} + \tan^{-1}\hat{z} \Big], \quad (\hat{z} > 0). \tag{71}$$

For a semi-permeable membrane, the boundary conditions (39) become

$$\begin{aligned}
&\hat{C} = 1 && \text{when } \sqrt{\hat{R}^2+\hat{z}^2} \to \infty \quad \text{and } \hat{z} > \hat{a}; \\
&\frac{\partial \hat{C}}{\partial \tilde{R}} = 0 && \text{when } \hat{R} = 0 \quad ; \\
&\frac{\partial \hat{C}}{\partial \hat{z}} = F^s_z \hat{C} \tilde{V}_z && \text{when } \hat{z} = \hat{a} \quad \text{and } \hat{R} \ge 1 \\
& && \text{or } \hat{z} = \sqrt{\hat{a}^2 - (1-\hat{R})^2} \quad \text{and } \hat{R} < 1 \,.
\end{aligned} \tag{72}$$

The flow rate across the semi-permeable membrane, from (47), is

$$\tilde{q} = \frac{N_1}{3+\frac{8}{\pi}\tilde{l}} \left[\tilde{C}(\tilde{z}_a^+) + \int_{\tilde{z}_a}^{\infty} \sigma(\tilde{z}) \frac{\partial \tilde{C}}{\partial \tilde{z}} d\tilde{z} \right] . \tag{73}$$

The pressure along the pore axis ($\tilde{R}=0$) for $-\infty<\tilde{z}<\tilde{z}_a$ can be evaluated by (69), (70) or (71) with $\tilde{C}_0=\tilde{C}_{\ell}=0$ and $\partial\tilde{C}/\partial\tilde{z}=0$. When $\tilde{z}>\tilde{z}_a$, along the pore axis ($\tilde{R}=0$) (44) gives

$$\tilde{p}(\tilde{z}) - \tilde{p}(0) = -\pi N_1 \left[\int_{\tilde{z}_a}^{\tilde{z}} \sigma(\tilde{z}) \frac{\partial \tilde{C}}{\partial \tilde{z}} d\tilde{z} + \tilde{C}(\tilde{z}_a^+) \right] - 3\tilde{q} \left(\frac{\tilde{z}}{\tilde{z}^2+1} + \tan^{-1}\tilde{z} \right) , \quad (\tilde{z} > \tilde{z}_a) . \tag{74}$$

We now proceed to solve (59), subject to boundary conditions (63), (64) or (72). Equation (59) is first cast into the form of a difference equation and then solved by an iterative procedure. The right half-space ($\tilde{z}>0$) is truncated to a big finite region as shown in Fig. 8 for the case of a permeable membrane. The grid system in a meridian plane consists of lines $\tilde{R}=\tilde{R}_i$ ($i=1,2,\ldots,M$) and $\tilde{z}=\tilde{z}_j$ ($j=1,2,\ldots,N$) such that

$$0 = \tilde{R}_1 < \tilde{R}_2 < \tilde{R}_3 < \ldots < \tilde{R}_M ;$$
$$\tilde{z}_1 < \tilde{z}_2 < \tilde{z}_3 < \ldots < \tilde{z}_N .$$

The line $\tilde{z}=\tilde{z}_1$ consists of part of the pore opening ($\tilde{z}=0$ for $\tilde{R}<1-\tilde{a}$) and part of the broken curve ($\tilde{z}=\tilde{a}$ for $\tilde{R}>1$ and $\tilde{z}=\sqrt{\tilde{a}^2-(1-\tilde{R})^2}$ for $1-\tilde{a}\leqslant\tilde{R}\leqslant 1$). The spacings in Fig. 8 are unevenly arranged so that the finer grids near the pore

opening may better describe the rapid concentration change there.

By using the overrelaxation scheme (Forsythe and Wasow 1960), the solute continuity equation (59) can be discretized, for an interior point (R_i, z_j) $(1 < i < M,\ 1 < j < N)$, as follows

$$\tilde{C}_{ij}^{(m+1)} = \tilde{C}_{ij}^{(m)} + \tilde{\omega}\left[P_{ij}^{L}\, \tilde{C}_{i-1,j}^{(m+1)} + P_{ij}^{R}\, \tilde{C}_{i+1,j}^{(m)} + P_{ij}^{U}\, \tilde{C}_{i,j+1}^{(m)} + P_{ij}^{B}\, \tilde{C}_{i,j-1}^{(m+1)} - \tilde{C}_{ij}^{(m)} \right], \tag{75}$$

where

$$P_{ij}^{L} = \frac{P_{ij}^{D}\, \hat{R}_{i-1}}{\Delta_i\, \tilde{R}_i} \left[\frac{\tilde{D}_{RR\, i-1,j}}{h_{i-1}} + \tilde{U}^{o}_{R\, i-1,j} \right],$$

$$P_{ij}^{R} = \frac{P_{ij}^{D}\, \hat{R}_{i+1}}{\Delta_i\, \hat{R}_i} \left[\frac{\tilde{D}_{RR\, i+1,j}}{h_i} - \tilde{U}^{o}_{R\, i+1,j} \right],$$

$$P_{ij}^{U} = \frac{P_{ij}^{D}}{\delta_j} \left[\frac{\tilde{D}_{zz\, i,j+1}}{k_j} - \tilde{U}^{o}_{z\, i,j+1} \right],$$

$$P_{ij}^{B} = \frac{P_{ij}^{D}}{\delta_j} \left[\frac{\tilde{D}_{zz\, i,j-1}}{k_{j-1}} + \tilde{U}^{o}_{z\, i,j-1} \right],$$

and

$$P_{ij}^{D} = \left[\frac{\tilde{D}_{RR\, i+1,j}\, \hat{R}_{i+1}}{h_i \Delta_i\, \tilde{R}_i} + \frac{\tilde{D}_{RR\, i-1,j}\, \hat{R}_{i-1}}{h_{i-1} \Delta_i\, \tilde{R}_i} + \frac{\tilde{D}_{zz\, i,j+1}}{k_j\, \delta_j} + \frac{\tilde{D}_{zz\, i,j-1}}{k_{j-1}\, \delta_j} \right]^{-1},$$

$$h_i = \hat{R}_{i+1} - \hat{R}_i \quad (1 \le i < M), \qquad k_j = \hat{z}_{j+1} - \hat{z}_j \quad (1 \le j < N),$$

$$\Delta_i = h_{i-1} + h_i \quad (1 < i < M), \qquad \delta_j = k_{j-1} + k_j \quad (1 < j < N).$$

The superscript m denotes the m-th iteration and $\tilde{\omega}$ is the relaxation factor. $\tilde{\omega}=1$ corresponds to a Seidel iteration. The boundary conditions (63) can be discretized as

$$\begin{aligned}
&\tilde{C}_{Mj}^{(m+1)} = 1 \quad , \quad (1 \le j < N) ; \\
&\tilde{C}_{iN}^{(m+1)} = 1 \quad , \quad (1 \le i \le M) ; \\
&\tilde{C}_{1,j}^{(m+1)} = \tilde{C}_{2,j}^{(m+1)} \quad , \quad (1 \le j < N) ; \\
&\tilde{C}_{i,1}^{(m+1)} = \tilde{C}_{i,2}^{(m+1)} \Big/ \left(1 + k_1 F_{\tilde{z}\, i,1}^{S} \tilde{V}_{\tilde{z}\, i,1}\right), \quad (i_a \le i < M) ; \\
&\tilde{C}_{i,1}^{(m+1)} = \tilde{C}_{0}^{(m+1)} = \tilde{C}_{1,2}^{(m+1)} - \frac{\tilde{z}_2}{2}\left[\frac{F_{\tilde{z}0}^{S}\tilde{q}\left(\tilde{C}_0^{(m)} - \tilde{C}_{\ell}^{(m)}\right)}{1 - e^{-F_{\tilde{z}0}^{S}\tilde{q}\tilde{\ell}}} + \frac{C_{1,3}^{(m+1)} - C_{1,2}^{(m+1)}}{k_2}\right], \\
&\qquad (1 \le i < i_a) .
\end{aligned} \tag{76}$$

Where $\tilde{R}_{i_a} \le 1-\tilde{a} < \tilde{R}_{i_a+1}$ and the last formula is derived by using a second order polynomial for $\tilde{C}(\tilde{z})$ connecting $\tilde{C}_0$ and $\tilde{C}_{1,2}$ smoothly. Boundary conditions (64) and (72) can be discretized likewise.

In this problem, there are three dimensionless characteristic parameters to be specified: $\tilde{a}$, N_q and $\tilde{\ell}$. However, in (75) and (76), $\tilde{D}_{RR}$, $\tilde{D}_{zz}$, $\tilde{U}_R^o/\tilde{q}$, $\tilde{U}_z^o/\tilde{q}$, $\tilde{V}_{zi,1}/\tilde{q}$ and $F_{zi,1}^{S}$ are functions of $\tilde{a}$ alone and independent of N_q and $\tilde{\ell}$. Thus for a given $\tilde{a}$, these quantities can be computed only once and used for all cases with different N_q and $\tilde{\ell}$.

To start the iterative procedure of solving (75), we have to arbitrarily specify the initial values of $\tilde{C}$ at all the grid points. One simple way is to assume that $\tilde{C}_{ij}=1$ at all the points in the right half-space and $\tilde{C}_{ij}=\tilde{C}_{-\infty}$ in the left. Different initial values do not change the final

results but do influence the speed of convergence. The relaxation factor $\tilde{\omega}$ should be chosen between 0 and 2 to secure the convergence. The choice of $\tilde{\omega}$ can influence the convergence speed significantly. Theoretically, there exists an optimum value of $\tilde{\omega}$; however, this value has to be determined by numerical tests for individual cases. In our computations the optimum values of $\tilde{\omega}$ fall in the range between 1.5 and 1.9. The convergence is tested by the following criterion:

$$\underset{\substack{1\le i\le M\\ 1\le j\le N}}{\text{Max.}} \left|\tilde{C}_{ij}^{(m+1)} - \tilde{C}_{ij}^{(m)}\right| \le \varepsilon \text{ , (in the whole flow field)} , \qquad (77)$$

where ε is a given small positive number. Numerical tests show that $\varepsilon = 10^{-6}$ is a good choice and $\varepsilon = 10^{-5}$ can occasionally lead to false convergence. For most cases sixty to a few hundred iterations are sufficient. In our computations, R_M and z_N were taken as 10 to 20 and M, N were approximately 30.

5. RESULTS AND DISCUSSION

Our computations were performed for the range of $\tilde{a}$=0.01--1.5 and $\tilde{\ell}$=5--500. The volume fraction of the solute in the right bulk solution ϕ is limited to values ≤ 0.05 to keep the solution dilute. The corresponding N_q, calculated from (66), ranges between 716.2 and 0.006. Without loss of generality, we assume $\tilde{C}_{-\infty}=0$, since one can always use the scale transformation $\hat{C}=(C-C_{-\infty})/(C_{\infty}-C_{-\infty})$ to convert a non-zero concentration $C_{-\infty}$ to this case.

Fig. 9 presents the profiles of concentration and pressure for the case of very small particles ($\tilde{a}$=0.01) in a long pore ($\tilde{\ell}$=500). For this case, the concentration gradient is, effectively, restricted to the entrance end in the pore, as Ray (1960) predicted, and the fast diffusion in this entrance region induces a passive solvent movement through the pore. The pressure drop is quite close to that for a Poiseuille flow in a tube, as indicated by a dash line in the figure, except near the entrance end, where the concentration gradient drives the solvent motion against the adverse pressure gradient. For such a long pore the flow outside the pore has little influence on the osmotic flow. However, if the pore is relatively short, the solution is substantially different, as can be observed in Fig. 10 for $\tilde{\ell}$=5. In this case, a large concentration change occurs outside the pore within a few radii of the entrance end and the driving force inside the pore is less important. The strong

nonlinear effects of concentration cause a large asymmetry between the entrance and exit regions.

Figs. 11, 12 and 13 show the effect of the particle size ($\tilde{a}$=0.1--0.9) at the same volume fraction (ϕ=0.05) in the right bulk solution. When ϕ is fixed, the molar concentration C_∞ of big particles is much less than that of small particles. As $\tilde{a}$ increases, the osmotic flow rate $\tilde{q}$ decreases and thus the nonlinearity in the concentration profile becomes less significant. Note that the scale for the pressure drop in these figures is two orders of magnitude smaller than in Figs. 9 and 10. For all these cases the maximum pressure drops are about one-tenth of the Poiseuille pressure drop along the whole pore length (e.g. the latter is equal to $8\tilde{q}\tilde{\ell}$=2.81 in Fig. 11) and the main driving force is the concentration gradient both inside and outside the pore. A fascinating feature of the pressure profile is the maximum that appears in the entrance region. In Figs. 11 and 12, the flow moves through most of the pore against an adverse pressure gradient.

Fig. 14 depicts the case of medium-sized particles ($\tilde{a}$=0.5) in a relative long pore ($\tilde{\ell}$=50). When compared with Fig. 12 for the same value of ϕ ($\tilde{a}$=0.5, $\tilde{\ell}$=5), the end effects are less important. When compared with Fig. 9 ($\tilde{a}$=0.01, $\tilde{\ell}$=500), there is no longer the sweeping-away effect of the solute near the exit end bacause the molar concentration C_∞ for $\tilde{a}$=0.5 is less than that for $\tilde{a}$=0.01 by a factor of 8×10^{-6} and thus the induced osmotic flow is

insignificant.

In Fig. 15, we consider the case of $\tilde{a}=0.1$ and $\tilde{\ell}=5$, in which the molar concentration C_∞, instead of the volume fraction ϕ, is chosen to be the same as in Fig. 12 ($\tilde{a}=0.5$, $\tilde{\ell}=5$). While the concentration profiles differ very little from each other, the pressure drop for $\tilde{a}=0.1$ is much less than for $\tilde{a}=0.5$, in accordance with the much lower values of N_q and $\tilde{q}$ for $\tilde{a}=0.1$. It is evident from Figs. 9--15 that the entrance and exit effects on the two sides of a permeable membrane are generally not symmetrical, as hypothesized by Lerche (1976). The side with higher concentration has a more significant disturbance due to nonlinear convective effects.

Fig. 16 illustrates the osmotic mechanism for a semi-permeable membrane ($\tilde{a}=1.5$). The steric exclusion of particles of radius $a>R_0$ produces an interface with a discontinuity in both concentration and pressure. To the left of this interface the concentration is identically zero and to the right the concentration is essentially uniform. As equation (40) indicates, the difference between hydrodynamic and osmotic pressures ($p-\bar{R}TC$) has to be continuous across the interface. Without an induced flow this could not be satisfied since $p_{-\infty}=p_\infty$ and $C_\infty \neq 0$. Therefore a solvent flow is generated through the pore such that the total hydrodynamic pressure drop is equal to the osmotic pressure difference across the interface. For these large particles the osmotic flow is so weak that the

convection at the pore entrance has only a very minor effect on the concentration profile.

Table 7 compares the hydrodynamic permeabilities L_p with entrance/exit effects, Eq. (50), and $(L_p)_o$ without these effects, Eq. (48). It is seen that the correction to L_p due to these effects is of the order of $R_o/\ell = \tilde{\ell}^{-1}$. However, from Table 8 one concludes that the effects of the entrance/exit on the osmotic flow rate $\tilde{q}$ of the solvent are much more significant, especially for cases of small particles, because of the additional changes due to the concentration profiles. As can be seen from Table 8 (for a constant volume fraction ϕ) and Table 9 (for a constant molar concentration C_∞ and a given pore radius R_o), the osmotic flow rate of the solvent may be overestimated by as much as two hundred percent for very small particles in short pores (e.g. $\tilde{a}$=0.01 and $\tilde{\ell}$=5) if the entrance/exit effects were not taken into consideration and the formula

$$\tilde{q}_o = \frac{\pi N_1}{8\tilde{\ell}} \sigma_o \tag{78}$$

were used. Similarly, the diffusional permeability may be either overestimated or underestimated considerably if (49) were used instead of (51). The smaller the solute particle, the shorter the pore, and the higher the volume fraction ϕ, the more important are the entrance/exit effects. Even with a relatively long pore ($\tilde{\ell}$=50) and a very low volume fraction ($\phi = 4\times10^{-7}$), the entrance/exit effects may still influence the osmotic flow rate $\tilde{q}$ by more than ten percent for

very small particles ($\tilde{a}$=0.01).

To provide some numerical estimates, we present the dimensional values of the total volume flux J_v/η and the solute flow rate J_s/η , see equations (21b) and (21a), in Figs. 17 and 18 for a pore radius R_o=5Å. When the volume fraction ϕ is fixed, both J_v and J_s decease rapidly as the particle size $\tilde{a}$ increases. However, when the molar concentration C_∞ is fixed, J_v increases but J_s decreases as $\tilde{a}$ increases. The decrease in J_s is due to both the lower diffusivity D_{zz} and the larger steric exclusion $(1-\tilde{a})^2$ for larger particles. Longer pores produce lower J_v and J_s, if the conditions are otherwise the same. The curves for C_∞=const. are truncated at $\tilde{a}$=0.5 since ϕ would exceed 0.05 for larger values of $\tilde{a}$.

In Fig. 19 curves of equal concentration $\tilde{C}$ are drawn for two different particle sizes with ϕ and $\tilde{\ell}$ being the same. While the concentration change occurs mainly inside the pore for $\tilde{a}$=0.5, the greatest gradient of concentration occurs immediately outside the pore entrance for $\tilde{a}$=0.01. However, in both cases the entrance/exit effects are essentially confined to the regions within a few pore-radii from the pore openings.

Fig. 19 clearly demonstrates the three-dimensional, local nature of the entrance/exit effects. This behavior is especially important in explaining osmosis in biological membranes, whose porosity is usually very low and the pore radius is small compared to the pore spacing. For these

membranes the local changes in concentration as indicated in this study would occur in the vicinity of the pore entrance/exit and not be affected by the interaction between pores. When the interaction between pores is considered, as diagrammatically shown in Fig. 20, a quasi-uniform concentration, say C_w, will be achieved at a distance δ_1 from the pore openings, where the length δ_1 is characteristic of the pore spacing. At this distance the flow may be treated as one-dimensional and thus Pedley's model for the unstirred layer applied, where C_w is the effective membrane concentration. At low porosities (e.g. η=0.01), the axial velocity of this one-dimensional flow would be much lower than the average velocity $\bar{V}_z$ inside the pore (by a factor η). Therefore, it can be expected that tha change beyond δ_1 would be much weaker and on a much longer length scale, say δ_2, than that within δ_1. In fact, as Pedley and Fischbarg (1978) estimated based on the experimental data of Lerche (1976), δ_2 is about 500μm and ΔC_2 in this region is less than two percent of the bulk concentration C_b for most biological membranes. The typical J_v was cited as 2.5×10^{-3} cm/s for an aqueous solution of sucrose (a=5.3Å). In contrast, our results in Table 8 and 9 show that δ_1 is at most tens of Angstroms and ΔC_1 within δ_1 ranges from a few percent to several tens of percent of the total concentration difference ($C_{0^+}-C_{0^-}$) except for the case of a semi-permeable membrane where the concentration beyond the discontinuity interface is almost uniform. A typical average velocity $\bar{V}_z$

is at least of the order of 0.1cm/s (see Fig. 17). Therefore, the concentration gradient $\Delta C_1/\delta_1$ within the entrance /exit region of fine length scale δ_1 may be several orders of magnitude greater than the concentration gradient $\Delta C_2/\delta_2$ in Pedley's unstirred layer of length scale δ_2 for the case of a permeable membrane.

The foregoing discussion and the results in Fig. 19 provide a much clearer picture of the substructure of the unstirred layer described by Dainty, Pedley and others. When the porosity is low the concentration C_w acts as the far field solution C_∞ for the isolated pore in Fig. 1 (a) since the concentration relaxes to this value in both the R and z directions within a few pore-radii. However, if the pores are closely spaced (less than approximately three pore-radii), the far field boundary conditions C_w or C_∞ on the inner length scale δ_1 cannot be applied for an isolated pore, but the interaction between pores must be considered. In this case the concentration in the exit plane of the membrane will not relax to C_w as R increases, and an intermediate layer relating the wall concentration and Pedley's C_m must be considered. For finite non-isotonic bathing solutions ($C_\infty \neq C_{-\infty}$), there would be a solute flow towards the dilute side and consequently C_∞ and $C_{-\infty}$ would change with time. A steady state could not be reached until $C_\infty = C_{-\infty}$. Lerche (1976) claimed that curve 3 (at t=121sec) in his Fig. 4 was a steady state, but curve 5 (at t=576sec) and curve 6 (at t=900sec) in the same figure show an obvious

continuing change. However, at any instant a quasi-steady state solution does exist within the fine scale δ_1 once the instantaneous value of C_w, as shown in Fig. 20, is used for our C_∞ in Fig. 1(a). This means that, corresponding to the two different length scales δ_1 and δ_2, there are also two different time scales for the local changes within δ_1 (fast) and for the long-scale changes within δ_2 (slow). A combined time-dependent analysis of both layers would be interesting.

In summary, our model has quantitatively considered the pore entrance/exit effects on osmosis. For permeable membranes, these effects are important in predicting the osmotic volume flux of the solvent, especially for relatively short pores, small particles and not very dilute solutions. The errors without taking these effects into account range from a few percent to two hundred percent for the calculated cases. The detailed concentration and pressure profiles are given for both permeable and semi-permeable membranes and it has been shown that the scale for these local three-dimensional changes is of the order of a few pore-radii when the interaction between pores does not have to be considered. These fine-scale changes are far more important than the long-scale, one-dimensional changes in Pedley's unstirred layer for the application to permeable membranes with low porosities.

While having shed light on the essential features of the fine structure of osmosis, the present model is greatly

simplified in geometry. A real membrane may have intricate distributions of tortuous pores of various shapes and sizes. The present model applies to dilute solutions only. For non-dilute solutions, the expressions (2) and (8) for the osmotic pressure and the thermodynamic force have to be modified. The hydrodynamic interactions between the solute particles cannot be neglected. Moreover, the solvent velocity $\vec{V}$ can no longer be approximated by that in the absence of particles as is done in this study.

It is hoped that a rigorous three-dimensional theory for the hydrodynamic interactions at the entrance will soon become available so that the approximations for the force and torque correction factors in Section 3 can be improved. Similarly, if a detailed solution for the hydrodynamic interaction of an off-axis positioned sphere in a circular cylindrical tube is developed in the future, the three-dimensional equation (28) for the solute conservation can be solved in the interior of the pore in place of the present one-dimensional version (15).

Table 1 Part of Force and Torque Correction Factors

z/a	F_x^t	F_x^r	F_x^s	T_y^r	$T_y^{t,x}$	$T_y^{s,x}$
1.0000	∞	∞	1.7005	∞	∞	0.9440
1.0032	-4.0223	0.5133	1.6982	-2.6793	0.3849	0.9443
1.0050	-3.7863	0.4558	1.6969	-2.5056	0.3419	0.9444
1.0453	-2.6475	0.1840	1.6682	-1.6996	0.1455	0.9477
1.1276	-2.1514	9.829×10^{-2}	1.6160	-1.3877	7.372×10^{-2}	0.9537
1.5431	-1.5675	1.953×10^{-2}	1.4391	-1.0998	1.456×10^{-2}	0.9742
2.3524	-1.3079	3.523×10^{-3}	1.2780	-1.0250	2.642×10^{-3}	0.9901
3.7622	-1.1738	5.621×10^{-4}	1.1671	-1.0059	4.216×10^{-4}	0.9971
10.0677	-1.0591	1.170×10^{-3}	1.0587	-1.0003	8.774×10^{-6}	0.9981
∞	-1.0000	0	1.0000	-1.0000	0	1.0000

Sources: F_x^t, $T_y^{t,x}$, F_x^r and T_y^r -- Goldman, Cox and Brenner(1967)
F_x^s and $T_y^{s,x}$ -- Cox and Brenner(1967)

Table 2 The Axisymmetric Force Correction Factor F^t_{zo}

z/a \ a/Ro	0.05	0.10	0.25	0.50	0.75	1.00	2.5	5.0	7.5	10.0	20.0	∞
1.0	-1.0241	-1.0503	-1.1388	-1.3688	-1.7878	-2.3805	-7.95	-21.1	-32.0	-43.8	-92	∞
1.1	-1.0242	-1.0503	-1.1412	-1.3777	-1.7666	-2.2867	-5.89	-8.94	-9.99	-10.5	-10.8	-11.4592
1.25	-1.0242	-1.0503	-1.1419	-1.3819	-1.7497	-2.1807	-4.0355	-4.9183	-5.1532	-5.2340	-5.25	-5.3053
1.5	-1.0243	-1.0504	-1.1433	-1.3882	-1.7164	-2.0334	-2.9207	-3.1535	-3.1889	-3.1983	-3.20	-3.2054
2.0	-1.0248	-1.0505	-1.1475	-1.3919	-1.6348	-1.8058	-2.0857	-2.1200	-2.1239	-2.1248	-2.125	-2.1255
3.0	-1.0254	-1.0510	-1.1579	-1.3581	-1.4679	-1.5168	-1.5649	-1.5687	-1.5690	-1.5691	-1.5691	-1.5692
4.0	-1.0262	-1.0519	-1.1637	-1.3091	-1.3491	-1.3655	-1.3791	-1.3801	-1.3802	-1.3802	-1.3802	-1.3802
5.0	-1.0266	-1.0532	-1.1617	-1.2509	-1.2728	-1.2795	-1.2841	-1.2850	-1.2851	-1.2851	-1.2851	-1.2851
6.0	-1.0271	-1.0549	-1.1541	-1.2110	-1.2222	-1.2254	-1.2277	-1.2279	-1.2279	-1.2279	-1.2279	-1.2279
8.0	-1.0278	-1.0579	-1.1328	-1.1571	-1.1608	-1.1617	-1.1624	-1.1625	-1.1625	-1.1625	-1.1625	-1.1625
10.0	-1.0283	-1.0596	-1.1125	-1.1240	-1.1255	-1.1262	-1.1262	-1.1262	-1.1262	-1.1262	-1.1262	-1.1262
20.0	-1.0319	-1.0507	-1.0587	-1.0595	-1.0595	-1.0595	-1.0595	-1.0595	-1.0595	-1.0595	-1.0595	-1.0595
30.0	-1.0290	-1.0368	-1.0388	-1.0389	-1.0389	-1.0389	-1.0389	-1.0389	-1.0389	-1.0389	-1.0389	-1.0389
100.0	-1.0112	-1.0114	-1.0114	-1.0114	-1.0114	-1.0114	-1.0114	-1.0114	-1.0114	-1.0114	-1.0114	-1.0114
∞	-1.0000	-1.0000	-1.0000	-1.0000	-1.0000	-1.0000	-1.0000	-1.0000	-1.0000	-1.0000	-1.0000	-1.0000

Sources: $a/R_o = \infty$ -- Brenner(1961)

$a/R_o = 0.05$ or 20.0
$z/a = 1.0, 20.0, 30.0$ or 100.0
} Calculated by the author of this thesis

All the others -- Dagan, Weinbaum and Pfeffer(1982b)

Table 3 The Axisymmetric Force Correction Factor F^s_{zo}

z/a \ a/R₀	0.05	0.10	0.25	0.50	0.75	1.00	2.5	5.0	7.5	10.0	20.0
1.0	1.0024	1.0432	1.0941	1.1646	1.2402	1.3566	2.18	5.38	11.0	18.9	72
1.1	1.0225	1.0435	1.0963	1.1797	1.2841	1.4148	2.53	5.97	11.6	18.2	65.5
1.25	1.0225	1.0435	1.0975	1.1912	1.3155	1.4743	3.04	6.37	8.33	9.21	9.59
1.5	1.0226	1.0436	1.1001	1.2121	1.3696	1.5704	2.9635	3.91	4.12	4.18	4.23
2.0	1.0230	1.0437	1.1067	1.2544	1.4463	1.6377	2.1531	2.2514	2.2641	2.2675	2.27
3.0	1.0237	1.0445	1.1234	1.2922	1.4137	1.4785	1.5526	1.5589	1.5596	1.5598	1.56
4.0	1.0245	1.0457	1.1371	1.2693	1.3232	1.3435	1.3612	1.3623	1.3625	1.3625	1.363
5.0	1.0251	1.0475	1.1423	1.2315	1.2558	1.2635	1.2695	1.2698	1.2698	1.2699	1.270
6.0	1.0257	1.0495	1.1400	1.1976	1.2096	1.2130	1.2156	1.2157	1.2157	1.2157	1.2157
8.0	1.0264	1.0534	1.1247	1.1492	1.1529	1.1539	1.1546	1.1546	1.1546	1.1546	1.1546
10.0	1.0269	1.0559	1.1072	1.1187	1.1202	1.1205	1.1208	1.1208	1.1208	1.1208	1.1208
20.0	1.0310	1.0495	1.0575	1.0580	1.0580	1.0580	1.0580	1.0580	1.0580	1.0580	1.0580
30.0	1.0285	1.0361	1.0381	1.0382	1.0382	1.0382	1.0382	1.0382	1.0382	1.0382	1.0382
100.0	1.0112	1.0113	1.0114	1.0114	1.0114	1.0114	1.0114	1.0114	1.0114	1.0114	1.0114
∞	1.0000	1.0000	1.0000	1.0000	1.0000	1.0000	1.0000	1.0000	1.0000	1.0000	1.0000

Sources: Conversion is made between the different definitions:

$$F^s_{zo} = \left[1 + (z/a)^2 \right] F^s_z ,$$

where the values of F^s_z are taken from Dagan, Weinbaum and Pfeffer(1982b), except that the values for $z/a = 1.0$, 20.0, 30.0 or 100.0 or for $a/R_o = 0.05$ or 20.0 are calculated by the author of this thesis.

Table 4 The Force Correction Factor F_{zc}^{t}

a/R_c / z/a	0.0	0.10	0.25	0.5	0.75	1.0	2.5	5.0	7.5	10.0
1.0	∞	∞	∞	∞	∞	∞	∞	∞	∞	∞
1.1	-11.4592	-11.4593	-11.464	-11.559	-11.768	-11.784	-7.09	-3.04	-1.96	-1.56
1.25	-5.3053	-5.3054	-5.3123	-5.4051	-5.5172	-5.3773	-2.8182	-1.5704	-1.2854	-1.1790
1.5	-3.2054	-3.2055	-3.2147	-3.2952	-3.2954	-3.0812	-1.7048	-1.2643	-1.1513	-1.1046
2.0	-2.1255	-2.1258	-2.1397	-2.1798	-2.0776	-1.8936	-1.3152	-1.1354	-1.0851	-1.0620
3.0	-1.5692	-1.5700	-1.5878	-1.5543	-1.4392	-1.3417	-1.1292	-1.0613	-1.0401	-1.0297
4.0	-1.3802	-1.3818	-1.3953	-1.3272	-1.2417	-1.1848	-1.0719	-1.0350	-1.0231	-1.0172
5.0	-1.2851	-1.2877	-1.2916	-1.2154	-1.1536	-1.1166	-1.0459	-1.0226	-1.0150	-1.0112
6.0	-1.2279	-1.2314	-1.2247	-1.1521	-1.1064	-1.0805	-1.0318	-1.0158	-1.0105	-1.0078
8.0	-1.1625	-1.1672	-1.1440	-1.0872	-1.0579	-1.0450	-1.0179	-1.0089	-1.0059	-1.0044
10.0	-1.1262	-1.1305	-1.0989	-1.0563	-1.0382	-1.0287	-1.0115	-1.0057	-1.0038	-1.0028
∞	-1.0000	-1.0000	-1.0000	-1.0000	-1.0000	-1.0000	-1.0000	-1.0000	-1.0000	-1.0000

Sources: $a/R_c = 0.0$ -- Brenner(1961)

All the others -- Dagan, Pfeffer and Weinbaum(1982)

Here R_c is the radius of the disk.

Table 5 The Force Correction Factor F^S_{zc}

z/a \ a/R_c	0.10	0.25	0.50	0.75	1.00	2.5	5.0	7.5	10.0
1.0	3.79	3.89	3.94	4.22	3.96	1.95	1.36	1.21	1.14
1.1	3.4562	3.5151	3.7436	3.7602	3.4298	1.7960	1.3188	1.1922	1.1301
1.25	3.0265	3.0740	3.5181	3.1587	2.8508	1.6342	1.2755	1.1674	1.1240
1.5	2.5511	2.5860	2.6614	2.5251	2.2719	1.4735	1.2141	1.1372	1.1008
2.0	2.0315	2.0516	2.0418	1.8885	1.7207	1.2845	1.1344	1.0874	1.0467
3.0	1.5942	1.6020	1.5324	1.4168	1.3276	1.1305	1.0634	1.0417	1.0310
4.0	1.4080	1.4071	1.3239	1.2400	1.1850	1.0736	1.0361	1.0239	1.0178
5.0	1.3077	1.2986	1.2162	1.1549	1.1182	1.0470	1.0232	1.0154	1.0108
6.0	1.2461	1.2292	1.1537	1.1078	1.0818	1.0325	1.0161	1.0107	1.0080
8.0	1.1751	1.1463	1.0884	1.0606	1.0457	1.0182	1.0091	1.0060	1.0045
10.0	1.1350	1.1003	1.0570	1.0387	1.0291	1.0116	1.0058	1.0039	1.0029
∞	1.0000	1.0000	1.0000	1.0000	1.0000	1.0000	1.0000	1.0000	1.0000

Sources: Conversion is made between the different definitions:

$$F^S_{zc} = \frac{\frac{1}{2}\pi F^S_z}{\tan^{-1}(z/R_c) - \frac{z/R_c}{1 + (z/R_c)^2}},$$

where the values of F^S_z are taken from Dagan, Pfeffer and Weinbaum(1982), except that the data for z/a = 1.0 are extropolated by the author of this thesis.

Table 6 The Hydrodynamic Data inside the Pore

a/R_0	p^t_{zo}	p^s_{zo}
0.0	-1.0000	1.0000
0.01	-1.0215	1.0147
0.1	-1.263	1.255
0.2	-1.680	1.636
0.3	-2.373	2.231
0.4	-3.599	3.223
0.5	-5.973	5.017
0.6	-11.20	8.696
0.7	-25.29	17.19
0.8	-31.4	20.0
0.9	-48.7	27.6

Sources: a/R_0=0.0--0.01 -- Happel & Brenner(1973, p.318)

a/R_0=0.1--0.7 -- Leichtberg, Pfeffer & Weinbaum(1976)

a/R_0=0.8--0.9 -- Wu & Skalak(1984)

Table 7 The Hydraulic Permeability L_p

$\tilde{l}$	$\frac{L_p \mu}{\eta R_0}$	$\frac{(L_p)_0 \mu}{\eta R_0}$	$(L_p)_0/L_p$
5	0.020233	0.025000	1.236
50	0.002442	0.002500	1.024
500	0.000249	0.000250	1.002

Table 8 Results for $\phi = 0.05$

$\hat{\ell}$	$\tilde{a}$	σ_o	N_q	total volume flux			diffusional permeability			concentration	
				$\tilde{q}$	$\tilde{q}_o$	$\tilde{q}_o/\tilde{q}$	$\omega\bar{V}_s/L_p$	$\omega\bar{V}_s/L_{po}$	ω_s/ω	$\tilde{c}_o$	$\tilde{c}_\ell$
	0.01	0.0264	716.2	4.807×10^{-1}	1.485	3.089	0.000083	0.000171	1.658	0.408	0.013
	0.1	0.1951	7.162	7.022×10^{-1}	1.097×10^{-1}	1.563	0.010843	0.011401	0.851	0.838	0.069
5	0.5	0.7862	0.286	1.365×10^{-1}	1.766×10^{-1}	1.294	0.020151	0.018602	0.747	0.924	0.047
	0.9	0.9943	0.088	5.426×10^{-2}	6.872×10^{-2}	1.267	0.000305	0.000296	0.783	0.886	0.051
	1.5	1.0000	0.032	2.034×10^{-2}	2.513×10^{-2}	1.236	0.000000	0.000000	---	0.000	0.000
	0.01	0.0264	716.2	1.184×10^{-1}	1.485×10^{-1}	1.254	0.000142	0.000171	1.173	0.814	0.000
	0.1	0.1951	7.162	1.043×10^{-1}	1.097×10^{-1}	1.052	0.011318	0.011401	0.983	0.978	0.008
50	0.5	0.7862	0.286	1.719×10^{-1}	1.766×10^{-1}	1.027	0.018774	0.018602	0.968	0.991	0.001
	0.9	0.9943	0.088	6.723×10^{-2}	6.892×10^{-2}	1.025	0.000297	0.000296	0.974	0.986	0.005
	1.5	1.0000	0.032	2.455×10^{-2}	2.513×10^{-2}	1.024	0.000000	0.000000	---	0.000	0.000

Table 9 Results for $C_\infty = 1.2690\times10^{-3}$ mole/cm^3 and $R_0 = 5$Å

$\tilde{\ell}$	$\tilde{a}$	σ_0	ϕ	N_q	total volume flux			diffusional permeability			concentration	
					$\tilde{q}$	$\tilde{q}_0$	$\tilde{q}_0/\tilde{q}$	$\omega\bar{V}_s/L_p$	$\omega_0\bar{V}_s/L_{po}$	ω_0/ω	$\tilde{C}_0$	$\tilde{C}_\ell$
5	0.01	0.0264	4×10^{-7}	0.006	7.191×10^{-6}	1.244×10^{-5}	1.730	0.000157	0.000171	1.000	0.872	0.128
	0.1	0.1951	4×10^{-4}	0.057	5.905×10^{-4}	8.734×10^{-4}	1.479	0.011430	0.011401	0.807	0.905	0.094
	0.3	0.5394	0.0108	0.172	5.409×10^{-3}	7.287×10^{-3}	1.347	0.035407	0.033038	0.755	0.930	0.063
	0.5	0.7862	0.0500	0.286	1.365×10^{-2}	1.766×10^{-2}	1.294	0.020151	0.018602	0.747	0.924	0.047
50	0.01	0.0264	4×10^{-7}	0.006	1.124×10^{-6}	1.244×10^{-6}	1.107	0.002442	0.002500	1.000	0.983	0.017
	0.1	0.1951	4×10^{-4}	0.057	8.405×10^{-5}	8.734×10^{-5}	1.039	0.011406	0.011401	0.976	0.989	0.011
	0.3	0.5394	0.0108	0.172	7.047×10^{-4}	7.287×10^{-4}	1.034	0.033308	0.033038	0.969	0.992	0.007
	0.5	0.7862	0.0500	0.286	1.719×10^{-3}	1.766×10^{-3}	1.027	0.018774	0.018602	0.968	0.991	0.001

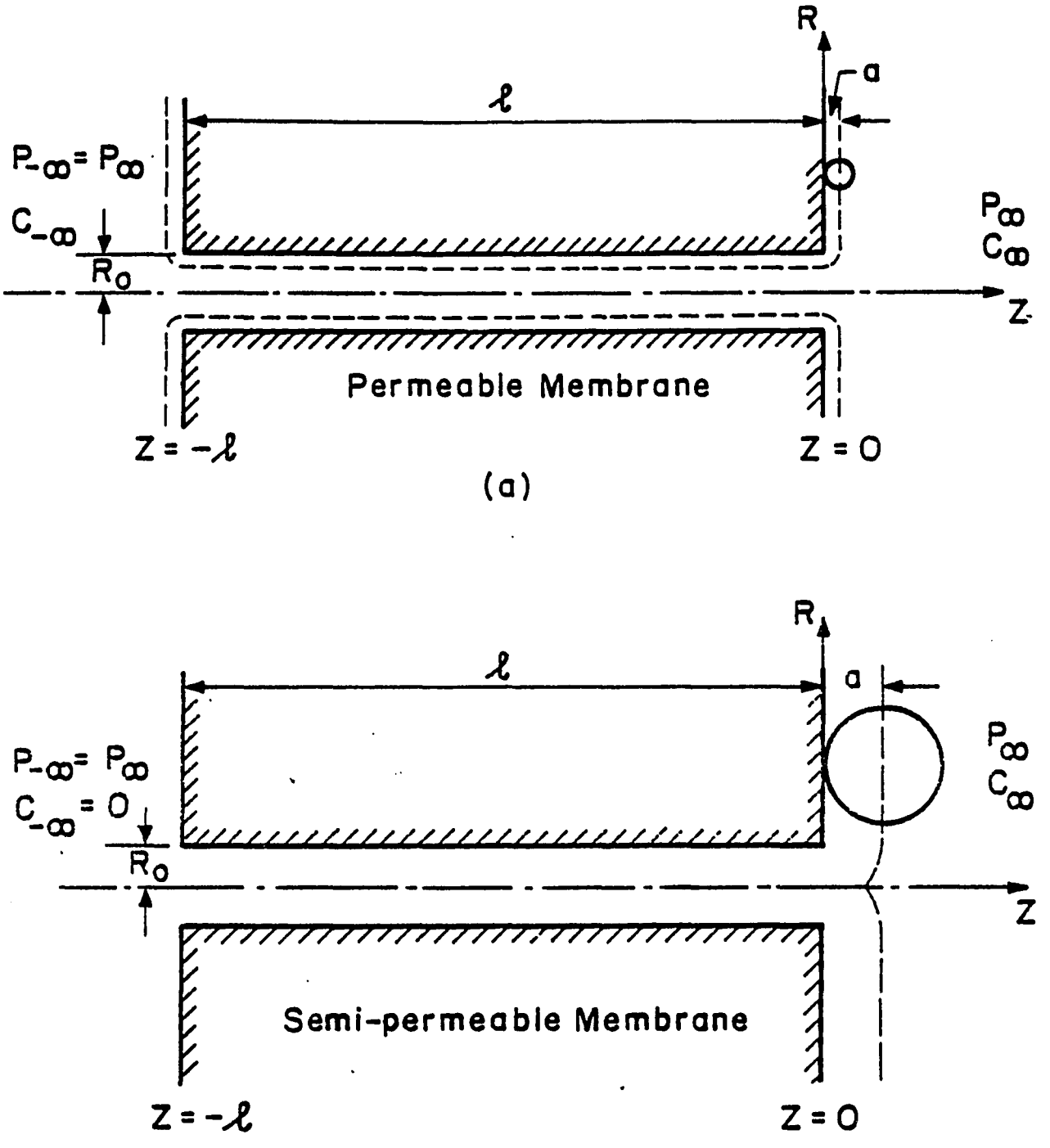

Fig. 1 Our models for the fine structure of osmosis

(a) the permeable membrane

(b) the semi-permeable membrane

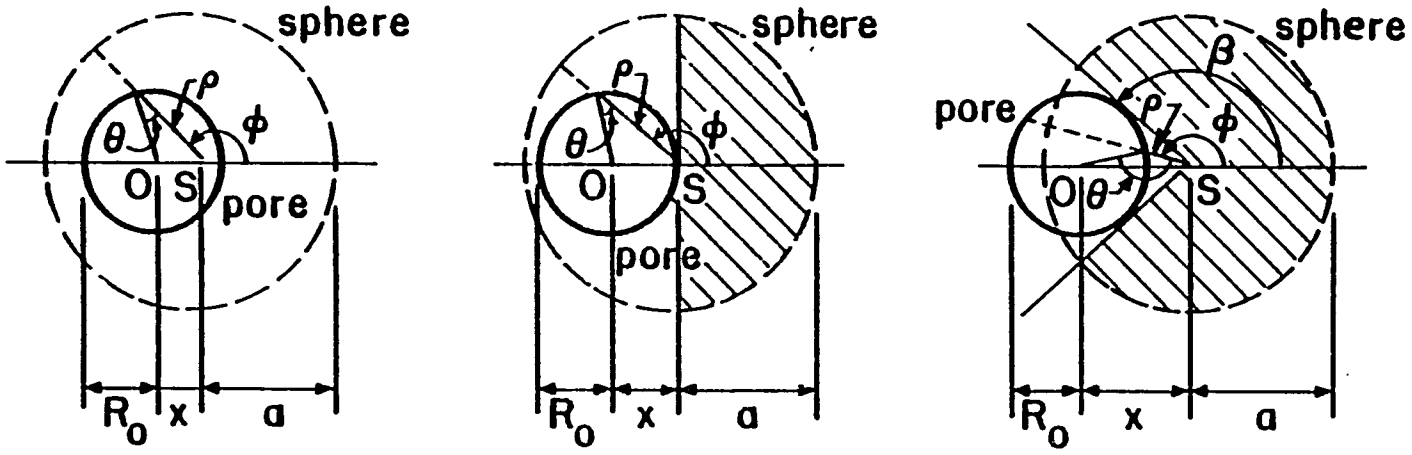

Case 1 ($0 \leq x < R_0$) Case 2 ($x = R_0$) Case 3 ($x > R_0$)

Fig. 2 Three cases for the calculations of F_z^t and F_z^s

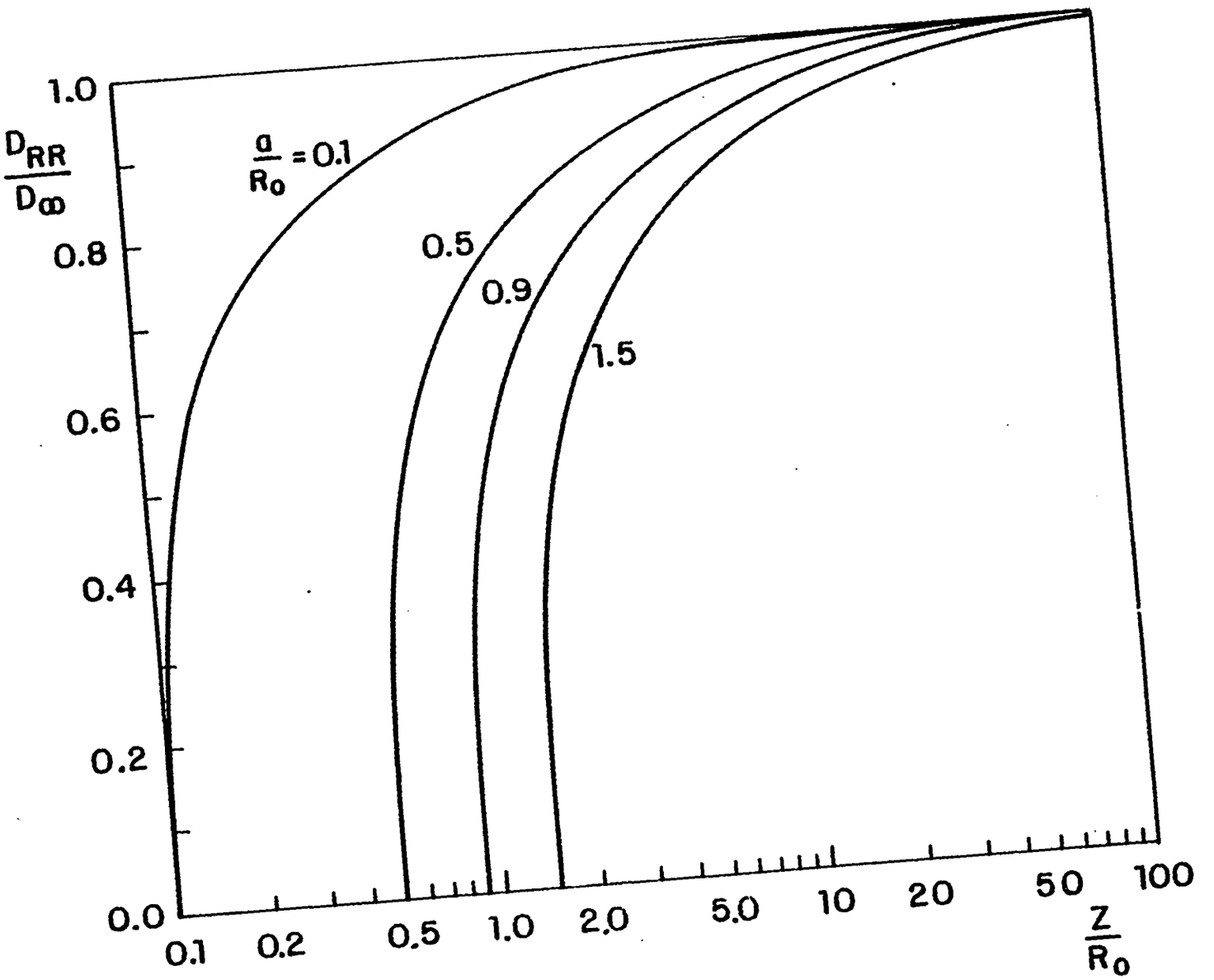

Fig. 3 The diffusivity D_{RR}

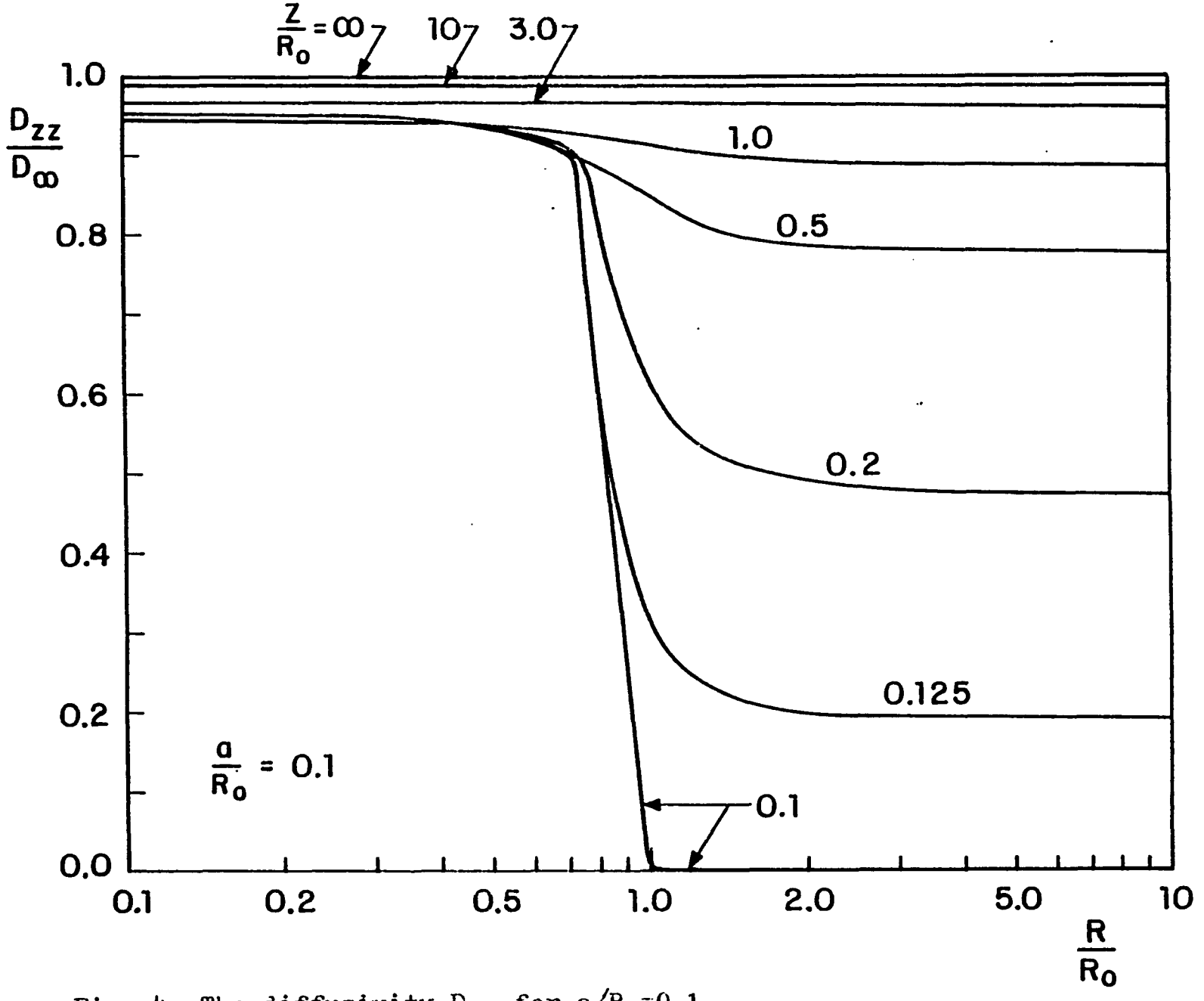

Fig. 4 The diffusivity D_{zz} for $a/R_0=0.1$

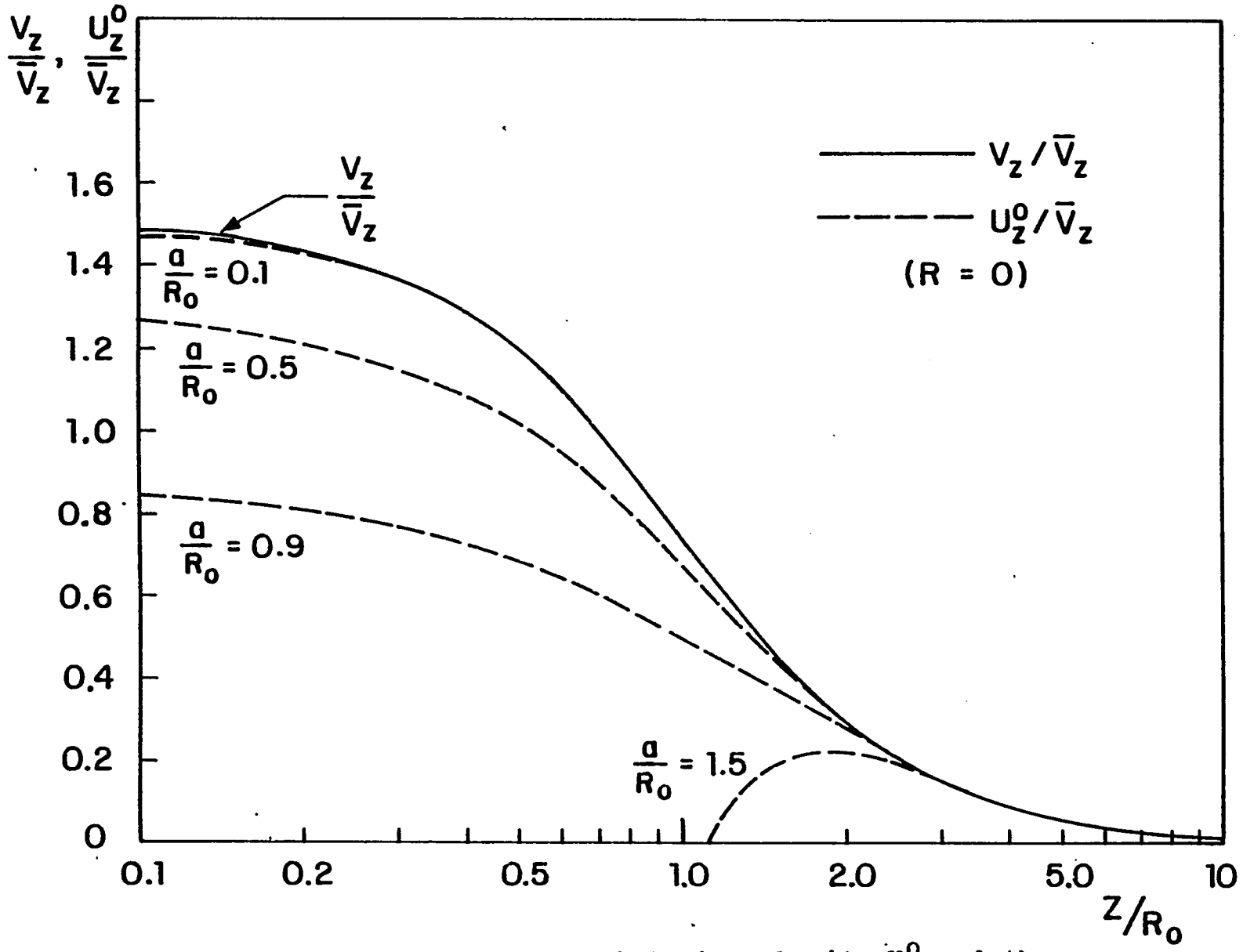

Fig. 5 The particle's deterministic velocity U_z^0 and the solvent velocity V_z along the centerline

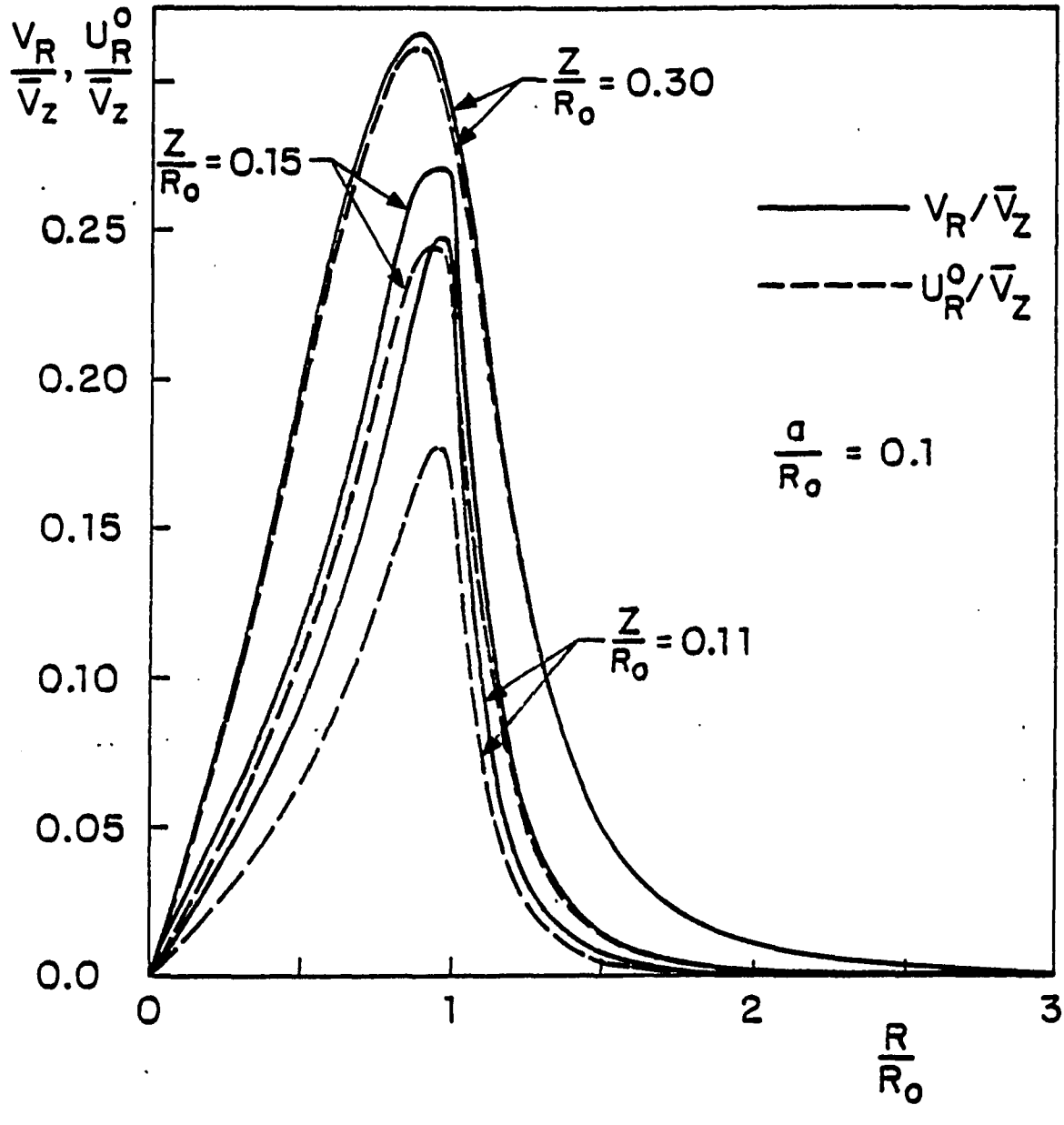

Fig. 6 The particle's deterministic velocity U_R^o and the solvent velocity V_R for $a/R_o=0.1$

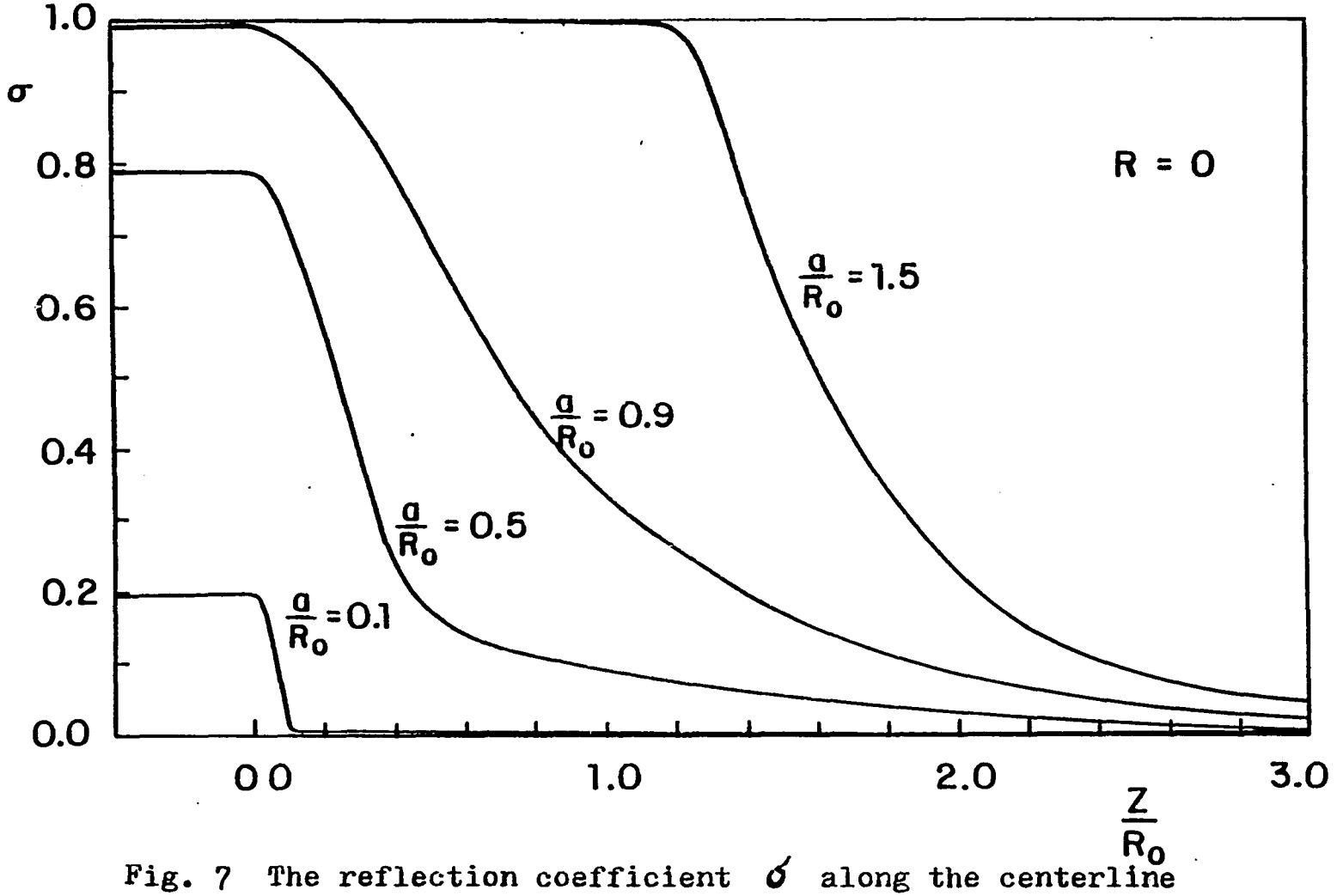

Fig. 7 The reflection coefficient σ along the centerline

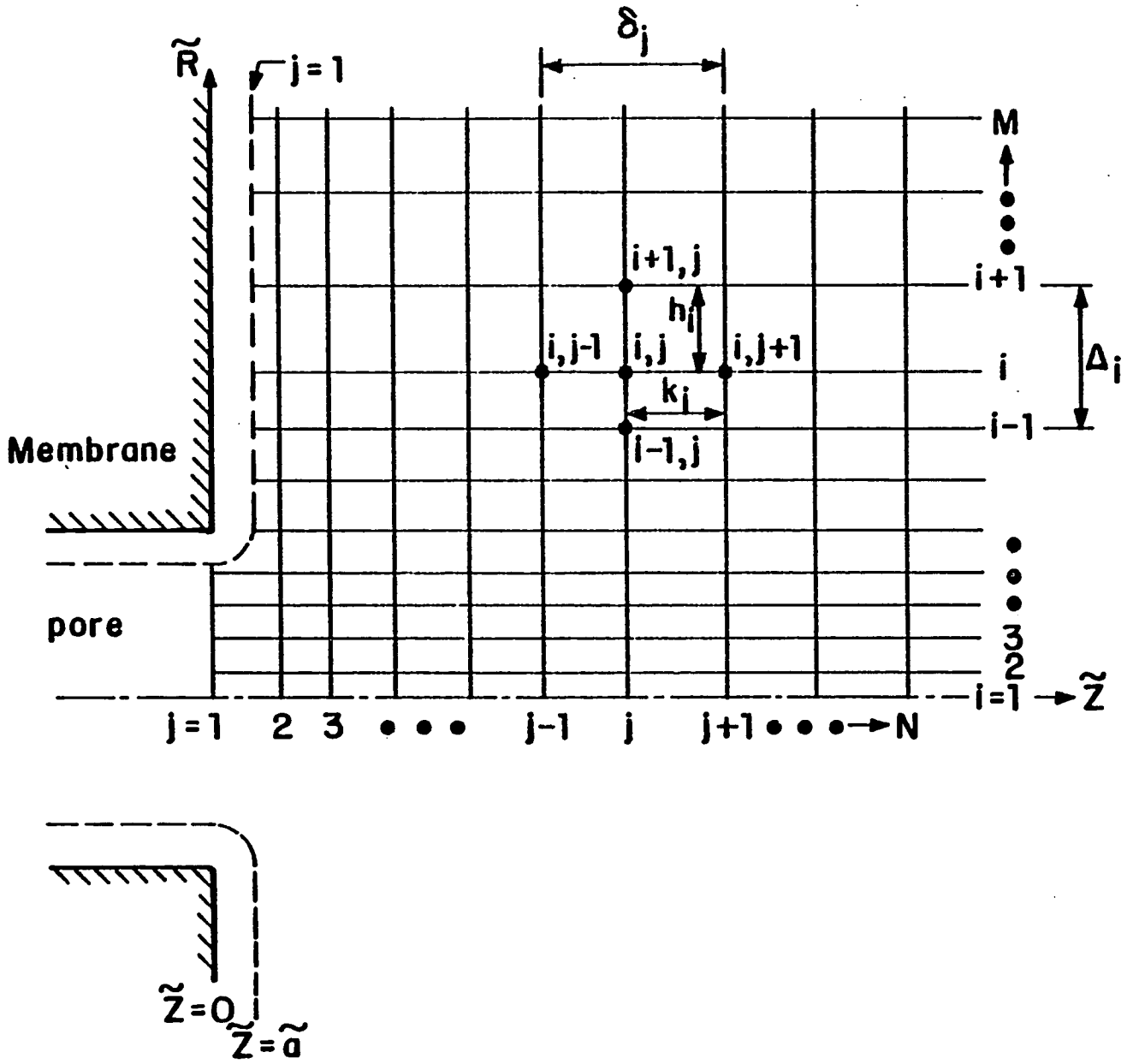

Fig. 8 The grid system for solving Eq. (75)

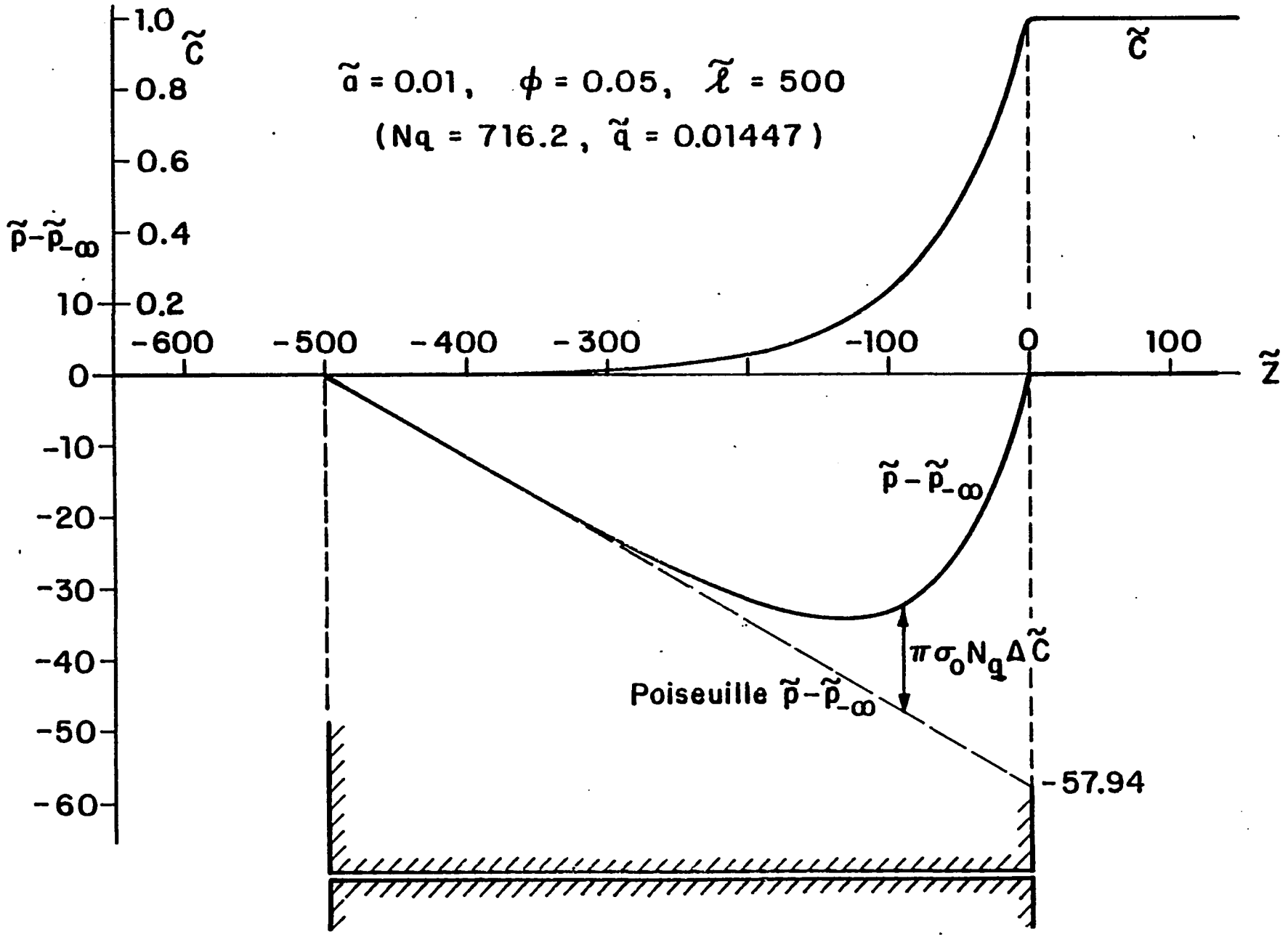

Fig. 9 The concentration and pressure profiles for $\tilde{a}$=0.01, ϕ=0.05 and $\tilde{\ell}$=500

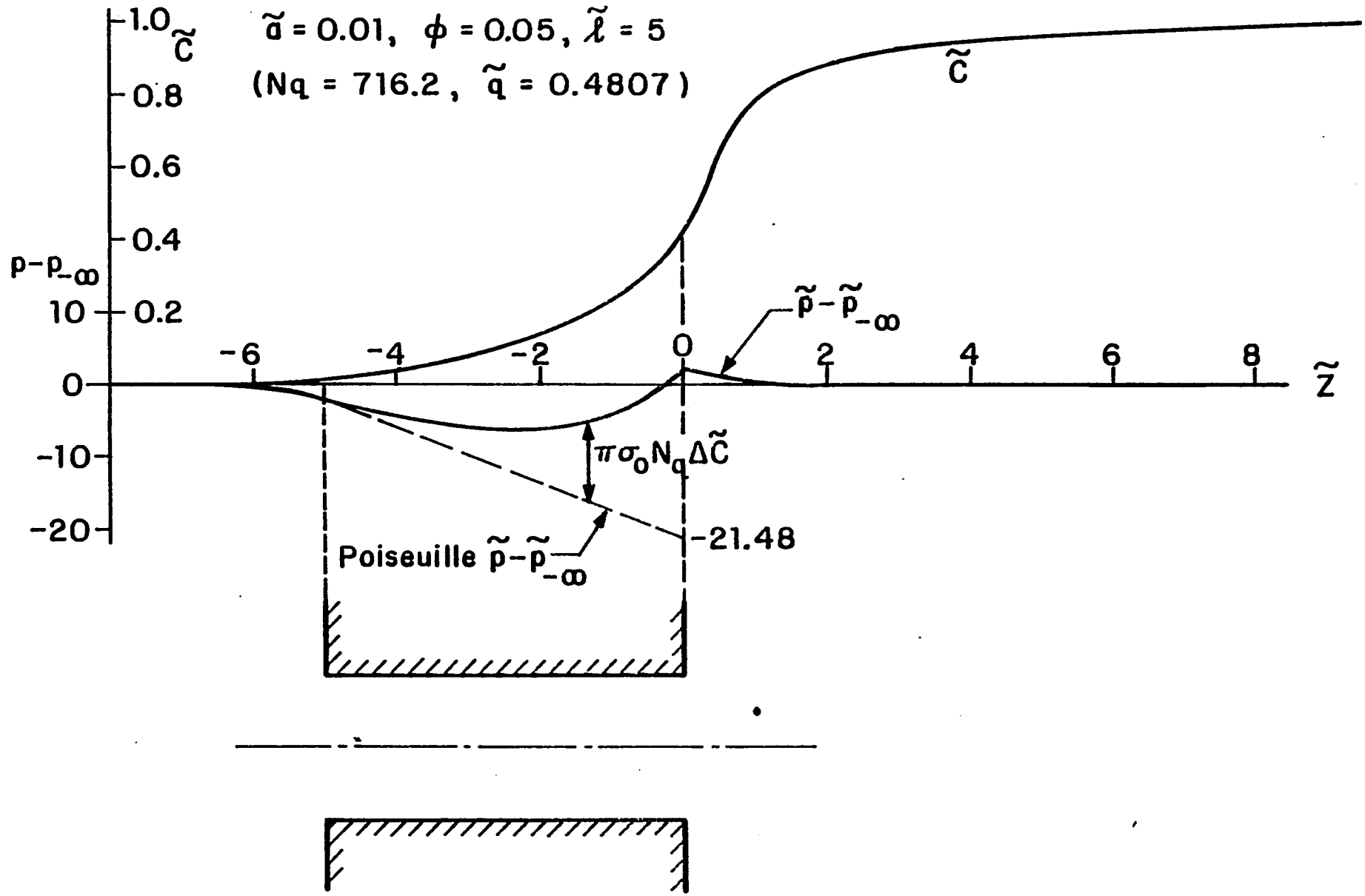

Fig. 10 The concentration and pressure profiles for $\tilde{a}$=0.01, ϕ=0.05 and $\tilde{\ell}$=5

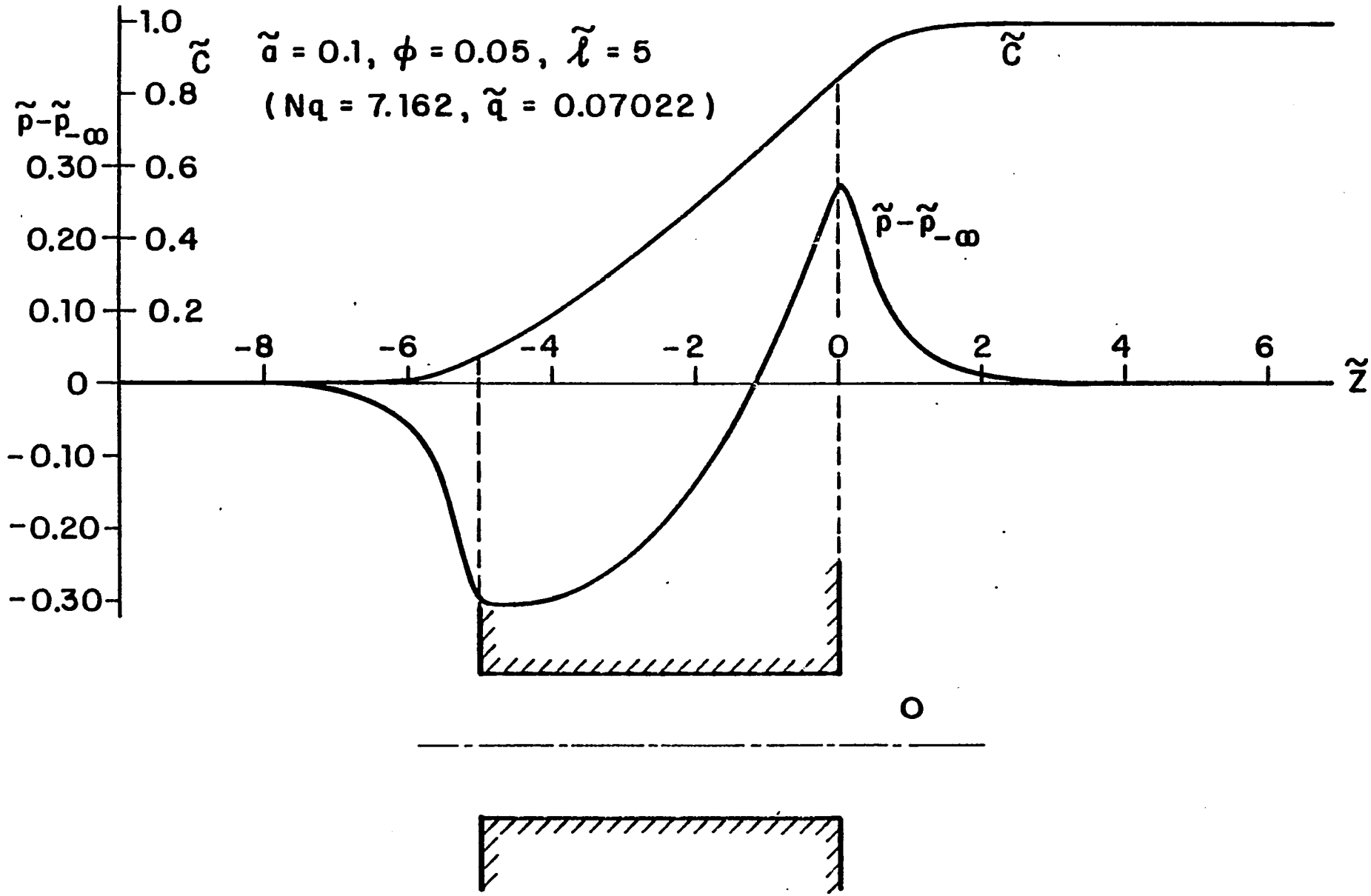

Fig. 11 The concentration and pressure profiles for $\tilde{a}$=0.1, ϕ=0.05 and $\tilde{\ell}$=5

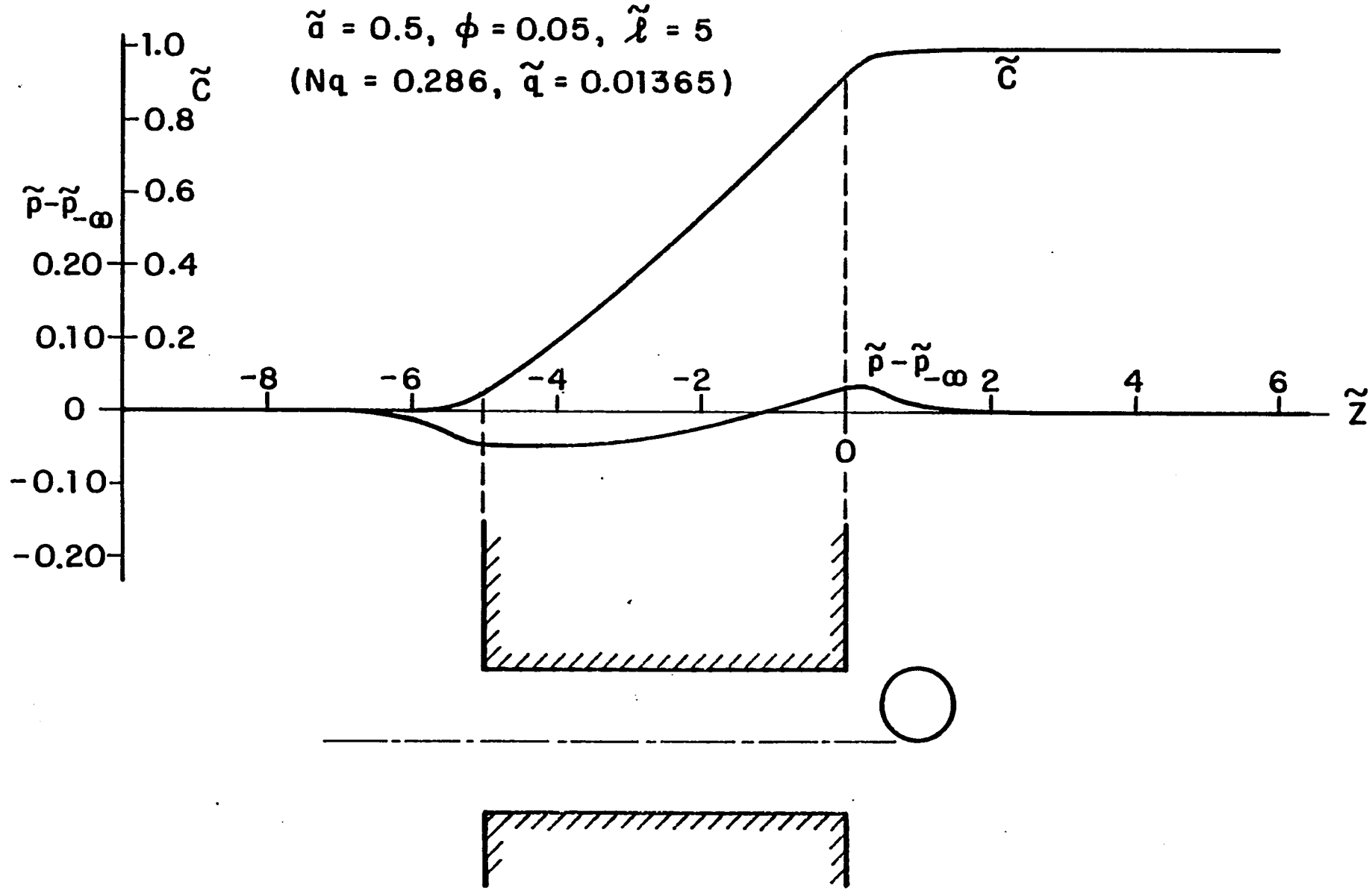

Fig. 12 The concentration and pressure profiles for $\tilde{a}$=0.5, ϕ=0.05 and $\tilde{\ell}$=5

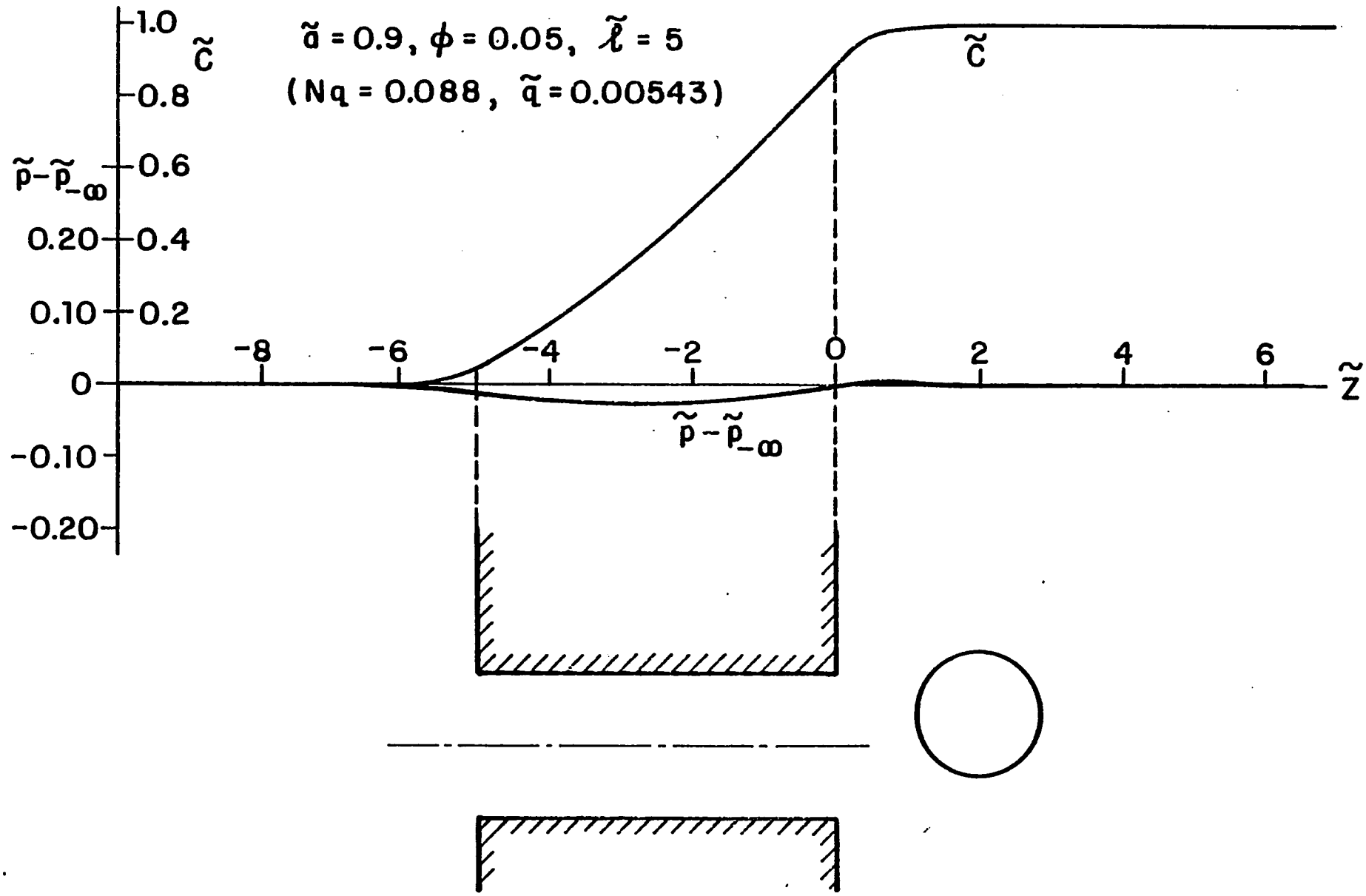

Fig. 13 The concentration and pressure profiles for $\tilde{a}$=0.9, ϕ=0.05 and $\tilde{\ell}$=5

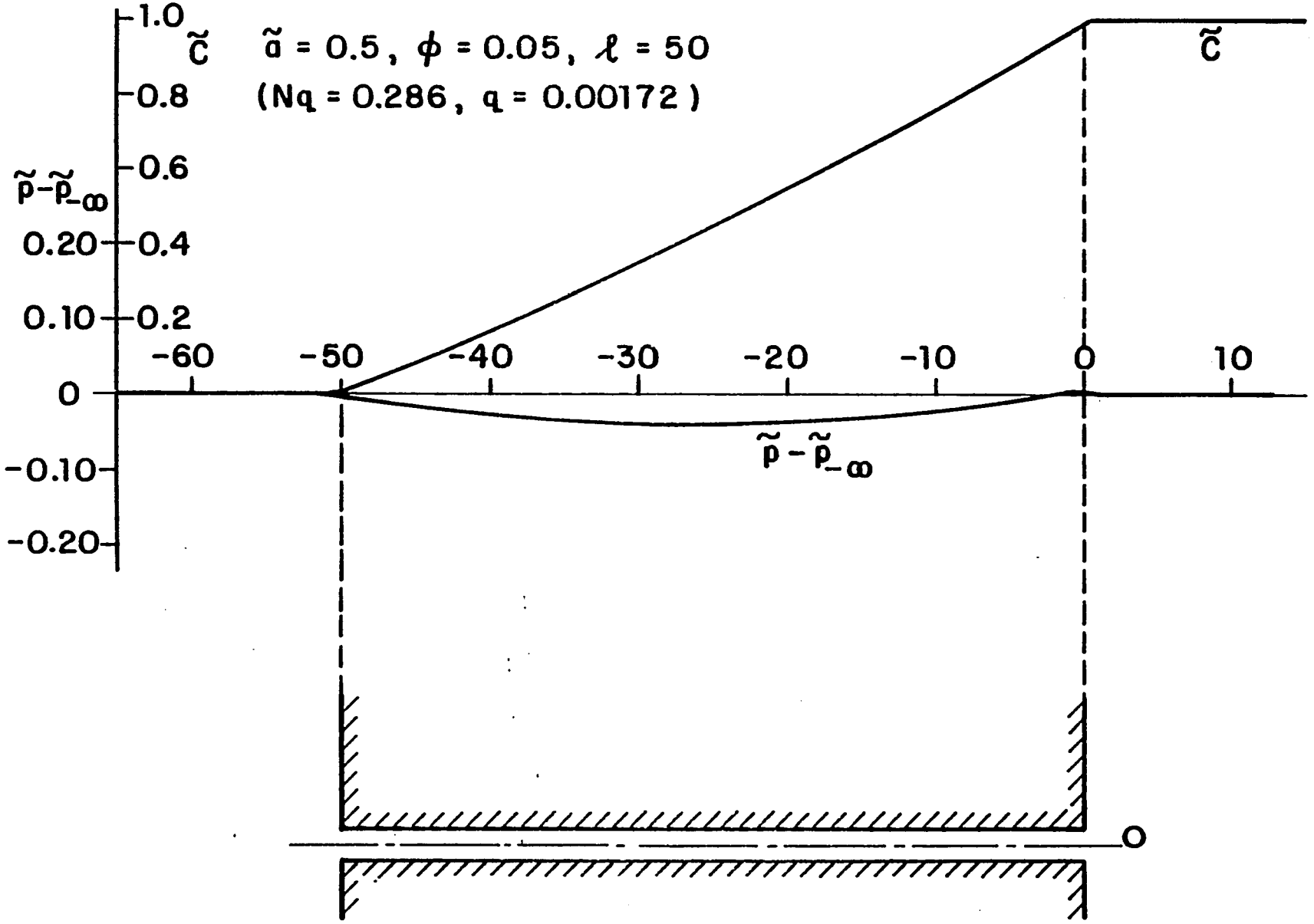

Fig. 14 The concentration and pressure profiles for $\tilde{a}$=0.5, ϕ=0.05 and $\tilde{\ell}$=50

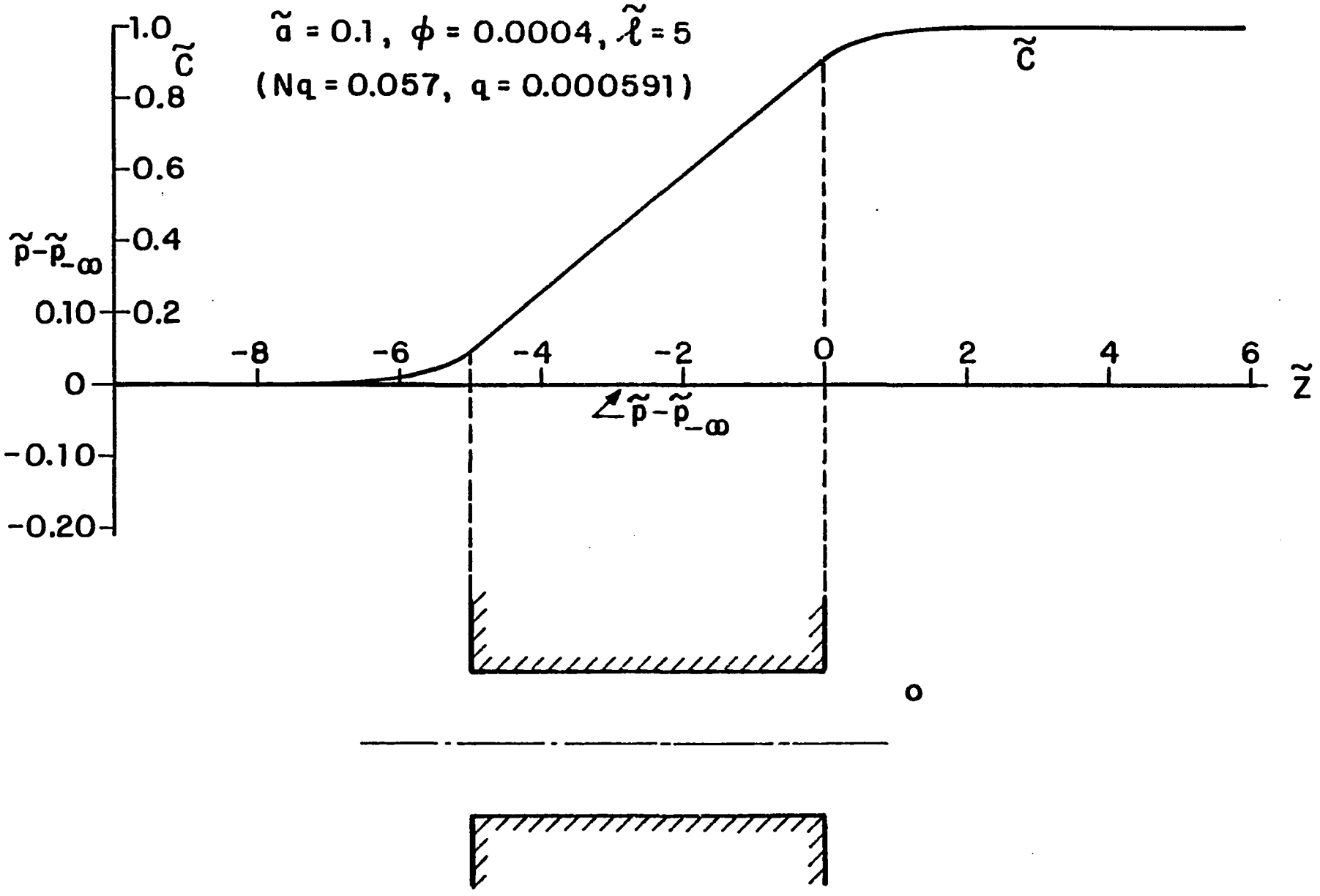

Fig. 15 The concentration and pressure profiles for $\tilde{a}$=0.1, ϕ=0.0004 and $\tilde{\ell}$=5

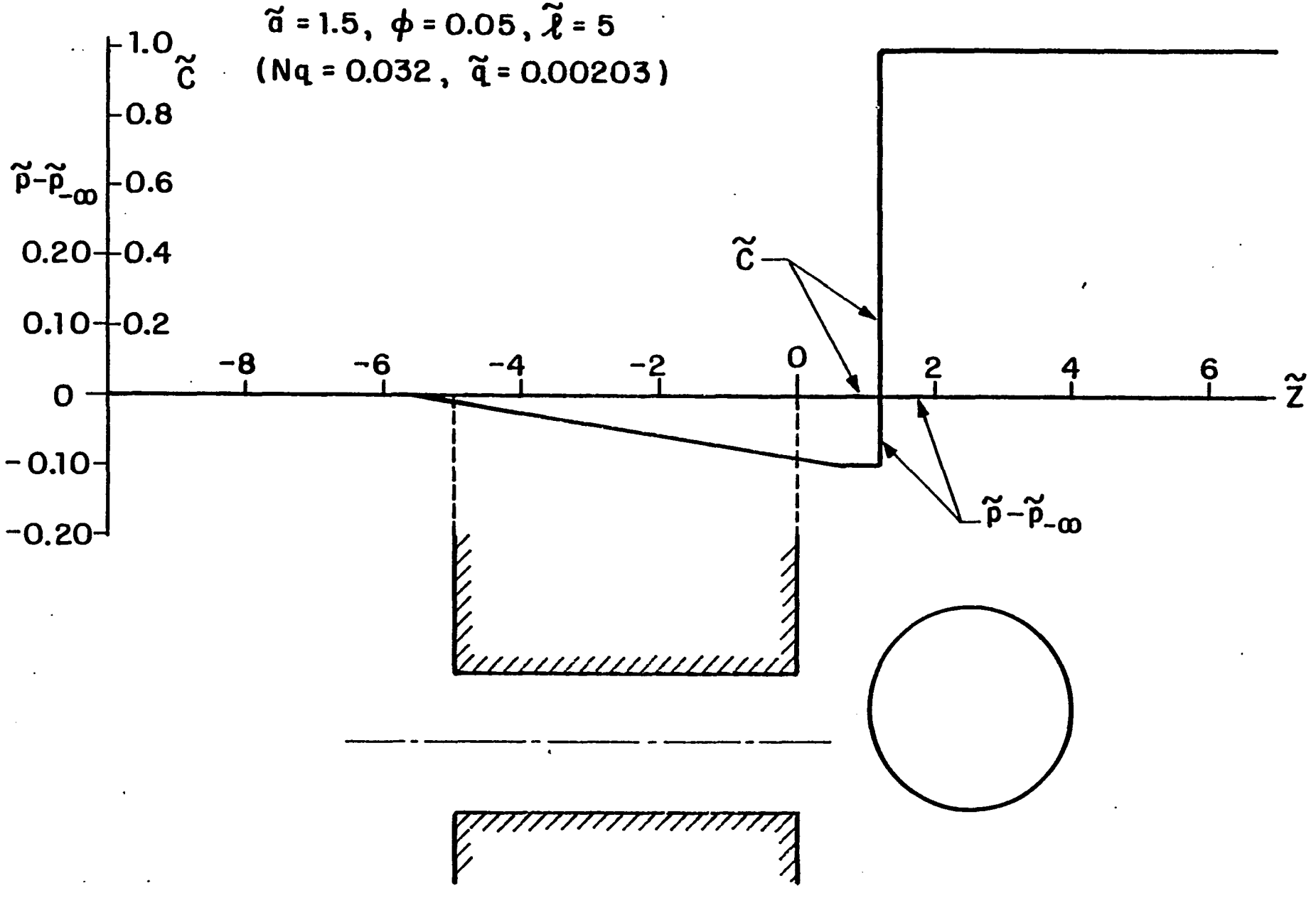

Fig. 16 The concentration and pressure profiles for $\tilde{a}$=1.5, ϕ=0.05 and $\tilde{\ell}$=5

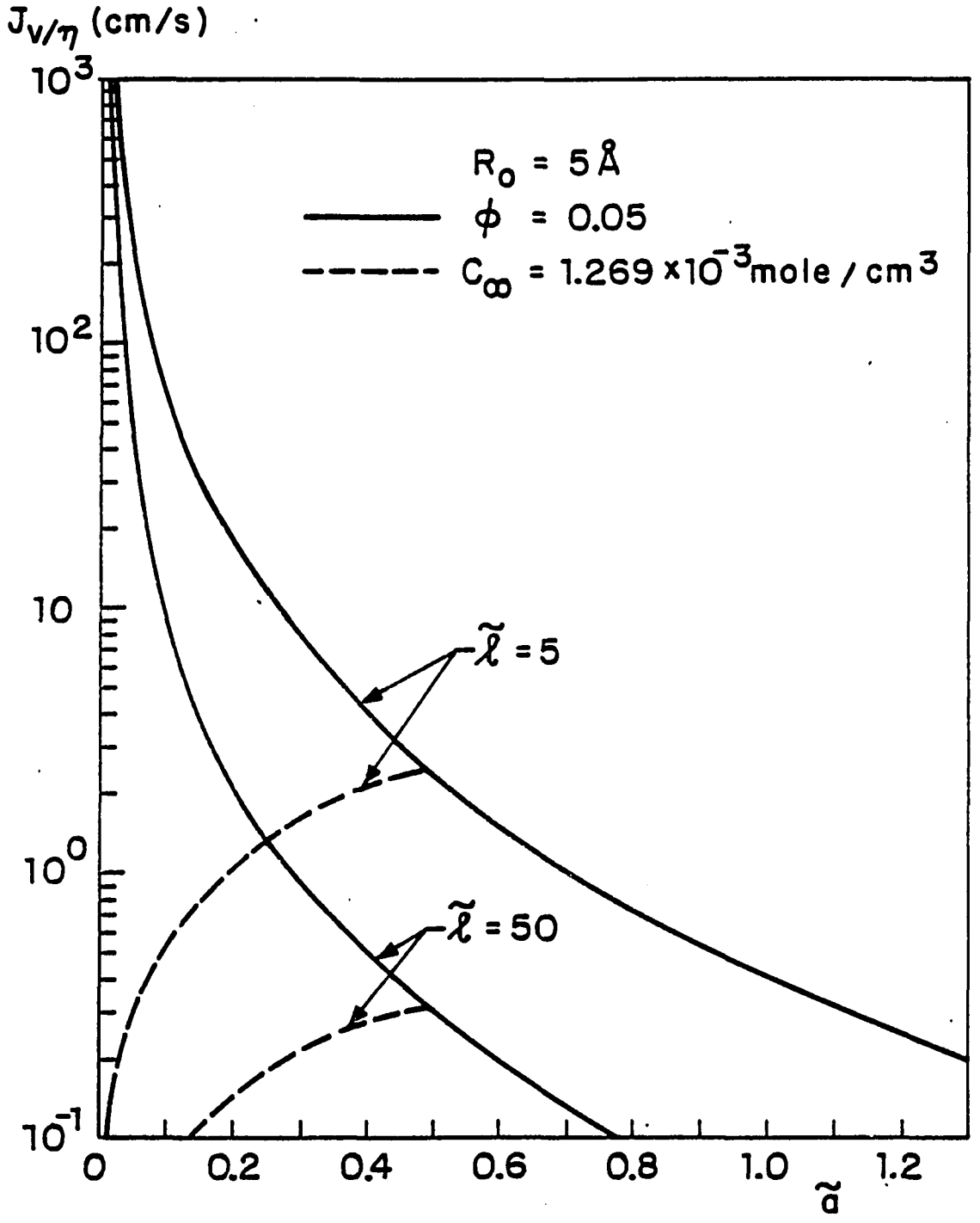

Fig. 17 The total volume flux J_v for R_o=5Å

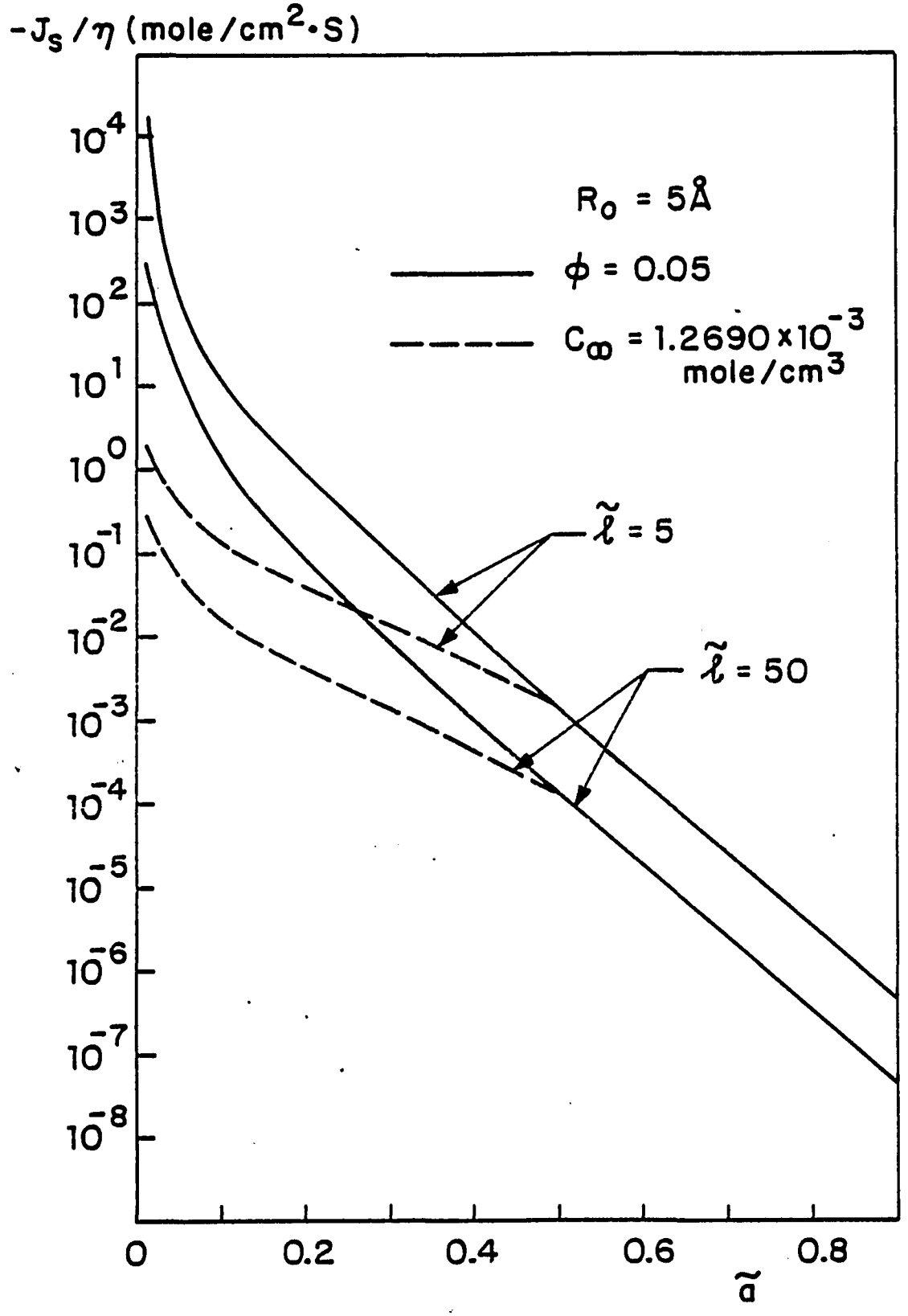

Fig. 18 The solute flow rate J_s for R_0=5Å

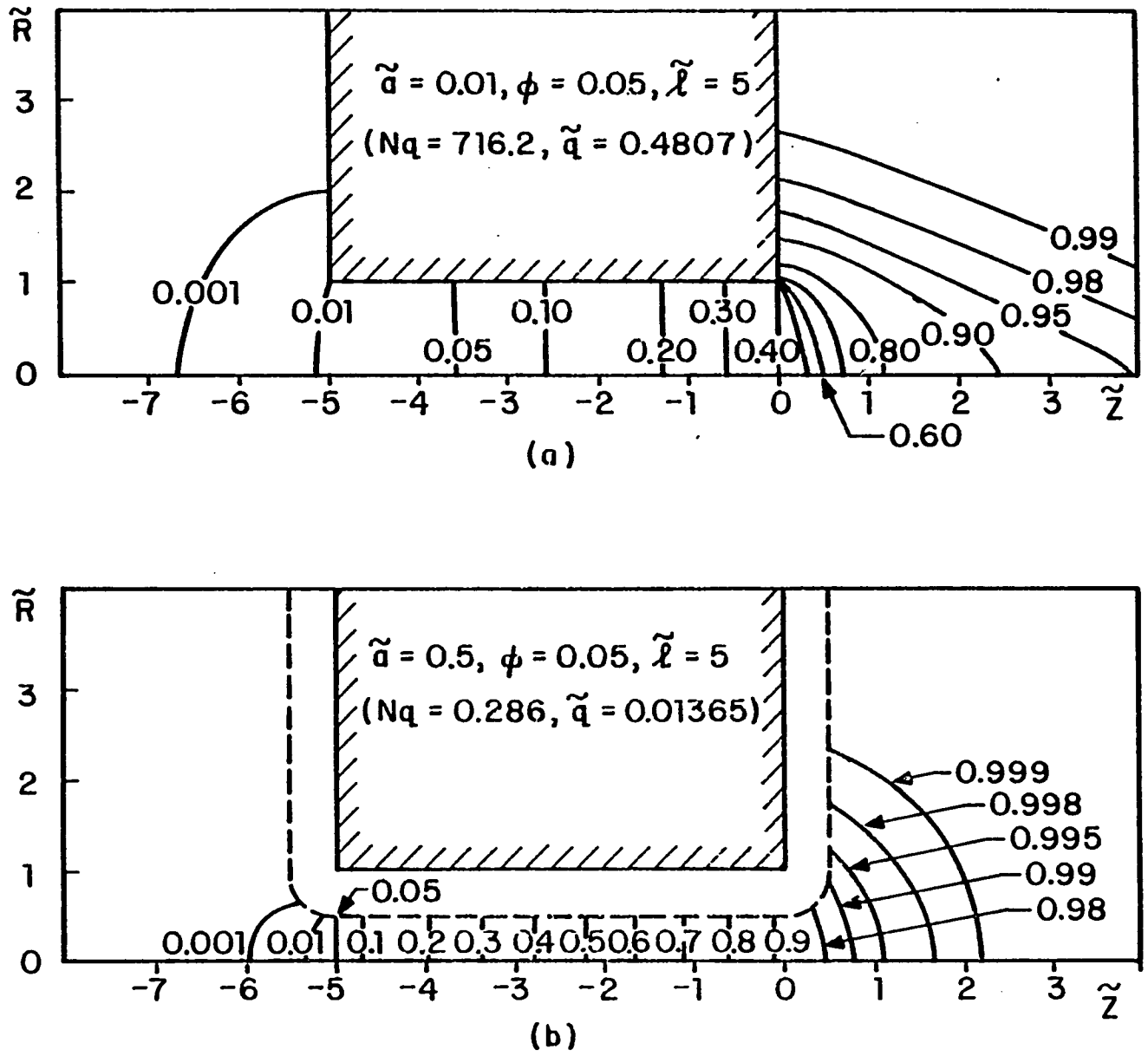

Fig. 19 The curves of equal concentration for (a) $\tilde{a}$=0.01, ϕ =0.05 and $\tilde{\ell}$=5
(b) $\tilde{a}$=0.5, ϕ =0.05 and $\tilde{\ell}$=5

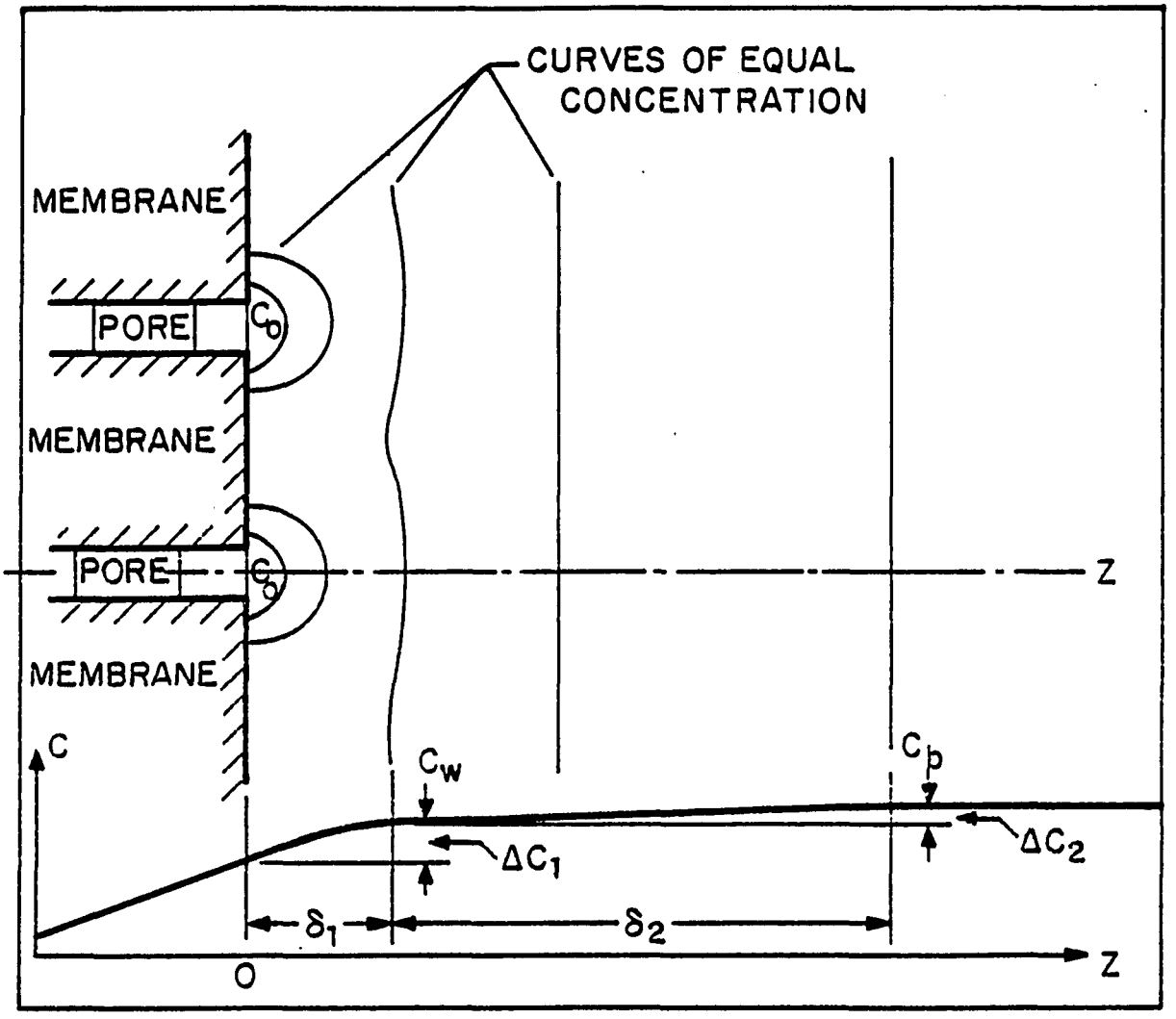

Fig. 20 Two length scales in the entrance region and the unstirred layer

CHAPTER 3

THE THREE-DIMENSIONAL HYDRODYNAMIC INTERACTIONS OF A FINITE SPHERE NEAR A ZERO-THICKNESS ORIFICE

1. INTRODUCTION

The motion of particles and macromolecules at the entrance to filters and membranes is a problem of long standing interest in aerosol and filter technology, osmotic phenomena and the filtration of particulates in whole blood. Prominent examples are: the plasma-screening effect of red cells entering small blood vessels or glass tubes; osmosis at the pore opening of semi-permeable or partially-permeable membranes; the molecular sieving of macromolecules in the loading of plasmalemma vesicles; the interaction of micron-sized particles with entrance geometry in nuclepore filters; the collection efficiency of synthetic membranes and filters; the entrance of highly deformable particles into pores such as in red blood cell deformability tests.

Because of the hydrodynamic interaction between the particle and the pore wall, the hydrodynamic resistance experienced by the particle can differ substantially from the Stokes resistance in an unbounded fluid. The correction factors for the hydrodynamic force and torque vary with the position of the particle and with the direction of the motion. Consequently, the neutrally buoyant velocity of the particle will differ from the velocity of the fluid surrounding it and the particle diffusivity is no longer a scaler but a second-order tensor (e.g. Brenner and Gaydos 1977). The three-dimensional hydrodynamic analysis of the motion of a finite neutrally buoyant particle towards a pore is an

essential input in all the problems involving entrance phenomena mentioned above.

The interaction between a single particle and a single pore entrance may be mathematically modeled by considering a sphere in one of the two semi-infinite regions which are connected by a circular pore in an infinitesimally thin plane wall (Fig. 1). The Reynolds number based upon the sphere or pore radius is usually very small so that the Stokes approximation of creeping flow is valid. However, even with such simplifications, the hydrodynamic problem remains analytically intractable because there is no natural coordinate system which fits the geometry of the sphere and the plane-with-a-pore and, hence, the no-slip conditions cannot be satisfied simultaneously on the two boundaries by any closed-form solution of the equations of motion. The reflections method, which was extensively used to treat weak hydrodynamic interactions of particles with boundaries, is shown to converge very slowly when the sphere-wall spacing is of the order of five sphere radii or less (Ganatos, Weinbaum and Pfeffer 1980). To attack such problems with strong hydrodynamic interactions, two numerical theories, the multipole series representation technique and the integral equation method, have been developed in recent years.

The multipole series representation technique, first developed by Gluckman, Pfeffer and Weinbaum (1971) for unbounded axisymmetric Stokes flow, is based on the idea

that the solution for any object conforming to a natural coordinate system can be approximated by a truncated series of multi-lobular disturbances in which the accuracy of the representation is systematically improved by the addition of higher order multipoles. The solution for a particle assemblage can be represented as the superposition of the above truncated series in several different coordinate systems. The coefficients in these series are then determined by the boundary collocation methods, in which the no-slip boundary conditions are satisfied simultaneously at a finite number of surface points on each particle in the flow field. The convergence of this solution procedure for close particle spacings is vastly superior to the reflections method. This technique has been extended to axisymmetric flows with infinite cylindrical boundaries (Leichtberg, Pfeffer and Weinbaum 1976) and to three-dimensional unbounded and bounded flows (Ganatos, Pfeffer and Weinbaum 1978; Ganatos, Weinbaum and Pfeffer 1980; Ganatos, Pfeffer and Weinbaum 1980). Three years ago Dagan, Weinbaum and Pfeffer (1982b) applied this technique to the entrance problem of the on-axis motion of a finite sphere approaching a circular pore in a zero-thickness plane wall. They obtained accurate results for the hydrodynamic resistance when the sphere center was located no less than 1.1 times the sphere radius from the plane wall. In their solution, different stream functions are constructed for the two half-spaces (Fig. 1) in terms of the unknown velocity profile at the orifice.

The disturbances due to the plane wall are represented by Fourier-Bessel integrals and the disturbance due to the sphere--by the multipole series. Through analytically matching the kinematic (velocity) and dynamic (stress) fields of the two half-spaces at the orifice, the unknown kernels of the Fourier integrals can be expressed in terms of the unknown coefficients in the multipole series for the disturbance due to the sphere such that the no-slip condition is automatically satisfied on the infinite plane wall. Thus the collocation method need only be applied on the sphere surface. The ability to match the two fields analytically is crucial for the successful application of the multipole technique. Similar procedures were used by Wu and Skalak (1984) to achieve a solution for the axisymmetric creeping motion of a sphere from a half-space to a semi-infinite circular cylindrical pore. In a separate paper, Dagan, Weinbaum and Pfeffer (1982a) obtained an infinite-series solution for the creeping motion of pure fluid through an orifice of finite length. Their results show that the velocity profile approaches to within 1.5 percent of a Poiseuille profile after a short entrance distance of half the pore radius. In the far field the solution is found to match exactly the streamline pattern for a flow through an orifice of zero thickness obtained by Sampson (1891), see Happel and Brenner(1973), p.153. This justifies the use of a zero wall thickness model (as shown in Fig. 1) as an approximation to the entrance geometry for a finite length

pore. The same authors, Dagan, Weinbaum and Pfeffer (1983), also tried to extend this technique to the three-dimensional case. However, for this case the analytical satisfaction of dynamic continuity at the orifice is impossible because of the extreme complexity of the form of the boundary conditions. Therefore, they developed a more approximate model in which the rotation of the sphere and the transverse curvature effect of the pore are neglected. Their results predicted for the first time the deviation of the trajectory of a neutrally buoyant sphere from the undisturbed fluid streamlines due to the hydrodynamic interaction with the entrance geometry of the orifice. This prediction is verified by experiment, and their approximate theory is shown to be quantitatively accurate provided that the particle center is at least two pore-radii away from the pore opening.

In the integral equation method, the velocity disturbance generated by the boundaries in the flow field is represented by the integrals of singularities distributed over the boundary surfaces (Ladyzhenskaya 1963). The application of the no-slip conditions on the surfaces, either by the collocation method (e.g. Youngren and Acrivos 1975) or by the weighted residual technique (Lewellen 1982), leads to a set of Fredholm's integral equations of the first kind for the unknown densities of the singularity distributions. These integral equations are then solved numerically, e.g. by dividing the boundary into discrete elements. This would lead to a system of

simultaneous linear algebraic equations. This method has been applied to Stokes flows past a particle of arbitrary shape (Youngren and Acrivos 1975), a gas bubble (Youngren and Acrivos 1976) and a viscous drop (Rallison and Acrivos 1978), and to the motion of an arbitrarily positioned sphere in the flow inside a circular cylindrical pore (Lewellen 1982). This method has also been extended to creeping flow with an infinite boundary (Lee and Leal 1982, Leal and Lee 1982). The singularities are distributed over both the finite particle surface and the infinite confining boundary, but the infinite domain of integration is truncated. The truncation distance is determined by numerical tests as well as order of magnitude estimates. This very general method, which can be used to treat problems with boundaries of arbitrary shape, so far has not been applied to problems with discontinuous boundaries such as the pore entrance geometry.

An alternative version of the integral equation method is the so called "Green's function method", in which the singularity solutions appearing in the integrals over the particle surfaces are required to satisfy the boundary conditions on the confining boundaries. For example, the creeping flow solution for a stokeslet near a stationary plane (Blake 1971) can be integrated over the surface of an arbitrary body to analyze the creeping flow past this body in the presence of the plane wall. Recently, the Green's functions for the entrance geometry have been derived either

for the axisymmetric case (Davis, O'Neill and Brenner 1981) or for the asymmetric case (Davis 1983; Miyazaki and Hasimoto 1984). While the stokeslet in their solutions can be considered as an approximation to a small particle, these solutions can also be integrated over the surface of a finite particle, in principle, to solve the entrance problem for a finite particle. However, the use of this singularity introduces significant difficulties in the numerical development because of the complicated forms of the Green's functions.

In comparison, both the multipole representation technique and the integral equation method have their own advantages and disadvantages. The multipole representation technique is very efficient and highly accurate for a finite body that conforms to some orthogonal geometry. The application of this technique to bounded flow requires the analytical satisfaction of no-slip conditions on the infinite confining boundaries, a really formidable task for many problems including the present one. In contrast, the integral equation method is very flexible in treating boundaries of arbitrary shape including infinite boundaries. Another advantage of this method lies in the fact that the density of the stokeslet distribution, which is identified as the local stress force on the surface, is given as part of the solutions. This is especially useful in problems with deformable interfaces. The drawbacks of this method are the lower accuracy and the longer computation time

compared with the multipole series representation technique. In this study we try to combine the two methods to make better use of each other's advantages and diminish their disadvantages. This combined method will enable us to find a rigorous three-dimensional solution for a finite sphere in the presence of the pore shown in Fig. 1, as well as an axisymmetric solution which is valid when the sphere arbitrarily intersects the pore opening.

The organization of this chapter is as follows: a combined series-integral representation of the disturbed velocity in the flow field for the entrance geometry will be derived and then be used to formulate both the axisymmetric and the three-dimensional hydrodynamic interaction problems in Section 2; the solutions to the axisymmetric and the three-dimensional problems will be presented in Section 3 and Section 4 respectively; Section 5 will summarize this study.

2. FORMULATION

In Fig. 1 all the lengths are scaled to the pore radius R_0. Two Cartesian coordinate systems are used: (x,y,z) is associated with the pore and (X,Y,Z) with the sphere. The center of the sphere of radius a is located at $(-x_0, 0, -z_0)$. For convenience, a cylindrical coordinate system (R, φ, z) associated with the pore and a spherical coordinate system (r, θ, ϕ) associated with the sphere are introduced. The transformation between the coordinates is as follows:

$$\begin{aligned} &X = x + x_0, \quad Y = y, \quad Z = z + z_0; \\ &x = R\cos\varphi, \quad y = R\sin\varphi; \\ &X = r\sin\theta\cos\phi, \quad Y = r\sin\theta\sin\phi, \quad Z = r\cos\theta. \end{aligned} \tag{1}$$

For a creeping flow, the dimensionless Stokes equations are

$$\begin{aligned} &\frac{\partial^2 V_i}{\partial x_j \partial x_j} = \frac{\partial p}{\partial x_i}, \quad (i=1,2,3), \\ &\frac{\partial V_k}{\partial x_k} = 0. \end{aligned} \tag{2}$$

Here the Einstein's convention of summation over repeated indices is adopted, (x_1, x_2, x_3) represent (x, y, z). The fluid velocity V_i is made dimensionless with respect to a characteristic velocity U_0 (e.g. the particle's velocity) and the fluid pressure p to a characteristic viscous stress $\mu U_0/R_0$, where μ is the viscosity of the fluid.

Due to the linearity of the governing equations (2), the

general motion of the sphere in the symmetric plane (x,z) in zero-Reynolds-number flow can be constructed as the superposition of (i) a pure translation of the sphere with velocity (U_x, 0, U_z) in a quiescent fluid; (ii) a pure rotation of the sphere with angular velocity Ω about the Y-axis in a quiescent fluid; and (iii) the flow past a stationary sphere with undisturbed velocity components V_x^s and V_z^s, which obey Sampson's solution (see (11a) and (11b)), at the sphere center ($-x_o$, 0, $-z_o$). According to Dagan, Weinbaum and Pfeffer (1983), the hydrodynamic force and torque on the sphere are approximately given by

$$
\begin{aligned}
F_x &= 6\pi\mu a\,(U_x F_x^t + a\Omega F_x^r + V_x^s F_x^s),\\
F_z &= 6\pi\mu a\,(U_z F_z^t + a\Omega F_z^r + V_z^s F_z^s),\\
T_y &= 8\pi\mu a^2(U_x T_y^{t,x} + U_z T_y^{t,z} + a\Omega T_y^r + \frac{a}{2z_o} V_x^s T_y^{s,x} + \frac{a}{2x_o} V_z^s T_y^{s,z}),
\end{aligned}
\tag{3}
$$

where F_x^t, F_x^r,...,$T_y^{s,z}$ are the force and torque correction factors obtained from the solutions of the three separated problems mentioned above, with the superscripts t, r, s denoting the three problems in sequence. The correction factors account for the hydrodynamic interactions between the sphere and the entrance boundary. For a neutrally buoyant sphere carried by the flow, equations (3) with $F_x=F_z=T_y=0$ yield three relations to determine U_x, U_z and Ω. These equations neglect the fact that the translation in the x-direction can produce a force in the z-direction, and vice versa, and that the torque correction factors for problem (iii) ($T_y^{s,x}$ and $T_y^{s,z}$) are not independent.

In this section, we shall mathematically formulate the problem in order to determine the force and torque correction factors.

2.1 INTEGRAL REPRESENTATION

Ladyzhenskaya (1963) considered two different problems of creeping flow. Problem 1 deals with an actual flow in a space Ω whose boundary is $\partial\Omega$ (Fig. 2). The disturbance velocity $\vec{V}(\vec{x})$ and pressure $p(\vec{x})$ satisfies equation (2), where $\vec{x}=(x_1, x_2, x_3)$ is the position vector for a field point. Both $\vec{V}(\vec{x})$ and $p(\vec{x})$ vanish at infinity and $\vec{V}(\vec{x})$ satisfies no-slip conditions on the solid boundary $\partial\Omega$. Problem 2 treats a fictitious flow due to a stokeslet (point force) in the k-direction at point $\vec{y}=(y_1, y_2, y_3)$ (Fig. 2). The dimensionless velocity $\vec{u}^k(\vec{x},\vec{y})$ and pressure $p^k(\vec{x},\vec{y})$ satisfies

$$\frac{\partial^2 u_i^k(\vec{x},\vec{y})}{\partial x_j \partial x_j} - \frac{\partial p^k(\vec{x},\vec{y})}{\partial x_i} = \delta(\vec{x}-\vec{y}), \qquad (4)$$

$$\frac{\partial u_j^k(\vec{x},\vec{y})}{\partial x_j} = 0 ,$$

where $\delta(\vec{x}-\vec{y})$ is Dirac delta function. The basic solutions of (4), which vanish at infinity, are

$$u_i^k(\vec{x},\vec{y}) = -\frac{1}{8\pi}\left[\frac{\delta_{ik}}{r_{xy}} - \frac{(x_i-y_i)(x_k-y_k)}{r_{xy}^3}\right], \qquad (5)$$

$$p^k(\vec{x},\vec{y}) = \frac{y_k - x_k}{4\pi\, r_{xy}^3},$$

where $r_{xy}=|\vec{x}-\vec{y}|$, $\vec{x}$ denotes the field point, $\vec{y}$ the position of the stokeslet and δ_{ik} is the Kronecker delta.

Ladyzhenskaya (1963) derived a Green's formula for these problems as follows:

$$\iiint_{\Omega}\left\{V_i(\vec{y})\left[\frac{\partial^2 u_i^k(\vec{x},\vec{y})}{\partial y_j\,\partial y_j} - \frac{\partial p^k(\vec{y},\vec{x})}{\partial y_i}\right] - u_i^k(\vec{x},\vec{y})\left[\frac{\partial^2 V_i(\vec{y})}{\partial y_j\,\partial y_j} - \frac{\partial p(\vec{y})}{\partial y_i}\right]\right\} d\Omega_y$$

$$= \iint_{\partial\Omega}\left\{V_i(\vec{y})\,T_{ij}[\vec{u}^k(\vec{x},\vec{y})]\,n_j(\vec{y}) - u_i^k(\vec{x},\vec{y})\,T_{ij}[\vec{V}(\vec{y})]\,n_j(\vec{y})\right\} dS_y, \qquad (6)$$

where

$$T_{ij}[\vec{V}(\vec{y})] = -\delta_{ij}\,p(\vec{y}) + \left[\frac{\partial V_i(\vec{y})}{\partial y_j} + \frac{\partial V_j(\vec{y})}{\partial y_i}\right] \qquad (7a)$$

and

$$T_{ij}[\vec{u}^k(\vec{x},\vec{y})] = -\delta_{ij}\,p^k(\vec{y},\vec{x}) + \left[\frac{\partial u_i^k(\vec{x},\vec{y})}{\partial y_j} + \frac{\partial u_j^k(\vec{x},\vec{y})}{\partial y_i}\right] \qquad (7b)$$

represent the stress tensors for problems 1 and 2, respectively. $\vec{n}=\{n_j\}$ is the exterior normal vector (with respect to space Ω) to the boundary $\partial\Omega$ and therefore points <u>inward</u> from the body surfaces. The subscript y in dS_y and $d\Omega_y$ indicates that the integrations are to be carried out over $\vec{y}$.

The Green's formula (6), when combined with (2) and (4), enables us to express the velocity $V_i(\vec{x})$ at any field point $\vec{x}$ inside Ω as the sum of two surface integrals, i.e. a

"single layer potential" $V_i^{(1)}(\vec{x})$ and a "double layer potential" $V_i^{(2)}(\vec{x})$:

$$V_i(\vec{x}) = V_i^{(1)}(\vec{x}) + V_i^{(2)}(\vec{x}) , \tag{8}$$

where

$$\begin{aligned} V_i^{(1)}(\vec{x}) &= -\iint_{\partial\Omega} \mathcal{U}_i^k(\vec{x},\vec{y})\, T_{kj}[\vec{V}(\vec{y})]\, n_j(\vec{y})\, dS_y \\ &= -\iint_{\partial\Omega} \mathcal{U}_i^k(\vec{x},\vec{y})\, f_k(\vec{y})\, dS_y \\ &= \frac{1}{8\pi} \iint_{\partial\Omega} \left[\frac{\delta_{ik}}{r_{xy}} + \frac{(x_i-y_i)(x_k-y_k)}{r_{xy}^3}\right] f_k(\vec{y})\, dS_y , \end{aligned} \tag{8a}$$

$$\begin{aligned} V_i^{(2)}(\vec{x}) &= \iint_{\partial\Omega} T_{ij}[\vec{u}^k(\vec{x},\vec{y})]\, V_k(\vec{y})\, n_j(\vec{y})\, dS_y \\ &= -\frac{3}{4\pi} \iint_{\partial\Omega} \frac{(x_i-y_i)(x_j-y_j)(x_k-y_k)}{r_{xy}^5} V_k(\vec{y})\, n_j(\vec{y})\, dS_y , \end{aligned} \tag{8b}$$

and

$$f_k(\vec{y}) = T_{kj}[\vec{V}(\vec{y})]\, n_j(\vec{y}) . \tag{8c}$$

Note that $f_k(\vec{y})$ represents the actual local stress force in the k-direction. The single and double layer potentials together are often referred to as the hydrodynamic potentials.

The above formulars are derived under the assumption that each of the boundaries $\partial\Omega$ is a Lyapunov surface. For surfaces of practical interest this requires $\partial\Omega$ to have a well defined tangent plane at every point. Under this assumption, the single layer potential $V_i^{(1)}(\vec{x})$ is continuous in Ω and $\partial\Omega$. But the double layer potential $V_i^{(2)}(\vec{x})$ undergoes a discontinuity across $\partial\Omega$:

$$\lim_{\vec{x}\to\vec{x}_o} V_i^{(2)}(\vec{x}) = V_i^{(2)}(\vec{x}_o) + \frac{1}{2} V_i(\vec{x}_o), \quad \begin{pmatrix} \vec{x}\in\Omega, \\ \vec{x}_o\in\partial\Omega \end{pmatrix}. \tag{9}$$

Physically, the single and double layer potentials can be thought as distributions of stokeslets and higher-order singularities, respectively, over the boundary surfaces $\partial\Omega$. Each potential, along with its corresponding pressure, satisfies the Stokes equations (2) individually inside Ω. The density functions $f_k(\vec{y})$ or $v_k(\vec{y})$ are unknown on the boundary $\partial\Omega$ and have to be determined from the requirement that the velocity should satisfy the no-slip conditions on the boundary $\partial\Omega$. With the densities so obtained, $V_i(\vec{x})$ in (8) represents the solution for problem 1 and the force and torque on a body can be determined from the integration of $f_k(\vec{y})$ over the body surface.

However, the above theory in the form of equation (8) cannot be applied directly to our configuration in Fig. 1. Some modifications are necessary.

Firstly, in deriving equations (6) and (8), the basic solutions $u_i^k(\vec{x},\vec{y})$ and $p^k(\vec{x},\vec{y})$ to (4) are assumed to vanish at infinity, but for our geometry in Fig. 1, the pressures on the two sides of the plane wall should approach different limiting values, say $p_{-\infty}$ and p_{∞}, at infinity for problem (iii). Thus $p_{-\infty}$ and p_{∞} cannot vanish at the same time. This difficulty is easily eliminated by decomposing the solution for our present problem into the sum of the Sampson's

solution (with superscript s) and a remaining disturbance (primed quantities), where both $V_i'(\vec{x})$ and $p'(\vec{x})$ vanish at infinity, namely

$$\begin{aligned} V_i(\vec{x}) &= V_i^s(\vec{x}) + V_i'(\vec{x}), \\ p(\vec{x}) &= p^s(\vec{x}) + p'(\vec{x}), \end{aligned} \tag{10}$$

The Sampson's solution is (Happel and Brenner 1973, p.153)

$$V_R^s(\vec{x}) = \frac{-3q}{8\pi} z \frac{\zeta}{R}(R_1 - R_2)\left(\frac{1}{R_1} - \frac{1}{R_2}\right), \tag{11a}$$

$$V_z^s(\vec{x}) = \frac{3q}{8\pi} \frac{\zeta}{R}(R_1 - R_2)\left(\frac{R-1}{R_1} - \frac{R+1}{R_2}\right), \tag{11b}$$

$$p^s(\vec{x}) = \frac{3q}{\pi}\left(\frac{\lambda}{\lambda^2+\zeta^2} + \tan^{-1}\lambda\right). \tag{11c}$$

Here the dimensionless volumetric flow rate q is related to the pressure difference $(p_{-\infty}-p_{\infty})$ and the oblate spheroidal coordinates (λ,ζ) are related to the cylindrical coordinates (R, φ, z), as follows:

$$q = \frac{1}{3}(p_{-\infty} - p_{\infty}) \tag{11d}$$

$$\lambda = \left[\frac{1}{4}(R_1+R_2)^2 - 1\right]^{1/2}, \tag{11e}$$

$$\zeta = \left[1 - \frac{1}{4}(R_2-R_1)^2\right]^{1/2}, \tag{11f}$$

$$R_1 = \left[z^2 + (R-1)^2\right]^{1/2}, \tag{11g}$$

$$R_2 = \left[z^2 + (R+1)^2\right]^{1/2}. \tag{11h}$$

Secondly, the plane wall with an orifice as shown in Fig. 1, having no definite tangent plane at the edge of the orifice, is not a Lyapunov surface as required in deriving equations (6) and (8). Thus, these equations cannot be applied directly to the whole flow field. However, we can divide the flow field in Fig. 1 into two regions as shown in Fig. 3. Then the boundaries of each region will be Lyapunov surfaces and, consequently, Green's formula (6) will be applicable to each region. The boundaries of region I consist of the sphere surface S_p, the left side of the plane wall S_{W^-} and the orifice opening S_H, whereas region II has the right side of the plane wall S_{W^+} and the orifice opening S_H as its boundary (Fig. 3). Assuming for the moment that $\vec{x}$ belongs to region I, the application of equation (6) to regions I and II gives the following:

In region I:

$$V_i'(\vec{x}) = -\iint_{S_b} u_i^k(\vec{x},\vec{y})\, T_{kj}^{(p)}(\vec{V}'(\vec{y}))\, n_j^{(p)}(\vec{y})\, dS_y + \iint_{S_b} T_{ij}(\vec{u}^k(\vec{x},\vec{y}))\, V_k'^{(p)}(\vec{y})\, n_j^{(p)}(\vec{y})\, dS_y$$

$$V_i'(\vec{x}) = -\iint_{S_p} u_i^k(\vec{x},\vec{y})\, T_{kj}^{(p)}(\vec{V}'(\vec{y}))\, n_j^{(p)}(\vec{y})\, dS_y + \iint_{S_p} T_{ij}(\vec{u}^k(\vec{x},\vec{y}))\, V_k'^{(p)}(\vec{y})\, n_j^{(p)}(\vec{y})\, dS_y$$

$$- \iint_{S_{W^-}} u_i^k(\vec{x},\vec{y})\, T_{kj}^{(-)}(\vec{V}'(\vec{y}))\, n_j^{(-)}(\vec{y})\, dS_y - \iint_{S_H} u_i^k(\vec{x},\vec{y})\, T_{kj}^{(H)}(\vec{V}'(\vec{y}))\, n_j^{(-)}(\vec{y})\, dS_y$$

In r

$$+ \iint_{S_H} T_{ij}(\vec{u}^k(\vec{x},\vec{y}))\, V_k'^{(H)}(\vec{y})\, n_j^{(-)}(\vec{y})\, dS_y \,, \qquad (12a)$$

$$0 = -\iint_{S_{W^+}} u_i^k(\vec{x},\vec{y})\, T_{kj}^{(+)}(\vec{V}'(\vec{y}))\, n_j^{(+)}(\vec{y})\, dS_y - \iint_{S_H} u_i^k(\vec{x},\vec{y})\, T_{kj}^{(H)}(\vec{V}'(\vec{y}))\, n_j^{(+)}(\vec{y})\, dS_y$$

$$+ \iint_{S_H} T_{ij}(\vec{u}^k(\vec{x},\vec{y}))\, V_k'^{(H)}(\vec{y})\, n_j^{(+)}(\vec{y})\, dS_y \,, \qquad (12b)$$

where the superscripts p, H, +, - denote S_p, S_H, S_{w+} and S_{w-} respectively and all the other symbols have the same meanings as in (5)--(8). The double layer potentials over S_{w-} and S_{w+} do not appear because their kernels $V_i'(\vec{y})$ are identically zero on the two sides of the plane wall. Using

$$n_j^{(-)}(\vec{y}) = -n_j^{(+)}(\vec{y}) = \begin{cases} 0 & \text{when } j = 1 \text{ or } 2, \\ 1 & \text{when } j = 3, \end{cases}$$

and adding (12a), (12b), we are able to derive an expression for the disturbance velocity:

$$V_i'(\vec{x}) = -\iint_{S_p} u_i^k(\vec{x},\vec{y})\, T_{kj}^{(p)}(\vec{V}'(\vec{y}))\, n_j^{(p)}(\vec{y})\, dS_y + \iint_{S_p} T_{ij}(\vec{u}^k(\vec{x},\vec{y}))\, V_k'^{(p)}(\vec{y})\, n_j^{(p)}(\vec{y})\, dS_y$$

$$- \iint_{S_{w-}} u_i^k(\vec{x},\vec{y})\, f_k^{(w)}(\vec{y})\, dS_y \quad , \tag{13}$$

where

$$f_k^{(w)}(\vec{y}) = T_{kz}^{(-)}(\vec{V}'(\vec{y})) - T_{kz}^{(+)}(\vec{V}'(\vec{y})), \quad k=1,2,3. \tag{14}$$

Although this is derived for the case where $\vec{x}$ belongs to region I, similar reasoning for the other cases ($\vec{x}$ belongs to region II or $\vec{x}$ is right at the pore opening) also yields the same expression. Hence (13) is a unified expression, valid for any point $\vec{x}$ in the whole flow field. There is futhermore no restriction on the position of the sphere. This means that (13) remains valid even if the sphere enters the pore, while such cases could not be treated by any previous method.

2.2 THE COMBINED SERIES-INTEGRAL REPRESENTATION

In (13), $f_k^{(w)}(\vec{y})$ represents the difference of stresses across the plane wall and $T_{kj}^{(p)}(\vec{v}'(\vec{y}))$ -- the stress on the sphere surface. Both of them are unknown and have to be determined by the application of no-slip conditions on S_p and S_w-. The resulting integral equations have to be solved numerically and approximations concerning $f_k^{(w)}(\vec{y})$ and $T_{kj}^{(p)}(\vec{v}'(\vec{y}))$ have to be made. These approximations usually produce considerable inaccuracy in calculating the force and torque correction factors, which are our primary goals. In addition, extensive numerical integrations have to be performed over both the sphere surface S_p and the plane wall S_w-. As mentioned in Section 1, we wish to combine the integral equation method with the multipole series representation technique in an attempt to improve the accuracy with which the surface stresses on S_p can be computed and also reduce the amount of numerical integration.

Lamb's fundamental harmonic solutions of the Stokes equations (2) in spherical coordinates describe an arbitrary disturbance on the surface of a sphere (see Happel and Brenner 1973, p.65). If the velocity vanishes at infinity, Lamb's solution can be written as

$$\vec{V}_p = \sum_{n=1}^{\infty} \left[\nabla \times (\vec{r}\, \chi_{-(n+1)}) + \nabla \Phi_{-(n+1)} - \frac{(n-2)}{2n(2n-1)} r^2 \nabla P_{-(n+1)} \right.$$

$$\left. + \frac{(n+1)}{n(2n-1)} \vec{r}\, P_{-(n+1)} \right], \qquad (15)$$

where $\chi_{-(n+1)}$, $\Phi_{-(n+1)}$ and $P_{-(n+1)}$ are solid spherical harmonic functions of order $-(n+1)$ and $\vec{r}$ is the radial position vector with the origin at the sphere center. In general, the harmonic functions have the following form:

$$\begin{Bmatrix} \chi_{-(n+1)} \\ \Phi_{-(n+1)} \\ P_{-(n+1)} \end{Bmatrix} = \sum_{m=0}^{n} P_n^m(\cos\theta) \frac{1}{r^{n+1}} \left[\begin{Bmatrix} A_{mn} \\ C_{mn} \\ E_{mn} \end{Bmatrix} \cos m\phi + \begin{Bmatrix} B_{mn} \\ D_{mn} \\ F_{mn} \end{Bmatrix} \sin m\phi \right], \quad (16)$$

where $P_n^m(\cos\theta)$ is the associated Legendre function and A_{mn}, B_{mn},...,F_{mn} are unknown constants to be determined from the boundary conditions. When the flow configuration has symmetry about the plane $\phi=0$, as is the case in Fig. 1, we have

$$A_{mn} = D_{mn} = F_{mn} = 0. \quad (17)$$

The hydrodynamic force and torque exerted on the sphere are simply evaluated by

$$\vec{F} = -4\pi \, (E_{11}\vec{i} + E_{01}\vec{k}), \quad (18)$$

$$\vec{T} = -8\pi \, B_{11}\vec{j}. \quad (19)$$

It has turned out that in a variety of applications of the multipole series representation technique in which there is planar symmetry, Lamb's solution always provides high accuracy in evaluating the force and torque on the sphere (Weinbaum 1981). The multipole technique was not used for

the orifice wall because of the difficulty in analytically satisfying the no-slip boundary conditions on this surface for nonaxisymmetric motion. The sphere surface offers no difficulty. Thus, we shall represent the disturbance on the sphere surface by Lamb's series solution (15),instead of the first two integrals (the hydrodynamic potentials on S_p) in (13), while retaining the third integral (the single layer potential on S_w-) in (13) to represent the disturbance on the orifice wall. This would enable us to evaluate the force and torque on the sphere with higher accuracy while avoiding the difficulty of analytically satisfying the boundary conditions on the pore and wall. In so doing, $\vec{V}'(\vec{x})$ becomes

$$V_i'(\vec{x}) = V_{pi}(\vec{x}) - \iint_{S_w-} u_i^k(\vec{x},\vec{y}) f_k^{(w)}(\vec{y}) dS_y \,. \tag{20}$$

After substituting (15)--(17) for $V_{pi}(\vec{x})$ and (5) for $u_i^k(\vec{x},\vec{y})$ in (20), we have

$$V_i'(\vec{x}) = \sum_{n=1}^{\infty}\sum_{m=0}^{n}\left[B_{mn}B_{mn}^{(i)}(r,\theta,\phi) + C_{mn}C_{mn}^{(i)}(r,\theta,\phi) + E_{mn}E_{mn}^{(i)}(r,\theta,\phi)\right]$$

$$+ \frac{1}{8\pi}\iint_{S_w-}\left[\frac{\delta_{ik}}{r_{xy}} + \frac{(x_i-y_i)(x_k-y_k)}{r_{xy}^3}\right] f_k^{(w)}(\vec{y}) dS_y \,, \quad i=1,2,3, \tag{21}$$

where

$$B_{mn}^{(1)}(r,\theta,\phi) = \frac{1}{r^{n+1}}\left[-\sin\theta\sin\phi\,\frac{dP_n^m(\xi)}{d\xi}\sin m\phi + m\frac{\cos\phi}{\tan\theta}P_n^m(\xi)\cos m\phi\right], \tag{21a}$$

$$C_{mn}^{(1)}(r,\theta,\phi) = \frac{1}{r^{n+2}}\left[-\left((n+1)P_n^m(\xi) + \xi\frac{dP_n^m(\xi)}{d\xi}\right)\sin\theta\cos\phi\cos m\phi\right.$$

$$\left. + m\frac{\sin\phi}{\sin\theta}P_n^m(\xi)\sin m\phi\right], \tag{21b}$$

$$E^{(1)}_{mn}(r,\theta,\phi) = \frac{1}{2(2n-1)r^n}\left[\left((n+1)P^m_n(\xi) + \frac{n-2}{n}\xi\frac{dP^m_n(\xi)}{d\xi}\right)\sin\theta\cos\phi\cos m\phi - \frac{m(n-2)}{n}\frac{\sin\phi}{\sin\theta}P^m_n(\xi)\sin m\phi\right], \quad (21c)$$

$$B^{(2)}_{mn}(r,\theta,\phi) = \frac{1}{r^{n+1}}\left[\sin\theta\cos\phi\frac{dP^m_n(\xi)}{d\xi}\sin m\phi + m\frac{\sin\phi}{\tan\theta}P^m_n(\xi)\cos m\phi\right], \quad (21d)$$

$$C^{(2)}_{mn}(r,\theta,\phi) = \frac{1}{r^{n+2}}\left[-\left((n+1)P^m_n(\xi) + \xi\frac{dP^m_n(\xi)}{d\xi}\right)\sin\theta\sin\phi\cos m\phi - m\frac{\cos\phi}{\sin\theta}P^m_n(\xi)\sin m\phi\right], \quad (21e)$$

$$E^{(2)}_{mn}(r,\theta,\phi) = \frac{1}{2(2n-1)r^n}\left[\left((n+1)P^m_n(\xi) + \frac{n-2}{n}\xi\frac{dP^m_n(\xi)}{d\xi}\right)\sin\theta\sin\phi\cos m\phi + \frac{m(n-2)}{n}\frac{\cos\phi}{\sin\theta}P^m_n(\xi)\sin m\phi\right], \quad (21f)$$

$$B^{(3)}_{mn}(r,\theta,\phi) = -\frac{m}{r^{n+1}}P^m_n(\xi)\cos m\phi, \quad (21g)$$

$$C^{(3)}_{mn}(r,\theta,\phi) = \frac{1}{r^{n+2}}(m-n-1)P^m_{n+1}(\xi)\cos m\phi, \quad (21h)$$

$$E^{(3)}_{mn}(r,\theta,\phi) = \frac{1}{2n(2n-1)r^n}\left[2(n+1)\xi P^m_n(\xi) + (n-2)(n-m+1)P^m_{n+1}(\xi)\right]\cos m\phi, \quad (21i)$$

and

$$\xi = \cos\theta, \quad (21j)$$

$$\frac{dP^m_n(\xi)}{d\xi} = \frac{1}{1-\xi^2}\left[(n+1)\xi P^m_n(\xi) - (n-m+1)P^m_{n+1}(\xi)\right]. \quad (21k)$$

The introduction of $V_{pi}(\vec{x})$ in the form of series, instead of integrals, results in a considerable reduction of the amount of numerical integration. As will be seen, this is of great significance.

The no-slip conditions on the sphere surface and the pore

wall are

$$V_i'(r=a) = V_i'^{(p)}(\theta,\phi), \quad (\text{on } S_p); \tag{22a}$$

$$V_i'(R\geq 1,\ z=0) = 0, \quad (\text{on } S_w-); \tag{22b}$$

where

$$V_x'^{(p)}(\theta,\phi) = U_x + a\Omega\cos\theta - V_R^S(a,\theta,\phi), \tag{23a}$$

$$V_z'^{(p)}(\theta,\phi) = U_z - a\Omega\sin\theta\cos\phi - V_z^S(a,\theta,\phi). \tag{23b}$$

$V_R^S(\vec{x})$ and $V_z^S(\vec{x})$ are evaluated by (11a) and (11b); U_x, U_z and Ω are the translational and angular velocities of the sphere, respectively. In the next two subsections, we shall discuss how to apply the no-slip conditions for the axisymmetric and three-dimensional cases, respectively, to determine the unknown functions $f_k^{(w)}(\vec{y})$ and the unknown coefficients B_{mn}, C_{mn}, E_{mn} in (21).

2.3 THE COLLOCATION TECHNIQUE

For the axisymmetric case we apply the no-slip conditions at M_1 discrete points on the sphere surface S_p and at N_2 discrete points on the pore wall S_w-. All the points are located in the same meridian plane, for convenience take $\phi = \varphi = 0$. Due to the axial symmetry, the unknown $f_k^{(w)}(\vec{y})$ is of the following form:

$$f_1^{(w)}(\vec{y}) = f_R(\tilde{R})\cos\tilde{\varphi},$$

$$f_2^{(w)}(\vec{y}) = f_R(\tilde{R})\sin\tilde{\varphi}, \qquad (24)$$

$$f_3^{(w)}(\vec{y}) = f_z(\tilde{R}),$$

where $f_R(\tilde{R})$ and $f_z(\tilde{R})$ are unknown functions of $\tilde{R}$ and $\vec{y}=(\tilde{R},\tilde{\varphi},0)$ is the location of the stokeslet on S_w-. In the Lamb's series in (21), only the terms with m=0 are retained for the axisymmetric case. Note that $B_{mn}^{(i)}(r,\theta,\phi)\equiv 0$ when m=0. The integral equations that result after the no-slip conditions are applied cannot be solved analytically for $f_R(\tilde{R})$, $f_z(\tilde{R})$, C_{0n} and E_{0n}. To reduce the integral equations to a set of linear algebraic equations, which can be solved numerically, one has to introduce approximations for the behavior of $f_R(\tilde{R})$ and $f_z(\tilde{R})$. For example, Youngren and Acrivos (1975) approximated them by piecewise constants such that

$$\iint_{\Delta_m}\left[\frac{\delta_{ik}}{r_{xy}}+\frac{(x_i-y_i)(x_k-y_k)}{r_{xy}^3}\right]f_k(\vec{y})\,dS_y \approx f_k(\vec{x}^{(m)})\iint_{\Delta_m}\left[\frac{\delta_{ik}}{r_{xy}}+\frac{(x_i-y_i)(x_k-y_k)}{r_{xy}^3}\right]dS_y, \qquad (25)$$

where $\vec{x}^{(m)}$ is a point inside the small surface element Δ_m. If a similar procedure is applied to our infinite domain of integration S_w-, it would produce a divergent integral when $\tilde{R}\to\infty$. Fortunately, the magnitude of $f_R(\tilde{R})$ and $f_z(\tilde{R})$, which represent the differences of stresses on the two sides of the wall, decays rapidly with increasing $\tilde{R}$ and thus it is possible to truncate the infinite domain $1\le\tilde{R}<\infty$ into a

large but finite region, say $1 \leqslant \tilde{R} \leqslant R_u$. We divide this region into (N_2-2) intervals $(\hat{R}_{n-1}, \hat{R}_n)$, assuming that

$$\begin{aligned} &\hat{R}_1 = 1; \qquad \hat{R}_{N_2-1} = R_u; \\ &\hat{R}_n = \tfrac{1}{2}(R_n + R_{n+1}), \quad (n=2,3,4\ldots,N_2-2). \end{aligned} \tag{26}$$

where $1 \leqslant R_1 < R_2 < \cdots < R_{N_2} \leqslant R_u$ are the radial coordinates of the chosen collocation points on the pore plane. Then, for each of the intervals, a procedure similar to (25) can be applied. Our numerical tests show that higher accuracy can be attained if $f_R(\tilde{R})$ and $f_z(\tilde{R})$ are approximated by the piecewise quadratic interpolation:

$$f_k(\tilde{R}) = \sum_{\alpha=1}^{3} f_k(R_{n-2+\alpha}) \left(A_\alpha^{(n)} \tilde{R}^2 + B_\alpha^{(n)} \tilde{R} + C_\alpha^{(n)} \right),$$

$$\text{when } \hat{R}_{n-1} \leqslant \tilde{R} < \hat{R}_n, \quad (n=2,3,4,\ldots,N_2-1), \tag{27}$$

where

$$A_1^{(n)} = \frac{1}{D_n}(R_n - R_{n+1}), \qquad B_1^{(n)} = \frac{1}{D_n}(R_{n+1}^2 - R_n^2), \qquad C_1^{(n)} = \frac{R_n R_{n+1}}{D_n}(R_n - R_{n+1});$$

$$A_2^{(n)} = \frac{1}{D_n}(R_{n+1} - R_{n-1}), \qquad B_2^{(n)} = \frac{1}{D_n}(R_{n-1}^2 - R_{n+1}^2), \qquad C_2^{(n)} = \frac{R_{n+1} R_{n-1}}{D_n}(R_{n+1} - R_{n-1});$$

$$A_3^{(n)} = \frac{1}{D_n}(R_{n-1} - R_n), \qquad B_3^{(n)} = \frac{1}{D_n}(R_n^2 - R_{n-1}^2), \qquad C_3^{(n)} = \frac{R_{n-1} R_n}{D_n}(R_{n-1} - R_n);$$

$$D_n = R_{n-1} R_n (R_{n-1} - R_n) + R_n R_{n+1}(R_n - R_{n+1}) + R_{n+1} R_{n-1}(R_{n+1} - R_{n-1}). \tag{27a}$$

In (27), $f_k(\tilde{R})$ can be either $f_R(\tilde{R})$ or $f_z(\tilde{R})$. With (27) substituted into the integral equations and Lamb's series in (21) truncated to $n \leqslant M_1$, the no-slip conditions, when applied at the designated collocation points on S_p and S_w,

yield the following linear system of equations (i=1 and 3 only):

$$\sum_{n=1}^{M_1}\left[C_{on}\,C_{on}^{(i)}(a,\theta_p,0)+E_{on}\,E_{on}^{(i)}(a,\theta_p,0)\right]$$
$$+\frac{1}{8\pi}\sum_{n=2}^{N_2-1}\sum_{\alpha=1}^{3}\left[f_R(R_{n-2+\alpha})\,G_{iR}^{n\alpha}(R_p,0,z_p)+f_z(R_{n-2+\alpha})\,G_{iz}^{n\alpha}(R_p,0,z_p)\right]=V_i^{\prime(p)}(\theta_p,0),$$

$$\text{at}\quad \vec{x}=(a,\theta_p,0)=(R_p,0,z_p)\in S_p\,,\quad p=1,2,\cdots,M_1\,; \tag{28a}$$

$$\sum_{n=1}^{M_1}\left[C_{on}\,C_{on}^{(i)}(r_q,\theta_q,0)+E_{on}\,E_{on}^{(i)}(r_q,\theta_q,0)\right]$$
$$+\frac{1}{8\pi}\sum_{n=2}^{N_2-1}\sum_{\alpha=1}^{3}\left[f_R(R_{n-2+\alpha})\,G_{iR}^{n\alpha}(R_q,0,0)+f_z(R_{n-2+\alpha})\,G_{iz}^{n\alpha}(R_q,0,0)\right]=0,$$

$$\text{at}\quad \vec{x}=(r_q,\theta_q,0)=(R_q,0,0)\in S_{w-}\,,\quad q=1,2,\cdots,N_2\,; \tag{28b}$$

where $V_i^{(p)}(\theta,\phi)$ are given by (23a) and (23b); $C_{On}^{(i)}(r,\theta,\phi)$ and $E_{On}^{(i)}(r,\theta,\phi)$ by (21b), (21c), (21h) and (21i); and

$$G_{iR}^{n\alpha}(R,\varphi,z)=A_\alpha^{(n)}\sum_{j=1}^{2}H_{ij}^{(3)}(R,\varphi,z;\hat{R}_{n-1},\hat{R}_n;1)$$
$$+B_\alpha^{(n)}\sum_{j=1}^{2}H_{ij}^{(2)}(R,\varphi,z;\hat{R}_{n-1},\hat{R}_n;1)$$
$$+C_\alpha^{(n)}\sum_{j=1}^{2}H_{ij}^{(1)}(R,\varphi,z;\hat{R}_{n-1},\hat{R}_n;1)\,; \tag{29a}$$

$$G_{iz}^{n\alpha}(R,\varphi,z)=A_\alpha^{(n)}H_{i3}^{(3)}(R,\varphi,z;\hat{R}_{n-1},\hat{R}_n;0)$$
$$+B_\alpha^{(n)}H_{i3}^{(2)}(R,\varphi,z;\hat{R}_{n-1},\hat{R}_n;0)$$
$$+C_\alpha^{(n)}H_{i3}^{(1)}(R,\varphi,z;\hat{R}_{n-1},\hat{R}_n;0)\,; \tag{29b}$$

$$H_{ij}^{(\beta)}(R,\varphi,z;b_1,b_2;m)=\begin{cases}\displaystyle\int_{b_1}^{b_2}\int_0^{2\pi}\left[\frac{\delta_{ij}}{r_{xy}}+\frac{(x_i-y_i)(x_j-y_j)}{r_{xy}^3}\right]\cos m\tilde{\varphi}\,\tilde{R}^{\beta}\,d\tilde{\varphi}\,d\tilde{R}\,, & \text{when } j=1 \text{ or } 3;\\ \displaystyle\int_{b_1}^{b_2}\int_0^{2\pi}\left[\frac{\delta_{ij}}{r_{xy}}+\frac{(x_i-y_i)(x_j-y_j)}{r_{xy}^3}\right]\sin m\tilde{\varphi}\,\tilde{R}^{\beta}\,d\tilde{\varphi}\,d\tilde{R}\,, & \text{when } j=2.\end{cases} \tag{29c}$$

Equations (28a) and (28b) constitute $2(M_1+N_2)$ equations, which can be solved for the $2(M_1+N_2)$ unknowns: C_{0n}, E_{0n} ($n=1,2,\cdots,M_1$) and $f_R(R_n)$, $f_z(R_n)$ ($n=1,2,\cdots,N_2$). The force and torque on the sphere are then found from (18) and (19).

The most tedious and time-consuming part of this work is the evaluation of integrals $H_{ij}^{(\beta)}(R,\varphi,z;\ b_1,b_2;\ m)$ as defined by (29c). For example, if we take $M_1=10$, $N_2=20$, then we have to evaluate $18(M_1+N_2)(N_2-2)=9720$ such integrals. Fortunately, the integration over $\tilde{\varphi}$ can be performed analytically and the results expressed in terms of complete elliptic integrals. For the collocation points on S_w- (where $z=0$), we are also able to perform the integration over $\tilde{R}$ analytically by expanding the elliptic integrals into various power series of their moduli or complimentary moduli. For the collocation points on S_p, part of the integration over $\tilde{R}$ has to be carried out numerically. In either case $H_{ij}^{(\beta)}(R,\varphi,z;\ b_1,b_2;\ m)$ can be expressed in the following forms:

$$H_{ij}^{(\beta)}(R,\varphi,z;b_1,b_2;m)=\begin{cases} g_{ij}^{a}(R;b_1,b_2;m,\beta)\cos m\varphi + g_{ij}^{b}(R;b_1,b_2;m,\beta)\cos(m-k)\varphi \\ \quad + g_{ij}^{c}(R;b_1,b_2;m,\beta)\cos(m+k)\varphi\,, \quad \text{when } i=1 \text{ or } 3\,; \\ g_{ij}^{a}(R;b_1,b_2;m,\beta)\sin m\varphi + g_{ij}^{b}(R;b_1,b_2;m,\beta)\sin(m-k)\varphi \\ \quad + g_{ij}^{c}(R;b_1,b_2;m,\beta)\sin(m+k)\varphi\,, \quad \text{when } i=2\,. \end{cases} \tag{30}$$

Here $k=1$ for $i=3$ or $j=3$, and $k=2$ otherwise. The derivation of this formula is extraordinarily lengthy and a brief description of it will be given in the Appendix.

2.4 THE MIXED WEIGHTED-RESIDUAL AND COLLOCATION TECHNIQUE

For the three-dimensional case, we expand $f_k^{(w)}(\vec{y})$ in the form of Fourier series:

$$f_k^{(w)}(\vec{y}) = \begin{cases} \sum_{m=0}^{\infty} f_{km}(\tilde{R}) \cos m\tilde{\varphi}, & \text{when } k=1 \text{ or } 3; \\ \sum_{m=1}^{\infty} f_{km}(\tilde{R}) \sin m\tilde{\varphi}, & \text{when } k=2. \end{cases} \tag{31}$$

The collocation technique described in last subsection can also be used for this case, in principle. However, the chosen colocation points have to be located in more than one meridian plane. The previous work (Ganatos, Pfeffer and Weinbaum 1978) and our numerical tests show that the results for the force and torque on the sphere are very sensitive to the configuration of the collocation points. It is impracticable to place a sufficient number of collocation points so that the distribution of the collocation points is reasonably dense on the infinite plane wall S_w- (even if it is truncated). Therefore, we shall use a weighted residual technique for the plane wall S_w-, but retain the collocation technique on the sphere surface S_p. The collocation technique presents little difficulty on S_p, whereas the weighted residual technique would require a much greater amount of numerical integration on S_p.

The weighted residual technique is based on the idea that the no-slip conditions should be satisfied not at discrete

boundary points, rather on the continuous boundary in the sense of weighted averaging. In our present problem, the no-slip conditions (22b) on S_w- can be written as follows:

$$V_i'(R, \varphi, 0) = 0, \quad \text{when } R \geq 1, \ 0 \leq \varphi < 2\pi. \tag{32a}$$

Choose a family of weight functions $w_{i\ell}(\varphi)$, $\ell = 0, 1, 2, \cdots$. Now multiplying (32a) by one of the $w_{i\ell}(\varphi)$ and integrating it over φ from 0 to 2π, we have

$$\int_0^{2\pi} V_i'(R, \varphi, 0) w_{i\ell}(\varphi) d\varphi = 0 \qquad , \text{ when } R \geq 1. \tag{32b}$$

In principle we can take a similar weighted averaging in the R-direction too. However we will not do this here because it would require an excessive amount of numerical integration in addition. Instead, we choose a number of values R_n, as we did for the axisymmetric case, and require that (32b) should be satisfied for these discrete R_n, i.e.

$$\int_0^{2\pi} V_i'(R_n, \varphi, 0) w_{i\ell}(\varphi) d\varphi = 0 \quad , \quad n = 1, 2, \cdots, N_2. \tag{32c}$$

Thus the no-slip conditions are satisfied at discrete rings on S_w-, in some average sense. In this work we choose

$$w_{i\ell}(\varphi) = \begin{cases} \cos \ell\varphi, & \text{when } i = 1 \text{ or } 3; \\ \sin \ell\varphi, & \text{when } i = 2. \end{cases} \tag{32d}$$

One advantage of such a choice is to make use of the orthogonality of trigonometric functions in evaluating the integration over φ of terms like $H_{ij}^{(\beta)}(R, \varphi, z; b_1, b_2; m)$ as given by (30), thus avoiding a lot of numerical

integration. However, terms $B_{mn}^{(i)}(r, \theta, \phi)$, $C_{mn}^{(i)}(r, \theta, \phi)$ and $E_{mn}^{(i)}(r, \theta, \phi)$ in the expression (21) for $V_i'(\vec{x})$ have to be integrated over φ numerically since the relationship between ϕ and φ is not straightforward for the three-dimensional case.

After applying the no-slip condition (22a) to M_1 discrete points on S_p and applying the weighted averaging condition (32c) to N_2 discrete rings on S_w- with M_2 weight functions chosen in (32d), we have (for i=1,2,3)

$$\underbrace{\sum_{n=1}^{n}\sum_{m=0}^{n}}_{M_1 \text{ terms}}\left[B_{mn} B_{mn}^{(i)}(a,\theta_p,\phi_p) + C_{mn} C_{mn}^{(i)}(a,\theta_p,\phi_p) + E_{mn} E_{mn}^{(i)}(a,\theta_p,\phi_p)\right]$$
$$+\frac{1}{8\pi}\sum_{n=2}^{N_2-1}\sum_{m=0}^{M_2-1}\sum_{j=1}^{3}\sum_{\alpha=1}^{3} f_{jm}(R_{n+\alpha-2})\, G_{ij}^{mn\alpha}(R_p,\varphi_p,z_p) = V_i'^{(p)}(\theta_p,\phi_p),$$

$$\text{at}\quad \vec{x} = (a,\theta_p,\phi_p) = (R_p,\varphi_p,z_p) \in S_p\ ,\quad p = 1,2,3,\cdots,M_1\ ; \tag{33a}$$

$$\underbrace{\sum_{n=1}^{n}\sum_{m=0}^{n}}_{M_1 \text{ terms}}\left[B_{mn} B_{mn\ell}^{(i)}(R_q) + C_{mn} C_{mn\ell}^{(i)}(R_q) + E_{mn} E_{mn\ell}^{(i)}(R_q)\right]$$
$$+\frac{1}{8}\sum_{n=2}^{N_2-1}\sum_{j=1}^{3}\sum_{\alpha=1}^{3}\Big\{ f_{j\ell}(R_{n+\alpha-2})\, I_{ij}^{n\alpha}(R_q,\ell)\,\epsilon_{i\ell} + f_{j,\ell+2}(R_{n+\alpha-2})\, I_{ij}^{n\alpha}(R_q,\ell+2)\,\epsilon_{i\ell}\left(1-\omega_{\ell-M_2+2}\right)$$
$$+ f_{j,\ell-2}(R_{n+\alpha-2})\, I_{ij}^{n\alpha}(R_q,\ell-2)\,\omega_{\ell-2}\Big\},\ \text{for}\quad \begin{array}{l} q = 1,2,3,\cdots,N_2, \\ \ell = 0,1,2,\cdots,M_2-1, \\ (\ell\neq 0 \text{ when } i=2)\ ; \end{array} \tag{33b}$$

where

$$\epsilon_{i\ell} = \begin{cases} 2 & \text{when } \ell = 0 \text{ and } i = 1 \text{ or } 3\ , \\ 1 & \text{when } \ell \neq 0\ ; \end{cases} \tag{33c}$$

$$\omega_s = \begin{cases} 0 & \text{when } s < 0\ , \\ 1 & \text{when } s \geq 0\ ; \end{cases} \tag{33d}$$

$$I_{ij}^{n\alpha}(R,\ell) = A_\alpha^{(n)} g_{ij}^a(R;\hat{R}_{n+1},\hat{R}_n;\ell,3) + B_\alpha^{(n)} g_{ij}^b(R;\hat{R}_{n+1},\hat{R}_n;\ell,2)$$
$$+ C_\alpha^{(n)} g_{ij}^c(R;\hat{R}_{n+1},\hat{R}_n;\ell,1) . \tag{33e}$$

Here $A_\alpha^{(n)}$, $B_\alpha^{(n)}$, $C_\alpha^{(n)}$ are given by (27a); $\hat{R}_n$ by (26); g_{ij}^a, g_{ij}^b and g_{ij}^c by Appendix. In (33a) and (33b), the Lamb's series is truncated to M_1 terms. Note that $B_{0n}^{(i)}(r,\theta,\phi)\equiv 0$ so that the sequence in which the terms are taken is C_{01}, E_{01}, B_{11}, C_{11}, E_{11}, C_{02}, E_{02}, B_{12}, C_{12}, E_{12}, B_{22},.... The term f_{20} does not appear since $\sin m\varphi\equiv 0$ when $m=0$. The $B_{mn\ell}^{(i)}(R_q)$, $C_{mn\ell}^{(i)}(R_q)$, $E_{mn\ell}^{(i)}(R_q)$ represent the weighted integrals of $B_{mn}^{(i)}(a,\theta,\phi)$, $C_{mn}^{(i)}(a,\theta,\phi)$, $E_{mn}^{(i)}(a,\theta,\phi)$ over φ and have to be numerically evaluated:

$$B_{mn\ell}^{(i)}(R) = \int_0^{2\pi} B_{mn}^{(i)}(r,\theta,\phi)\, w_{i\ell}(\varphi)\, d\varphi, \tag{33f}$$

$$C_{mn\ell}^{(i)}(R) = \int_0^{2\pi} C_{mn}^{(i)}(r,\theta,\phi)\, w_{i\ell}(\varphi)\, d\varphi, \tag{33g}$$

$$E_{mn\ell}^{(i)}(R) = \int_0^{2\pi} E_{mn}^{(i)}(r,\theta,\phi)\, w_{i\ell}(\varphi)\, d\varphi, \tag{33h}$$

where $(R,\varphi,0)=(r,\theta,\phi)$ with R=const. is a ring in the plane wall and $w_{i\ell}(\varphi)$ is given by (32d).

Equations (33a) and (33b) constitute $N_T=3M_1+(3M_2-1)N_2$ equations, which can be solved for N_T unknowns: B_{mn}, C_{mn}, E_{mn} and $f_{jm}(R_q)$. The force and torque then are found from (18) and (19).

3. AXISYMMETRIC SOLUTIONS

Solutions will be presented for two axisymmetric cases: (i) the sphere moves along the orifice axis in quiescent fluid; (ii) Sampson's flow past a stationary sphere. Due to the axial symmetry, $F_x=T_y=0$ in (3). To compare the results with Dagan, Weinbaum and Pfeffer (1982b), we redefine the force and torque correction factors as follows:

$$F_z = 6\pi\mu a\ (U_z F_z^t + V_{zo}\tilde{F}_z^s), \tag{34}$$

where

$$V_{zo} = \frac{3q}{2\pi} \tag{34a}$$

is the flow velocity at the center of the orifice opening (0, 0, 0) and $\tilde{F}_z^s$ is related to F_z^s, defined by (3), as follows:

$$F_z^s = \tilde{F}_z^s\ (1 + z^2). \tag{34b}$$

We follow the second scheme by Dagan, Weinbaum and Pfeffer (1982b) for selection of collocation points on the sphere surface S_p, i.e. for a given even number M_2, taking $\vartheta=(i-1)(180^\circ/(M_2-2))$ for $i=1,2,\cdots,M_2-1$ and then replacing 0°, 90°, 180° by $0^\circ+\delta$, $90^\circ-\delta$, $90^\circ+\delta$ and $180^\circ-\delta$ to avoid the singularity of the coefficient matrix in (28a) and (28b). Our numerical tests show that a choice of $\delta=0.01^\circ$ can secure the convergence to five significant digits of both F_z^t and $\tilde{F}_z^s$ for all spacings and radii, if all the other collocation points on S_p and S_w are unchanged. Part of

these tests are listed in Table 1, where the last case, a large radius (a=10) and a small spacing ($z_o/a=1.1$), is among the most unfavorable. Table 2 shows the convergence tests for M_1. It can be seen that while for the case with a small radius (a=0.1) and a big spacing ($z_o/a=5.0$), $M_1=6$ is sufficient to give five significant digits accurately, for the worst case (a=10.0, $z_o/a=1.1$) $M_1=28$ can only give three or two significant digits for F_z^t and $\tilde{F}_z^s$ respectively.

It is more difficult to select the collocation points on the infinite plane wall S_w-. To account for the sharp changes in the wall stresses near the pore edge, $R_1=1.0$ should be included and more points should be concentrated near R=1.0, in any reasonable scheme. To eliminate the arbitrariness in selecting points, we conducted convergence tests for N_2 using a particular scheme:

$$R_n = 1.0 + (R_u - 1.0)\left(\frac{n-1}{N_2-1}\right)^3 , \quad n=1,2,3,\cdots,N_2. \qquad (35)$$

Some results of such tests are summarized in Table 3. It can be seen that the convergence range from five to four significant digits except for the worst case (a=10, $z_o/a=1.1$) where there is only two or three digit accuracy. Other schemes for selection of the collocation points on S_w- were also tested and convergence was also reached. For example, a scheme with exponentially increasing spacings between the points gave $F_z^t=-1.0663$ and $\tilde{F}_z^s=0.84823$ for a=0.1 and $z_o/a=5.0$ when $N_2 \geq 14$ (Compare with Table 3).

As mentioned in Section 2.3, the infinite plane wall S_w-

is truncated to a large but finite region ($1.0 \leqslant \tilde{R} \leqslant R_u$). The convergence tests are conducted for R_u. A typical test is presented in Table 4, where a fixed set of collocation points is chosen. The tests indicate that it is adequate to choose R_u as equal to twenty times either a or z_o, whichever is larger. However, R_u should be no less than 3, to account for the pore edge effect. This truncation can be justified by the rapid decay of $f_z(\tilde{R})$ with the increase of $\tilde{R}$, as shown in Fig. 4. It can be seen from the figure that when $\tilde{R}$ is large, $f_z(\tilde{R})$ decays in proportion to at least the fourth power of $(1/\tilde{R})$. In the case of a=10.0 and z_o=11.0, the wall stresses change tremendously near the pore edge ($\tilde{R}$=1) and the high stress region extends to a larger distance. This explains the relative slower convergence for the case with a large sphere and a small spacing. For the axisymmetric case, $f_R(\tilde{R})$ is less important than $f_z(\tilde{R})$.

In tables 5 and 6, the force correction factors F_z^t and $\tilde{F}_z^s$ are compared with the solutions given by Dagan, Weinbaum and Pfeffer (1982b), valid for $z_o/a \geqslant 1.1$, and by Davis (1983), correct to the order of a^3. Dagan, Weinbaum and Pfeffer (1982b) satisfied the no-slip conditions analytically on the plane wall and numerically using the collocation technique on the sphere surface, whereas the present work have used the collocation technique on both the boundaries. Therefore the former should be more accurate in principle. It can be seen that the present results differ

from those of Dagan, Weinbaum and Pfeffer (1982b) by one to a few percent for most of the cases in the tables, a reasonable accuracy for the integral equation method in general. On the other hand, the results by Davis (1983), while having a comparable accuracy with ours for small particles ($a \leqslant 1.0$), deteriorates with the increase of the sphere radius a, as expected.

Although the solutions by Dagan, Weinbaum and Pfeffer (1982b) is more accurate in principle and more efficient in computation, it cannot treat the case in which the sphere crosses the orifice opening. In contrast, our present method applies to this case without difficulty. In Tables 7 and 8, we present the typical force correction factors F_z^t and $\tilde{F}_z^s$ for $z_o/a \leqslant 1.1$. These values in the immediate vicinity of the pore opening are very important in treating the entrance phenomena such as the fine structure of a permeable membrane (see Chapter 2) and the collection efficiency of membranes and filters. The latter is critically dependent on the values of F_z^t and $\tilde{F}_z^s$ near the pore opening. In these tables, no convergence is reached within reasonable computation efforts when $a=1.0$ and $z_o/a < 0.1$ (i.e. almost chocking of the pore opening by the sphere) because of the very sharp stress changes in the narrow gap between the sphere and the pore edge. In fact, F_z^t should approach infinity as z_o approaches zero when $a=1.0$.

The neutrally buoyant velocity of a sphere carried by the flow towards the pore is obtained by requiring a zero drag

force on the sphere, i.e. $F_z=0$ in (34). Then

$$\frac{U_z}{V_{zo}} = -\frac{\tilde{F}_z^s}{F_z^t} . \qquad (35)$$

The results from this equation are plotted for $z_o/a=0.0--1.1$ in Fig. 5. At $z_o/a=1.1$, the present solution matches the solution by Dagan , Weinbaum and Pfeffer (1982b), as shown by the arrowheads on the right side of the figure. For comparison, the figure also indicates the zero-drag velocity of a sphere carried axisymmetrically by the flow in an infinite circular cylindrical tube (Haberman and Sayre 1958), shown by the arrowheads on the left side. Obviously, the present results for $z_o=0$ are quite close to this limiting case, in spite of our neglecting the pore length.

4. THREE-DIMENSIONAL SOLUTIONS

As noted in Section 2, for the general three-dimensional motion of a sphere near a pore, equation (3), suggested by Dagan, Weinbaum and Pfeffer (1983), is not a rigorous description for the force and torque on the sphere. Firstly, when the sphere translates in one direction (e.g. the x-direction), a side force is usually generated in the lateral direction (e.g. the z-direction) due to the geometric asymmetry. This side force is small and would vanish for a rigid sphere translating next to an infinite plane wall without an orifice. Secondly, in the last equation of (3), two separate shearing flows were used to represent the effect of the Sampson flow through an orifice in the presence of a stationary sphere. This formulation was an acceptable approximation, since no better solution was available. However, it is not rigorous theoretically since the V_x^s and V_z^s in (3) are not independent of each other (see (11a) and (11b)) and thus $T_y^{s,x}$ and $T_y^{s,z}$ are related. The actual Sampson flow is described by a single torque correction factor scaled by the chracteristic velocity for this flow. Subject to these considerations, we replace equation (3) by the following formulas for the force and torque on the sphere:

$$F_x = 6\pi\mu a\ (U_x F_x^{t,x} + U_z F_x^{t,z} + a\Omega F_x^r + V_{zo}\tilde{F}_x^s),$$

$$F_z = 6\pi\mu a\ (U_x F_z^{t,x} + U_z F_z^{t,z} + a\Omega F_z^r + V_{zo}\tilde{F}_z^s), \qquad (36)$$

$$T_y = 8\pi\mu a^2 (U_x T_y^{t,x} + U_z T_y^{t,z} + a\Omega T_y^r + V_{zo}\tilde{T}_y^s),$$

where V_{zo}, given by (34a), is the flow velocity at the center of the pore opening and the other notations are the same as in (3).

One peculiar feature of the three-dimensional problem is the requirement of excessive computation time, mainly due to the great amount of numerical integration in (33f), (33g) and (33h). The practical consideration of both the cost and the accuracy has restricted the order of harmonics in (31) to $m < 8$ in this work. For most of our computations, the number of collocation points on the sphere surface is chosen as $M_1=4$ and the position of points is selected as shown in Fig. 6, according to Ganatos, Pfeffer and Weinbaum (1978). Some schemes with $M_1=12$ were also tested for the axisymmetric case. They did not always give improvement in accuracy. The number of collocation rings on the plane wall was chosen to lie in the range $N_2=10--18$. With $M_1=4$, $M_2=8$ and $N_2=10$, the number of simultaneous equations to be solved is $N_T=242$, which is close to the limit of the IBM 3081 computer. One run of such a job requires the CPU time of 16 minutes and a memory of 683kB. In view of the excessive cost, only a limited number of representative convergence tests were run.

Table 9 shows the convergence tests for M_2. It can be seen that in order for the major correction factors ($F_x^{t,x}$, $F_z^{t,z}$, $\tilde{F}_z^s$ and T_y^r) to converge to three significant digits, the required M_2 increases as the sphere goes from the pore axis outward. Table 10 presents the convergence test of all the twelve correction factors defined in (36) for M_2=5--8, with a=0.5, x_o=1.0 and z_o=1.0. Table 11 presents the corresponding convergence test for N_2=8--12. Both the tables show convergence to at least three significant digits for the major correction factors and to at least two digits for the rest of the factors, which are by themselves small.

The three-dimensional scheme described in Section 2.4 can also be applied to the axisymmetric case (x_o=0, U_x=0, Ω=0). In Table 12, such solutions for a small sphere (a=0.1) are favorably compared with our solutions using the method in Section 2.3 and with those by Dagan, Weinbaum and Pfeffer (1982b), by Davis (1983) and by Miyazaki and Hasimoto (1984). Miyazaki and Hasimoto's solution is derived for a translating stokeslet near a pore and is valid to the order of a. They present neither solutions for a rotating particle nor for flow past a stationary particle near a pore. In Fig. 7 and Fig. 8, the present solutions of both $F_x^{t,x}$ and $F_z^{t,z}$ for a=0.1 are compared with those by Miyazaki and Hasimoto (1984) for either x_o=0 (along the pore axis) or z_o=0 (at the pore opening). The agreement is excellent.

In Table 13, additional comparisons are shown for axisymmetric cases with a=0.5--2.5. Compared to the more accurate

solution of Dagan, Weinbaum and Pfeffer (1982b), the error for a=0.5 is within three percent and thus acceptable. But with the increase of the sphere radius a, the present method become less accurate; for a=2.5, the error is as high as thirty percent. Here the accuracy is limited not by the method itself, but by the small number of collocation points or rings (M_1 or N_2) that can be handled for a reasonable computation cost.

It is expected that when the sphere is positioned far away from the pore opening, the effect of the pore should be negligible. Therefore our solutions should approach those for a sphere near an infinite solid plane, as given by Brenner (1961), Goldman, Cox and Brenner (1967) and Cox and Brenner (1967). As can be seen from Table 14, when the sphere is distant from the wall ($z_o/a=10$), this is true. However, when the sphere is close to the wall, our solutions break down. To explain this, let us compare the zeroth to fourth harmonics, $f_{3m}(\tilde{R})$ as defined by (31), for $z_o/a=10$ (Fig. 9) and 1.1 (Fig. 10). When the sphere is close to the wall, very sharp changes in stresses would occur in a local area, corresponding to a very narrow range of φ. Therfore, very high order of harmonics should be required to describe such changes adequately. Since we restricted our program to $M_2 \leq 8$, our solutions are neither accurate in the neighborhood of the plane wall, nor for a very large x_o. With a faster computer one would be able to include higher order harmonics and thus be able to expand the range of validity.

In spite of the above restriction, our present solutions are valid within a few pore radii from the pore axis, including the vicinity of the pore opening but excluding the neighborhood of the plane wall. As mentioned in Section 3, the sphere motion in the vicinity of the pore opening is of primary importance for many entrance phenomena. The approximate theory by Dagan, Weinbaum and Pfeffer (1983) fails to treat this vicinity. Miyazaki and Hasimoto's solutions (1984) for a translating stokeslet provides a reasonable approximation for the translation of a very small sphere. The present solutions are the first three-dimensional solutions for a finite sphere near the pore opening, including the cases where the sphere translates, rotates or stays in a Sampson flow.

In Figs. 11--19, we present the force and torque correction factors $F_z^{t,z}$, $\tilde{F}_z^s$, $F_x^{t,x}$, T_y^r, $F_x^{t,z}$, $\tilde{F}_x^s$, $\tilde{T}_y^s$, F_z^r, F_x^r for a medium size sphere (a=0.5 and z_o/a=0--10). The curves are plotted only for the ranges of x_o, in which our solutions are considered to be valid. The remaining correction factors in (36) can be found through the reciprocal theorem (Happel and Brenner 1973, p.85) as follows:

$$F_z^{t,x} = F_x^{t,z}, \quad T_y^{t,z} = \frac{3}{4} F_z^r, \quad T_y^{t,x} = \frac{3}{4} F_x^r. \tag{37}$$

Of the above twelve correction factors, those related to the sphere rotation (with superscript r) and the off-axis Sampson flow (with superscript s) have not been previously presented for a particle or for a stokeslet, for the orifice

entrance geometry. It can be observed from these figures that

(1) $F_z^{t,z}$, $\tilde{F}_z^s$, $F_x^{t,x}$ and T_y^r are of the order of unity whereas the others are one order of magnitude smaller;

(2) While $F_z^{t,z}$ and $\tilde{F}_z^s$ change remarkably between the axisymmetric values for $x_o=0$ and the far field solutions for large x_o, $F_x^{t,x}$ and T_y^r are relatively insensitive to the radial position x_o of the sphere center. This can be explained by the fact that the translation normal to the wall or the Sampson flow induces a much larger flow through the pore than the translation parallel to the wall or the rotation so that the pore opening has a greater influence on $F_z^{t,z}$ and $\tilde{F}_z^s$;

(3) $F_x^{t,z}$, $F_z^{t,x}$, F_z^r, $T_y^{t,z}$ and $\tilde{T}_y^s$ vanish for the two extreme cases, namely $x_o \to 0$ and $x_o \to \infty$. All these correction factors are negligible except in the vicinity of the pore edge;

(4) $\tilde{F}_x^s$, F_x^r and $T_y^{t,x}$ change from zero to almost the far field values when x_o increases from zero to about 1.0 or 1.5.

The above observations agree with our qualitative assumptions regarding the three-dimensional behavior of the correction factors in Chapter 2. It is seen that most of the rapid changes in the hydrodynamic force and torque coefficients occur in the range of validity of the present solution. The relatively slow transition to the far field

solutions, described by Brenner and co-workers, can be reasonably extrapolated by the method proposed in Section 3 of Chapter 2.

In Figs. 20 and 21, the present results are compared with the approximate evaluations of $F_Z^{t,z}$ and F_Z^s (defined as $F_Z^s=(V_{ZO}/V_Z^s)\tilde{F}_Z^s$) by the method proposed in Section 3 of Chapter 2. It seems that the latter method gives fairly good, if not quantitatively accurate, approximations. In view of the expensive computation cost of the present method, the approximate method in Chapter 2 may be preferred in problems where lower accuracy is adequate.

5. CONCLUDING REMARKS

In this chapter we have proposed a combined multipole series and integral equation method to treat the problem of a finite sphere entering a zero thickness orifice. This combined method takes advantage of the flexibility of the integral equation method in treating a complicated geometry and reduces its disadvantages of lower accuracy and greater computation time by using the multipole series representation for the disturbance on the sphere surface.

For the axisymmetric case, the present solutions compare favorably with other solutions. In addition, the present solutions are valid irrespective of the position of the sphere along the pore axis. This more difficult case of a finite sphere crossing the pore opening could not be treated previously.

For the three-dimensional case, a mixed weighted residual and collocation technique is developed. This enables us to obtain a solution for the general three-dimensional motion of an arbitrarily positioned finite sphere not far off-the-pore-axis, including the case where the sphere is close to the pore opening. For a small sphere, the present solution is in good agreement with Miyazaki and Hasimoto's solution for a translating stokeslet in the same geometry. When the sphere is finite, no other solution is presently available for the entrance region near the pore opening. This region is very important in many problems concerning

entrance penomena because most of the rapid changes in the hydrodynamic force and torque occur there.

The main restriction to the validity of the present three-dimensional solution is the excessive computation cost. The limited number of collocation points or rings makes the present solution invalid in the neighborhood of the plane wall or beyond a few pore radii from the pore axis. However, if one could work with a faster computer, the range of validity could be extended in principle by including more terms in the present series-integral solution.

APPENDIX

The Evaluation of $H_{ij}^{(\beta)}(R,\varphi,z;\ b_1,b_2;\ m)$

If all the variables in formula (29c), defining $H_{ij}^{(\beta)}(R,\varphi,z;\ b_1,b_2;\ m)$, are written in the coordinates $(\tilde{R},\tilde{\varphi},\tilde{z})$, the inner integrals over $\tilde{\varphi}$ can be expressed in terms of the following integrals:

$$C_0(l,p,A,B,\varphi) = \int_0^{2\pi} \frac{\cos l\tilde{\varphi}\, d\tilde{\varphi}}{[A^2-B^2\cos(\tilde{\varphi}-\varphi)]^{p/2}},$$

$$S_0(l,p,A,B,\varphi) = \int_0^{2\pi} \frac{\sin l\tilde{\varphi}\, d\tilde{\varphi}}{[A^2-B^2\cos(\tilde{\varphi}-\varphi)]^{p/2}}, \tag{A1}$$

where l=m-2, m-1, m, m+1, m+2; p=1, 3; A and B are given by

$$A^2 = \tilde{R}^2 + R^2 + z^2, \quad B^2 = 2\tilde{R}R. \tag{A2}$$

Here (R, φ, z) is a fixed field point, $(\tilde{R}, \tilde{\varphi}, 0)$ is the variable point under integration.

By expressing the $\cos l\tilde{\varphi}$ or $\sin l\tilde{\varphi}$ in (A1) in terms of a polynomial of $\cos\tilde{\varphi}$, these integrals can be calculated as follows:

$$C_0(l,p,A,B,\varphi) = \cos l\varphi\, D(l,p,A,B),$$

$$S_0(l,p,A,B,\varphi) = \sin l\varphi\, D(l,p,A,B), \tag{A3}$$

where

$$D(l,p,A,B) = \frac{1}{[A^2+B^2]^{p/2}} \sum_{q=0}^{l} \alpha_{lq}\, G(q,p,k), \tag{A4}$$

$$k^2 = \frac{2B^2}{A^2+B^2} = \frac{4\tilde{R}R}{(\tilde{R}+R)^2+z^2}, \quad (0 \leqslant k < 1), \tag{A5}$$

$$\alpha_{00} = 1, \quad \alpha_{\ell q} = \frac{(-1)^q 2^{2q} \ell\, \Gamma(\ell+q)}{\Gamma(2q+1)\Gamma(\ell-q+1)}, \tag{A6}$$

$$G(q,p,k) = \int_0^{\pi/2} \frac{\cos^{2q}\tau\, d\tau}{[1-k^2\sin^2\tau]^{p/2}}, \tag{A7}$$

The G(q,p,k) can be related to the complete elliptic integrals K(k) and E(k) of the first and second kinds through the recurrence formulas. These formulas are exact mathematically. But they turn out to be unstable numerically unless k is quite close to unity, say $k \geqslant 0.90$.

For $k \leqslant 0.90$, we find $B^2/A^2 = k^2/(2-k^2) < 0.681$ and thus can expand the denominator of (A1) in a series of B^2/A^2 to obtain

$$D(\ell,p,A,B) = \frac{2\pi}{A^p} \sum_{s=0}^{\infty} \beta_{\ell+2s,\ell,p}\, u^{\ell+2s}, \tag{A8}$$

where

$$u \equiv \frac{B^2}{A^2} = \frac{2\tilde{R}R}{\tilde{R}^2+R^2+z^2}, \tag{A9}$$

$$\beta_{00p} = 1, \quad \beta_{\ell+2s,\ell,p} = \frac{1}{2^{\ell+2s}} \cdot \frac{(2\ell+4s+p-2)!!\,\Gamma(\ell+2s+1)}{(2\ell+4s)!!\,\Gamma(s+1)\Gamma(\ell+s+1)}. \tag{A10}$$

To explain the meaning of k, we can see from (A5) that k reaches the maximum at $\tilde{R}=\sqrt{R^2+z^2}$. If z=0, we would have k=1 at $\tilde{R}=R$, a singularity for the integrals in (A1) or (A7). The values of $k \geqslant 0.90$ corresponds to $\left(\frac{1-k_c}{1+k_c}R \leqslant \tilde{R} \leqslant \frac{1+k_c}{1-k_c}R\right)$ for the case of z=0, or to a smaller neighborhood of $\tilde{R}=\sqrt{R^2+z^2}$

for the case of $z \neq 0$. Here $k_c = \sqrt{1-(0.90)^2}$. Outside such a neighborhood we have $k \leq 0.90$. If $z \geq \frac{2k_c}{0.90} R$, the whole plane wall ($1 \leq \tilde{R} < \infty$) would correspond to $k \leq 0.90$.

In the range of $k \leq 0.90$, we can also carry out the integration over $\tilde{R}$ in (29c) analytically, by integrating (A8) term by term with respect to $\tilde{R}$ and using

$$\int_{b_1}^{b_2} \frac{\hat{R}^n}{(\hat{R}^2+R^2+z^2)^{p/2}} \left(\frac{2\hat{R}R}{\hat{R}^2+R^2+z^2}\right)^{l+2s} d\hat{R} = \frac{(2R)^{l+2s}}{(R^2+z^2)^{\frac{1}{2}(l-n+2s+p-1)}} Y\left(l+2s+n, l+2s+\frac{p-1}{2}, R, z; b_1, b_2\right), \tag{A11}$$

where

$$Y(i,q,R,z;b_1,b_2) \equiv \int_{b_1/\sqrt{R^2+z^2}}^{b_2/\sqrt{R^2+z^2}} \frac{x^i\,dx}{(x^2+1)^{q+\frac{1}{2}}}$$

$$= \begin{cases} \sum_{j=0}^{\infty} \hat{C}_{jq}\, P_1\left(i+2j+1, \frac{b_1}{\sqrt{R^2+z^2}}, \frac{b_2}{\sqrt{R^2+z^2}}\right), & \text{when } b_1 < b_2 < \sqrt{R^2+z^2}; \\ \sum_{j=0}^{\infty} \hat{C}_{jq}\, P_2\left(2q+2j-i, \frac{b_1}{\sqrt{R^2+z^2}}, \frac{b_2}{\sqrt{R^2+z^2}}\right), & \text{when } b_2 > b_1 > \sqrt{R^2+z^2}. \end{cases} \tag{A12}$$

$$P_1(i, b_1', b_2') \equiv \int_{b_1'}^{b_2'} x^{i-1} dx = \frac{1}{i}\left[b_2'^{\,i} - b_1'^{\,i}\right], \tag{A13a}$$

$$P_2(i, b_1', b_2') \equiv \int_{b_1'}^{b_2'} x^{-i-1} dx = \begin{cases} \frac{1}{i}\left[b_1'^{\,-i} - b_2'^{\,-i}\right], & \text{when } i \neq 0; \\ \ln \frac{b_2'}{b_1'}, & \text{when } i = 0. \end{cases} \tag{A13b}$$

$$\hat{C}_{0q} = 1, \quad \hat{C}_{jq} = (-1)^j \prod_{n=1}^{j} \left[\frac{2(q+j)-(2n-1)}{(2n)}\right]. \tag{A14}$$

In the range of $k \geq 0.90$, the integration over $\tilde{R}$ in (29c) has to be performed numerically if $z \neq 0$, but it can be performed analytically if $z=0$. In the latter case we expand the elliptic integrals, related to $G(q,p,k)$ in (A4), with respect to its complimentary modulus $k'=\sqrt{1-k^2}$ to give

$$D(l,1,A,B) = \frac{1}{(A^2+B^2)^{1/2}} \sum_{s=0}^{\infty} \left[\gamma_{ls}^{(1)} - \gamma_{ls}^{(2)} \ln k'\right] k'^{2s}, \tag{A15a}$$

$$D(l,3,A,B) = \frac{1}{(A^2+B^2)^{3/2}} \left\{ \sum_{s=0}^{\infty} \left[\delta_{ls}^{(1)} - \delta_{ls}^{(2)} \ln k'\right] k'^{2s} + k'^{-2} \right\}, \tag{A15b}$$

where

$$k' \equiv \sqrt{1-k^2} = \left[\frac{(\tilde{R}-R)^2 + z^2}{(\tilde{R}+R)^2 + z^2}\right]^{1/2}, \tag{A16}$$

$$\gamma_{ls}^{(1)} = \sum_{q=0}^{l} \alpha_{lq} C_{qs}, \qquad \gamma_{ls}^{(2)} = \sum_{q=0}^{l} \alpha_{lq} d_{qs},$$

$$\delta_{ls}^{(1)} = \sum_{q=0}^{l} \alpha_{lq} p_{qs}, \qquad \delta_{ls}^{(2)} = \sum_{q=0}^{l} \alpha_{lq} q_{qs}. \tag{A17}$$

$$\begin{aligned}
&d_{00} = 1, \\
&d_{0s} = \left[\frac{(2s-1)!!}{(2s)!!}\right]^2, \quad (s \geq 1), \\
&d_{1s} = d_{0s} - q_{1s}, \\
&d_{ms} = \frac{2m-2}{2m-1} 2 d_{m-1,s} - \frac{2m-3}{2m-1} d_{m-2,s} \\
&\qquad + \sum_{p=0}^{s} \left[\left(\frac{2m-3}{2m-1}\right) d_{m-2,p} - \left(\frac{2m-2}{2m-1}\right) d_{m-1,p}\right], \quad (m \geq 2).
\end{aligned} \tag{A18}$$

$$\begin{aligned}
&C_{00} = \ln 4, \\
&C_{0s} = d_{0s}\left[\ln 4 - \sum_{p=1}^{s} \frac{1}{p(2p-1)}\right], \quad (s \geq 1), \\
&C_{1s} = C_{0s} - p_{1s}, \\
&C_{ms} = \frac{2m-2}{2m-1} 2 C_{m-1,s} - \frac{2m-3}{2m-1} C_{m-2,s} + \sum_{p=0}^{s} \left[\left(\frac{2m-3}{2m-1}\right) C_{m-2,p} - \left(\frac{2m-2}{2m-1}\right) C_{m-1,p}\right], \\
&\qquad (m \geq 2).
\end{aligned} \tag{A19}$$

$$p_{0s} = e_{s+1} \quad , \qquad p_{1s} = \sum_{p=0}^{s} (C_{0p} - e_p) \ ,$$

$$p_{ms} = p_{m-1,s} + \sum_{p=0}^{s} (C_{m-1,p} - p_{m-1,p}) \ , \ (m \geq 2) \ . \tag{A20}$$

$$q_{0s} = g_{s+1} \ , \qquad q_{1s} = \sum_{p=0}^{s} (d_{0p} - g_p) \ ,$$

$$q_{ms} = q_{m-1,s} + \sum_{p=0}^{s} (d_{m-1,p} - q_{m-1,p}) \ , (m \geq 2) \ . \tag{A21}$$

$$g_0 = 0 \ ,$$

$$g_s = d_{0s} \frac{2s}{(2s-1)} \ , \ (s \geq 1) \ . \tag{A22}$$

$$e_0 = 1 \ ,$$

$$e_s = g_s \left[\ln 4 - \sum_{p=1}^{s-1} \frac{1}{p(2p-1)} - \frac{1}{2s(2s-1)} \right] , \ (s \geq 1) \ . \tag{A23}$$

and δ_{pq} is given by (A6). After substituting (A3) and (A4) along with (A15)--(A23) into (29c), we need to evaluate the following integrals:

$$T_{1s}(R, n, b_1, b_2) = \int_{b_1}^{b_2} \frac{\tilde{R}^n}{(\tilde{R}+R)^3} \left(\frac{\tilde{R}-R}{\tilde{R}+R} \right)^{2s} d\tilde{R} \ , \tag{A24a}$$

$$T_{2s}(R, n, b_1, b_2) = \int_{b_1}^{b_2} \frac{\tilde{R}^n}{(\tilde{R}+R)^3} \left(\frac{\tilde{R}-R}{\tilde{R}+R} \right)^{2s} \ln \left| \frac{\tilde{R}-R}{\tilde{R}+R} \right| d\tilde{R} \ , \tag{A24b}$$

$$J_{3s}(R, n, b_1, b_2) = \int_{b_1}^{b_2} \frac{\tilde{R}^n}{\tilde{R}+R} \left(\frac{\tilde{R}-R}{\tilde{R}+R} \right)^{2s} d\tilde{R} \ , \tag{A24c}$$

$$J_{4s}(R, n, b_1, b_2) = \int_{b_1}^{b_2} \frac{\tilde{R}^n}{\tilde{R}+R} \left(\frac{\tilde{R}-R}{\tilde{R}+R} \right)^{2s} \ln \left| \frac{\tilde{R}-R}{\tilde{R}+R} \right| d\tilde{R} \ . \tag{A24d}$$

These integrals can be evaluated by using transformation $t=(\tilde{R}-R)/(\tilde{R}+R)$ and expanding the integrands with respect to t as follows:

$$T_{1S}(R,n,b_1,b_2)=\frac{R^{n-1}}{4}\sum_{m=0}^{\infty}\frac{\lambda_{mn}}{m+2S+1}\left[\left(\frac{b_2-R}{b_2+R}\right)^{m+2S+1}-\left(\frac{b_1-R}{b_1+R}\right)^{m+2S+1}\right], \tag{A25a}$$

$$T_{2S}(R,n,b_1,b_2)=\frac{R^{n-1}}{4}\sum_{m=0}^{\infty}\frac{\lambda_{mn}}{m+2S+1}\left[\left(\frac{b_2-R}{b_2+R}\right)^{m+2S+1}\left(\ln\left|\frac{b_2-R}{b_2+R}\right|-\frac{1}{m+2S+1}\right)\right.$$
$$\left.-\left(\frac{b_1-R}{b_1+R}\right)^{m+2S+1}\left(\ln\left|\frac{b_1-R}{b_1+R}\right|-\frac{1}{m+2S+1}\right)\right], \tag{A25b}$$

$$J_{30}(R,n,b_1,b_2)=R^n\left\{(-1)^n\ln\frac{b_2+R}{b_1+R}+\sum_{m=0}^{n}\frac{(-1)^{n-m}}{m}\left[\left(\frac{b_2}{R}\right)^m-\left(\frac{b_1}{R}\right)^m\right]\right\}, \tag{A25c}$$

$$J_{3S}(R,n,b_1,b_2)=R^n\sum_{m=0}^{\infty}\frac{\omega_{mn}}{m+2S+1}\left[\left(\frac{b_2-R}{b_2+R}\right)^{m+2S+1}-\left(\frac{b_1-R}{b_1+R}\right)^{m+2S+1}\right],$$

$$(S\geq 1), \tag{A25d}$$

$$J_{4S}(R,n,b_1,b_2)=R^n\sum_{m=0}^{\infty}\frac{\omega_{mn}}{m+2S+1}\left[\left(\frac{b_2-R}{b_2+R}\right)^{m+2S+1}\left(\ln\left|\frac{b_2-R}{b_2+R}\right|-\frac{1}{m+2S+1}\right)\right.$$
$$\left.-\left(\frac{b_1-R}{b_1+R}\right)^{m+2S+1}\left(\ln\left|\frac{b_1-R}{b_1+R}\right|-\frac{1}{m+2S+1}\right)\right]. \tag{A25e}$$

where

$$\left.\begin{aligned}&\lambda_{0n}=1\ ;\quad \lambda_{1n}=2n-1\ ;\\ &\lambda_{m1}=0\ ,\quad \lambda_{m2}=4\ ,\quad \lambda_{m3}=8m-4\ ,\\ &\lambda_{m4}=8(m^2-m+1)\ ,\\ &\lambda_{m5}=\tfrac{1}{3}(16m^3-24m^2+56m-24).\end{aligned}\right\}\ (m\geq 2). \tag{A26}$$

$$\omega_{m1}=2m+1\ ,\quad \omega_{m2}=2m^2+2m+1\ ,$$
$$\omega_{m3}=\tfrac{1}{3}(4m^3+6m^2+8m+3)\ . \tag{A27}$$

The series appearing in (A8)--(A23) converge rapidly.

Now we can express the coefficients g^a_{ij}, g^b_{ij}, g^c_{ij} in (30) in terms of the notation just introduced in this Appendix for either $k \leq 0.90$ or $k \geq 0.90$ (with z=0 only). If an interval (b_1, b_2) covers both the ranges of $k \leq 0.90$ and $k \geq 0.90$, this interval should be divided accordingly and then the integrals in each subinterval should be evaluated using the appropriate formulas respectively.

For brevity, in the following we omit the first three arguments of $g^a_{ij}(R; b_1, b_2; m, \beta)$ etc., namely $g^a_{ij}(m, \beta)$ standing for $g^a_{ij}(R; b_1, b_2; m, \beta)$ and so like.

<u>In the range of $k \leq 0.90$</u>

$$g^a_{11}(0,\beta) = \Lambda_0'(\beta) + \tfrac{1}{2} R^2 \Lambda_0(\beta) - R\Lambda_1(\beta+1) + \Lambda_0(\beta+2),$$

$$g^b_{11}(0,\beta) = 0,$$

$$g^c_{11}(0,\beta) = \tfrac{1}{2} R^2 \Lambda_0(\beta) - R\Lambda_1(\beta+1) + \tfrac{1}{2}\Lambda_2(\beta+2),$$

$$g^a_{11}(1,\beta) = \Lambda_1'(\beta) + \tfrac{3}{4} R^2 \Lambda_1(\beta) - R\Lambda_0(\beta+1) - \tfrac{1}{2} R\Lambda_2(\beta+1) + \tfrac{3}{4}\Lambda_1(\beta+2),$$

$$g^b_{11}(1,\beta) = 0$$

$$g^c_{11}(1,\beta) = \tfrac{1}{4} R^2 \Lambda_1(\beta) - \tfrac{1}{2} R\Lambda_2(\beta+1) + \tfrac{1}{4}\Lambda_3(\beta+2),$$

$$g^a_{11}(m,\beta) = \Lambda_m'(\beta) + \tfrac{1}{2} R^2 \Lambda_m(\beta) - \tfrac{1}{2} R\Lambda_{m-1}(\beta+1) - \tfrac{1}{2} R\Lambda_{m+1}(\beta+1) + \tfrac{1}{2}\Lambda_m(\beta+2),$$

$$(m \geq 2),$$

$$g^b_{11}(m,\beta) = \tfrac{1}{4} R^2 \Lambda_m(\beta) - \tfrac{1}{2} R\Lambda_{m-1}(\beta+1) + \tfrac{1}{4}\Lambda_{m-2}(\beta+2), \quad (m \geq 2),$$

$$g^c_{11}(m,\beta) = \tfrac{1}{4} R^2 \Lambda_m(\beta) - \tfrac{1}{2} R\Lambda_{m+1}(\beta+1) + \tfrac{1}{4}\Lambda_{m+2}(\beta+2), \quad (m \geq 2);$$

$$g^a_{12}(0,\beta) = g^b_{12}(0,\beta) = g^c_{12}(0,\beta) = 0,$$

$$g^a_{12}(1,\beta) = \tfrac{1}{4}R^2\Lambda_1(\beta) - \tfrac{1}{2}R\Lambda_0(\beta+1) + \tfrac{1}{4}\Lambda_1(\beta+2),$$

$$g^b_{12}(1,\beta) = 0$$

$$g^c_{12}(1,\beta) = -\tfrac{1}{4}R^2\Lambda_1(\beta) + \tfrac{1}{2}R\Lambda_2(\beta+1) - \tfrac{1}{4}\Lambda_3(\beta+2),$$

$$g^a_{12}(m,\beta) = 0, \quad (m\geq 2),$$

$$g^b_{12}(m,\beta) = \tfrac{1}{4}R^2\Lambda_m(\beta) - \tfrac{1}{2}R\Lambda_{m-1}(\beta+1) + \tfrac{1}{4}\Lambda_{m-2}(\beta+2), \ (m\geq 2),$$

$$g^c_{12}(m,\beta) = -\tfrac{1}{4}R^2\Lambda_m(\beta) + \tfrac{1}{2}R\Lambda_{m+1}(\beta+1) - \tfrac{1}{4}\Lambda_{m+2}(\beta+2), \ (m\geq 2);$$

$$g^a_{13}(0,\beta) = g^b_{13}(0,\beta) = 0$$

$$g^c_{13}(0,\beta) = R\tfrac{z}{2}\Lambda_0(\beta) - \tfrac{z}{2}\Lambda_1(\beta+1),$$

$$g^a_{13}(m,\beta) = 0, \quad (m\geq 1)$$

$$g^b_{13}(m,\beta) = \tfrac{1}{2}R\tfrac{z}{2}\Lambda_m(\beta) - \tfrac{1}{2}\tfrac{z}{2}\Lambda_{m-1}(\beta+1), \ (m\geq 1),$$

$$g^c_{13}(m,\beta) = \tfrac{1}{2}R\tfrac{z}{2}\Lambda_m(\beta) - \tfrac{1}{2}\tfrac{z}{2}\Lambda_{m+1}(\beta+1), \ (m\geq 1);$$

$$g^a_{21}(0,\beta) = g^b_{21}(0,\beta) = 0,$$

$$g^c_{21}(0,\beta) = \tfrac{1}{2}R^2\Lambda_0(\beta) - R\Lambda_1(\beta+1) + \tfrac{1}{2}\Lambda_2(\beta+2),$$

$$g^a_{21}(1,\beta) = \tfrac{1}{4}R^2\Lambda_1(\beta) - \tfrac{1}{2}R\Lambda_0(\beta+1) + \tfrac{1}{4}\Lambda_1(\beta+2),$$

$$g^b_{21}(1,\beta) = 0,$$

$$g^c_{21}(1,\beta) = \tfrac{1}{4}R^2\Lambda_1(\beta) - \tfrac{1}{2}R\Lambda_2(\beta+1) + \tfrac{1}{4}\Lambda_3(\beta+2),$$

$$g^a_{21}(m,\beta) = 0, \quad (m\geq 2)$$

$$g^b_{21}(m,\beta) = -\tfrac{1}{4}R^2\Lambda_m(\beta) + \tfrac{1}{2}R\Lambda_{m-1}(\beta+1) - \tfrac{1}{4}\Lambda_{m-2}(\beta+2), \ (m\geq 2),$$

$$g^c_{21}(m,\beta) = \tfrac{1}{4}R^2\Lambda_m(\beta) - \tfrac{1}{2}R\Lambda_{m+1}(\beta+1) + \tfrac{1}{4}\Lambda_{m+2}(\beta+2), \ (m\geq 2);$$

$$g^a_{22}(0,\beta) = g^b_{22}(0,\beta) = g^c_{22}(0,\beta) = 0,$$

$$g^a_{22}(1,\beta) = \Lambda_1'(\beta) + \tfrac{3}{4}R^2\Lambda_1(\beta) - R\Lambda_0(\beta+1) - \tfrac{1}{2}R\Lambda_2(\beta+1) + \tfrac{3}{4}\Lambda_1(\beta+2),$$

$$g^b_{22}(1,\beta) = 0$$

$$g^c_{22}(1,\beta) = -\tfrac{1}{4}R^2\Lambda_1(\beta) + \tfrac{1}{2}R\Lambda_2(\beta+1) - \tfrac{1}{4}\Lambda_3(\beta+2),$$

$$g^a_{22}(m,\beta) = \Lambda_m'(\beta) + \tfrac{1}{2}R^2\Lambda_m(\beta) - \tfrac{1}{2}R\Lambda_{m-1}(\beta+1) - \tfrac{1}{2}R\Lambda_{m+1}(\beta+1) + \tfrac{1}{2}\Lambda_m(\beta+2),$$

$(m \geq 2)$,

$$g^b_{22}(m,\beta) = -\tfrac{1}{4}R^2\Lambda_m(\beta) + \tfrac{1}{2}R\Lambda_{m-1}(\beta+1) - \tfrac{1}{4}\Lambda_{m-2}(\beta+2), \quad (m \geq 2),$$

$$g^c_{22}(m,\beta) = -\tfrac{1}{4}R^2\Lambda_m(\beta) + \tfrac{1}{2}R\Lambda_{m+1}(\beta+1) - \tfrac{1}{4}\Lambda_{m+2}(\beta+2), \quad (m \geq 2);$$

$$g^a_{23}(0,\beta) = g^b_{23}(0,\beta) = 0,$$

$$g^c_{23}(0,\beta) = Rz\Lambda_0(\beta) - z\Lambda_1(\beta+1),$$

$$g^a_{23}(m,\beta) = 0, \quad (m \geq 1),$$

$$g^b_{23}(m,\beta) = -\tfrac{1}{2}Rz\Lambda_m(\beta) + \tfrac{1}{2}z\Lambda_{m+1}(\beta+1), \quad (m \geq 1),$$

$$g^c_{23}(m,\beta) = \tfrac{1}{2}Rz\Lambda_m(\beta) - \tfrac{1}{2}z\Lambda_{m+1}(\beta+1), \quad (m \geq 1);$$

$$g^a_{31}(0,\beta) = g^b_{31}(0,\beta) = 0,$$

$$g^c_{31}(0,\beta) = Rz\Lambda_0(\beta) - z\Lambda_1(\beta+1),$$

$$g^a_{31}(m,\beta) = 0, \quad (m \geq 1),$$

$$g^b_{31}(m,\beta) = \tfrac{1}{2}Rz\Lambda_m(\beta) - \tfrac{1}{2}z\Lambda_{m+1}(\beta+1), \quad (m \geq 1),$$

$$g^c_{31}(m,\beta) = \tfrac{1}{2}Rz\Lambda_m(\beta) - \tfrac{1}{2}z\Lambda_{m+1}(\beta+1), \quad (m \geq 1);$$

$$g^a_{32}(0,\beta) = g^b_{32}(0,\beta) = g^c_{32}(0,\beta) = 0,$$

$$g^a_{32}(m,\beta) = 0 \quad , \quad (m \geq 1),$$

$$g^b_{32}(m,\beta) = \frac{1}{2} R z \Lambda_m(\beta) - \frac{1}{2} z \Lambda_{m-1}(\beta+1), \quad (m \geq 1),$$

$$g^c_{32}(m,\beta) = -\frac{1}{2} R z \Lambda_m(\beta) + \frac{1}{2} z \Lambda_{m+1}(\beta+1), \quad (m \geq 1);$$

$$g^a_{33}(m,\beta) = \Lambda'_m(\beta) + z^2 \Lambda_m(\beta) \quad , \quad (m = 0, 1, 2, \cdots),$$

$$g^b_{33}(m,\beta) = g^c_{33}(m,\beta) = 0 \quad , \quad (m = 0, 1, 2, \cdots).$$

where

$$\Lambda'_m(\beta) = 2\pi \sum_{s=0}^{\infty} \beta_{m+2s,m,1} \frac{(2R)^{m+2s}}{(R^2+z^2)^{\frac{1}{2}(m-\beta+2s)}} Y(m+2s+\beta, m+2s, R, z; b_1, b_2),$$

$$\Lambda_m(\beta) = 2\pi \sum_{s=0}^{\infty} \beta_{m+2s,m,3} \frac{(2R)^{m+2s}}{(R^2+z^2)^{\frac{1}{2}(m-\beta+2s+2)}} Y(m+2s+\beta, m+2s+1, R, z; b_1, b_2),$$

and $Y(i,q,R,z;\ b_1,b_2)$ is defined by (A12).

<u>In the range of $k \geq 0.90$ (for $z=0$ only)</u>

$$g^a_{11}(0,\beta) = J_0(\beta) + 2J_{30}(R,\beta,b_1,b_2) + \frac{1}{2} R^2 W_0(\beta) - R W_1(\beta+1) + \frac{1}{2} W_0(\beta+2),$$

$$g^b_{11}(0,\beta) = 0 \ ,$$

$$g^c_{11}(0,\beta) = 2J_{30}(R,\beta,b_1,b_2) + \frac{1}{2} R^2 W_0(\beta) - R W_1(\beta+1) + \frac{1}{2} W_2(\beta+2),$$

$$g^a_{11}(1,\beta) = J_1(\beta) + 3J_{30}(R,\beta,b_1,b_2) + \frac{3}{4} R^2 W_1(\beta) - R W_0(\beta+1) - \frac{1}{2} R W_2(\beta+1) + \frac{3}{4} W_1(\beta+2),$$

$$g^b_{11}(1,\beta) = 0 \ ,$$

$$g^c_{11}(1,\beta) = J_{30}(R,\beta,b_1,b_2) + \tfrac{1}{4}R^2W_1(\beta) - \tfrac{1}{2}RW_2(\beta+1) + \tfrac{1}{4}W_3(\beta+2),$$

$$g^a_{11}(m,\beta) = J_m(\beta) + 2J_{30}(R,\beta,b_1,b_2) + \tfrac{1}{2}R^2W_m(\beta) - \tfrac{1}{2}RW_{m-1}(\beta+1) - \tfrac{1}{2}RW_{m+1}(\beta+1)$$
$$+ \tfrac{1}{2}W_m(\beta+2), \quad (m\geq 2),$$

$$g^b_{11}(m,\beta) = J_{30}(R,\beta,b_1,b_2) + \tfrac{1}{4}R^2W_m(\beta) - \tfrac{1}{2}RW_{m-1}(\beta+1) + \tfrac{1}{4}W_{m-2}(\beta+2), \ (m\geq 2),$$

$$g^c_{11}(m,\beta) = J_{30}(R,\beta,b_1,b_2) + \tfrac{1}{4}R^2W_m(\beta) - \tfrac{1}{2}RW_{m+1}(\beta+1) + \tfrac{1}{4}W_{m+2}(\beta+2), \ (m\geq 2);$$

$$g^a_{12}(0,\beta) = g^b_{12}(0,\beta) = g^c_{12}(0,\beta) = 0,$$

$$g^a_{12}(1,\beta) = J_{30}(R,\beta,b_1,b_2) + \tfrac{1}{4}R^2W_1(\beta) - \tfrac{1}{2}RW_0(\beta+1) + \tfrac{1}{4}W_1(\beta+2),$$

$$g^b_{12}(1,\beta) = 0,$$

$$g^c_{12}(1,\beta) = -J_{30}(R,\beta,b_1,b_2) - \tfrac{1}{4}R^2W_1(\beta) + \tfrac{1}{2}RW_2(\beta+1) - \tfrac{1}{4}W_3(\beta+2),$$

$$g^a_{12}(m,\beta) = 0, \quad (m\geq 2),$$

$$g^b_{12}(m,\beta) = J_{30}(R,\beta,b_1,b_2) + \tfrac{1}{4}R^2W_m(\beta) - \tfrac{1}{2}RW_{m-1}(\beta+1) + \tfrac{1}{4}W_{m-2}(\beta+2), \ (m\geq 2),$$

$$g^c_{12}(m,\beta) = -J_{30}(R,\beta,b_1,b_2) - \tfrac{1}{4}R^2W_m(\beta) + \tfrac{1}{2}RW_{m+1}(\beta+1) - \tfrac{1}{4}W_{m+2}(\beta+2), \ (m\geq 2);$$

$$g^a_{21}(0,\beta) = g^b_{21}(0,\beta) = 0,$$

$$g^c_{21}(0,\beta) = 2J_{30}(R,\beta,b_1,b_2) + \tfrac{1}{2}R^2W_0(\beta) - RW_1(\beta+1) + \tfrac{1}{2}W_2(\beta+2),$$

$$g^a_{21}(1,\beta) = J_{30}(R,\beta,b_1,b_2) + \tfrac{1}{4}R^2W_1(\beta) - \tfrac{1}{2}RW_0(\beta+1) + \tfrac{1}{4}W_1(\beta+2),$$

$$g^b_{21}(1,\beta) = 0,$$

$$g^c_{21}(1,\beta) = J_{30}(R,\beta,b_1,b_2) + \tfrac{1}{4}R^2W_1(\beta) - \tfrac{1}{2}RW_2(\beta+1) + \tfrac{1}{4}W_3(\beta+2),$$

$$g^a_{21}(m,\beta) = 0, \quad (m\geq 2),$$

$$g^b_{21}(m,\beta) = -J_{30}(R,\beta,b_1,b_2) - \tfrac{1}{4}R^2W_m(\beta) + \tfrac{1}{2}RW_{m-1}(\beta+1) - \tfrac{1}{4}W_{m-2}(\beta+2), \ (m\geq 2),$$

$$g^c_{21}(m,\beta) = J_{30}(R,\beta,b_1,b_2) + \tfrac{1}{4}R^2W_m(\beta) - \tfrac{1}{2}RW_{m+1}(\beta+1) + \tfrac{1}{4}W_{m+2}(\beta+2), \ (m\geq 2);$$

$$g^a_{22}(0,\beta) = g^b_{22}(0,\beta) = g^c_{22}(0,\beta) = 0\ ,$$

$$g^a_{22}(1,\beta) = J_1(\beta) + 3J_{30}(R,\beta,b_1,b_2) + \tfrac{3}{4}R^2W_1(\beta) - RW_0(\beta+1) - \tfrac{1}{2}RW_2(\beta+1) + \tfrac{3}{4}W_1(\beta+2),$$

$$g^b_{22}(1,\beta) = 0,$$

$$g^c_{22}(1,\beta) = -J_{30}(R,\beta,b_1,b_2) - \tfrac{1}{4}R^2W_1(\beta) + \tfrac{1}{2}RW_2(\beta+1) - \tfrac{1}{4}W_3(\beta+2)\ ,$$

$$g^a_{22}(m,\beta) = J_m(\beta) + 2J_{30}(R,\beta,b_1,b_2) + \tfrac{1}{2}R^2W_m(\beta) - \tfrac{1}{2}RW_{m+1}(\beta+1) - \tfrac{1}{2}RW_{m-1}(\beta+1) + \tfrac{1}{2}W_m(\beta+2)\ ,\quad (m\geq 2),$$

$$g^b_{22}(m,\beta) = -J_{30}(R,\beta,b_1,b_2) - \tfrac{1}{4}R^2W_m(\beta) + \tfrac{1}{2}RW_{m-1}(\beta+1) - \tfrac{1}{4}W_{m-2}(\beta+2),\ (m\geq 2),$$

$$g^c_{22}(m,\beta) = -J_{30}(R,\beta,b_1,b_2) - \tfrac{1}{4}R^2W_m(\beta) + \tfrac{1}{2}RW_{m+1}(\beta+1) - \tfrac{1}{4}W_{m+2}(\beta+2),\ (m\geq 2);$$

$$g^a_{33}(m,\beta) = J_m(\beta)\ ,\quad (m=0,1,2,\cdots),$$

$$g^b_{33}(m,\beta) = g^c_{33}(m,\beta) = 0\ ,\quad (m=0,1,2,\cdots);$$

and all the other $g^a_{ij}(m,\beta) = g^b_{ij}(m,\beta) = g^c_{ij}(m,\beta) = 0$.
Here

$$W_m(\beta) = 4\sum_{s=0}^{\infty}\left[\delta^{(1)}_{ms}T_{1s}(R,\beta,b_1,b_2) - \delta^{(2)}_{ms}T_{2s}(R,\beta,b_1,b_2)\right],$$

$$J_m(\beta) = 4\sum_{s=0}^{\infty}\left[\gamma^{(1)}_{ms}J_{3s}(R,\beta,b_1,b_2) - \gamma^{(2)}_{ms}J_{4s}(R,\beta,b_1,b_2)\right],$$

and $\delta^{(i)}_{ms}$, $\gamma^{(i)}_{ms}$, $T_{is}(R,\beta,b_1,b_2)$, $J_{is}(R,\beta,b_1,b_2)$ are defined by (A17) and (A24).

Numerical tests show taht the algorithms listed above can reduce the computation time for $H^{(\beta)}_{ij}(R,\varphi,z;\ b_1,b_2;\ m)$ to a few thousandths of the time required by a numerical quadrature and give an accuracy to 10^{-7} at worst for m=0--7 and β=1--3.

Table 1 The Axisymmetric Solution

(Convergence tests for δ)

	$a = 0.1$, $z_o = 0.5$ ($z_o/a = 5.0$) $M_1=4$, $N_2=20$		$a = 10.0$, $z_o = 20.0$ ($z_o/a = 2.0$) $M_1=10$, $N_2=20$		$a = 10.0$, $z_o = 11.0$ ($z_o/a = 1.1$) $M_1=20$, $N_2=40$	
δ	F_z^t	$\tilde{F}_z^s$	F_z^t	$\tilde{F}_z^s$	F_z^t	$\tilde{F}_z^s$
1°	-1.0661	0.84810	-2.1241	0.0056469	-10.502	0.18036
0.1°	-1.0661	0.84810	-2.1241	0.0056465	-10.451	0.19032
0.01°	-1.0661	0.84810	-2.1241	0.0056465	-10.450	0.19057
0.001°	-1.0661	0.84810	-2.1241	0.0056465	-10.450	0.19057

Table 2 The Axisymmetric Solution

(Convergence tests for M_1)

$a = 0.1$, $z_o = 0.5$, $(z_o/a = 5.0)$, $N_2 = 20$			$a = 10.0$, $z_o = 20.0$, $(z_o/a = 2.0)$, $N_2 = 20$			$a = 10.0$, $z_o = 11.0$, $(z_o/a = 1.1)$, $N_2 = 40$		
M_1	F_z^t	$\tilde{F}_z^s$	M_1	F_z^t	$\tilde{F}_z^s$	M_1	F_z^t	$\tilde{F}_z^s$
4	-1.0661	0.84810	4	-2.1400	0.0091578	14	-10.413	0.19736
6	-1.0661	0.84814	6	-2.1241	0.0057613	16	-10.470	0.18249
8	-1.0661	0.84814	8	-2.1241	0.0056307	18	-10.467	0.18686
			10	-2.1241	0.0056465	20	-10.450	0.19057
			12	-2.1241	0.0056488	22	-10.437	0.19257
			14	-2.1241	0.0056492	24	-10.432	0.19392
						26	-10.429	0.19480
						28	-10.424	0.19539

Table 3 The Axisymmetric Solution

(Convergence tests for N_2)

	a = 0.1 z_o = 0.5 (z_o/a = 5.0) M_1 = 4		a = 10.0 z_o = 20.0 (z_o/a = 2.0) M_1 = 10		a = 10.0 z_o = 11.0 (z_o/a = 1.1) M_1 = 20	
N_2	F_z^t	$\tilde{F}_z^s$	F_z^t	$\tilde{F}_z^s$	F_z^t	$\tilde{F}_z^s$
12	-1.0638	0.84625	-2.1113	0.0055464		
14	-1.0648	0.84711	-2.1185	0.0056009		
16	-1.0655	0.84760	-2.1219	0.0056281		
18	-1.0659	0.84791	-2.1234	0.0056404		
20	-1.0661	0.84810	-2.1241	0.0056465		
22	-1.0663	0.84823	-2.1245	0.0056496		
24	-1.0664	0.84832	-2.1247	0.0056513		
26	-1.0665	0.84838	-2.1248	0.0056523		
28	-1.0665	0.84844	-2.1249	0.0056529		
30	-1.0665	0.84846	-2.1250	0.0056533	-10.390	0.18152
32	-1.0666	0.84850	-2.1250	0.0056535		
34	-1.0666	0.84852	-2.1250	0.0056537	-10.423	0.18608
36	-1.0666	0.84852	-2.1250	0.0056539	-10.435	0.18831
38			-2.1250	0.0056539	-10.441	0.18915
39					-10.446	0.18994
40			-2.1250	0.0056540	-10.450	0.19057

Table 4 The Axisymmetric Solution

(Convergence test for R_u)

$a=0.1$, $z_o=0.5$, $z_o/a=5.0$, $M_1=4.$

Ru/z_o	R_u	N_2	F_z^t	$\tilde{F}_z^s$
4.76	2.38	10	-1.0657	0.84777
5.80	2.90	11	-1.0659	0.84793
7.04	3.52	12	-1.0660	0.84802
8.54	4.27	13	-1.0660	0.84806
10.32	5.16	14	-1.0661	0.84808
12.40	6.20	15	-1.0661	0.84809
14.80	7.40	16	-1.0661	0.84810
17.52	9.76	17	-1.0661	0.84810
20.62	10.31	18	-1.0661	0.84810

Table 5 The Axisymmetric Solution

(Comparison of F_z^t)

z_o/a		a=0.1	a=0.5	a=1.0	a=5.0	a=10.0
10.0	YN	-1.0723	-1.1246	-1.1259	-1.1251	-1.1253
	DG	-1.0596	-1.1240	-1.1262	-1.1262	-1.1262
	DV	-1.0730	-1.1248	-1.1259	-1.1261	---
5.0	YN	-1.0666	-1.2638	-1.2814	-1.2850	-1.2822
	DG	-1.0532	-1.2509	-1.2795	-1.2850	-1.2851
	DV	-1.0667	-1.2618	-1.2804	-1.2837	---
2.0	YN	-1.0540	-1.4264	-1.8654	-2.1194	-2.1250
	DG	-1.0505	-1.3919	-1.8058	-2.1200	-2.1248
	DV	-1.0542	-1.4843	-1.8396	-1.9981	---
1.5	YN	-1.0523	-1.4205	-2.1042	-3.153	-3.185
	DG	-1.0504	-1.3882	-2.0334	-3.1535	-3.1983
	DV	-1.0526	-1.4872	-2.0863	-2.5059	---
1.1	YN	-1.0513	-1.3946	-2.360	-8.47	-10.4
	DG	-1.0503	-1.3777	-2.2867	-8.94	-10.5
	DV	-1.0516	-1.4593	-2.2659	-2.8380	---

Sources: YN -- The present work;

DG -- Dagan, Weinbaum and Pfeffer (1982b);

DV -- Davis (1983).

Table 6 The Axisymmetric Solution

(Comparison of $\tilde{F}_z^s$)

z_o/a		a=0.1	a=0.5	a=1.0	a=5.0	a=10.0
10.0	YN	0.53439	0.043079	0.011102	0.00044801	0.00011204
	DG	0.52797	0.043026	0.011094	0.00044814	0.00011207
	DV	0.53485	0.043220	0.011139	0.0004499	---
5.0	YN	0.84852	0.17298	0.049182	0.0020527	0.0005126
	DG	0.83796	0.16986	0.048597	0.0020285	0.00050774
	DV	0.84824	0.17554	0.050131	0.0020924	---
2.0	YN	1.0069	0.65155	0.3593	0.0222	0.00565
	DG	1.0036	0.62720	0.32754	0.022291	0.0056546
	DV	1.0068	0.70094	0.45763	0.030870	---
1.5	YN	1.0224	0.79839	0.568	0.069	0.018
	DG	1.0206	0.77576	0.48320	0.0863	0.0185
	DV	1.0225	0.81957	0.82430	0.10522	---
1.1	YN	1.0319	0.91163	0.753	0.24	0.20
	DG	1.0310	0.90571	0.64018	0.191	0.149
	DV	1.0321	0.88548	1.0681	0.42048	---

Sources: YN -- The present work;

DG -- Dagan, Weinbaum and Pfeffer (1982b);

DV -- Davis (1983).

Table 7 The Axisymmetric Solution

(Results of F_z^t for $z_o/a \leq 1.1$)

z_o/a	a=0.1	a=0.25	a=0.5	a=0.75	a=1.0
1.1	-1.0513	-1.1448	-1.3946	-1.9234	-2.360
1.0	-1.0511	-1.1424	-1.3856	-1.9438	-2.457
0.5	-1.0503	-1.1327	-1.3364	-1.9163	-3.332
0.1	-1.0501	-1.1307	-1.3116	-1.8194	-10
0.05	-1.0501	-1.1305	-1.3107	-1.7888	---
0.0	-1.0501	-1.1291	-1.3104	-1.7768	---

Table 8 The Axisymmetric Solution

(Results of $\tilde{F}_z^s$ for $z_o/a \leq 1.1$)

z_o/a	a=0.1	a=0.25	a=0.5	a=0.75	a=1.0
1.1	1.0319	1.0209	0.91163	0.8082	0.753
1.0	1.0338	1.0314	0.93779	0.8964	0.794
0.5	1.0408	1.0705	1.0460	1.0531	0.957
0.1	1.0431	1.0837	1.0888	1.230	1.2
0.05	1.0431	1.0842	1.0903	1.249	---
0.0	1.0431	1.0843	1.0908	1.255	---

Table 9 The Three-dimensional Solution

(Convergence tests for M_2)

(a) $a=0.5$, $x_o=0$, $z_o=0.55$ ($z_o/a=1.1$)

M_1	M_2	N_2	T_y^r	F_x^r	F_z^r
4	1	14	-1.0084	-0.045989	-2×10^{-10}
4	3	14	-1.0092	-0.048010	-8×10^{-10}

(b) $a=0.1$, $x_o=0.25$, $z_o=0$ ($z_o/a=0.0$)

M_1	M_2	N_2	$F_x^{t,x}$	$F_z^{t,x}$	$T_y^{t,x}$
4	3	10	-1.1109	3×10^{-6}	-5×10^{-7}
4	5	10	-1.1144	3×10^{-6}	-5×10^{-7}

(c) $a=0.1$, $x_o=0.75$, $z_o=0.11$ ($z_o/a=1.1$)

M_1	M_2	N_2	$F_z^{t,z}$	$F_x^{t,z}$	$T_y^{t,z}$
4	5	10	-1.1329	0.022389	-0.017069
4	6	10	-1.1347	0.023698	-0.017851
4	8	10	-1.1361	0.024924	-0.018536

(d) $a=0.5$, $x_o=1.00$, $z_o=0.75$ ($z_o/a=1.5$)

M_1	M_2	N_2	$F_z^{t,z}$	$F_x^{t,z}$	$T_y^{t,z}$
4	6	10	-1.9500	0.049420	-0.059137
4	8	10	-1.9525	0.050361	-0.059231

Table 10 The Three-dimensional Solution

(Convergence test for M_2)

$a=0.5$, $x_o=1.001$, $z_o=1.00$ $(z_o/a=2.0)$

$M_1 = 4$, $N_2 = 10$

M_2	$F_x^{t,x}$	$F_z^{t,x}$	$T_y^{t,x}$
5	-1.2818	0.029797	-0.029155
6	-1.2824	0.030520	-0.029064
7	-1.2825	0.030726	-0.029078
8	-1.2826	0.030784	-0.029089
M_2	$F_x^{t,z}$	$F_z^{t,z}$	$T_y^{t,z}$
5	0.033099	-1.6328	-0.021424
6	0.033490	-1.6334	-0.021570
7	0.033576	-1.6340	-0.021527
8	0.033612	-1.6340	-0.021511
M_2	F_x^r	F_z^r	T_y^r
5	-0.040494	0.0071884	-1.0209
6	-0.040372	0.0071132	-1.0209
7	-0.040348	0.0070646	-1.0209
8	-0.040337	0.0070535	-1.0209
M_2	$\tilde{F}_x^s$	$\tilde{F}_z^s$	$\tilde{T}_y^s$
5	0.13183	0.36149	-0.061373
6	0.13196	0.36169	-0.061439
7	0.13204	0.36115	-0.061408
8	0.13206	0.36112	-0.061402

Table 11 The Three-dimensional Solution

(Convergence test for N_2)

$a=0.5$, $x_o=1.001$, $z_o=1.00$ $(z_o/a=2.0)$

$M_1 = 4$, $M_2 = 5$

N_2	$F_x^{t,x}$	$F_z^{t,x}$	$T_y^{t,x}$
8	-1.2817	0.031532	-0.028912
9	-1.2817	0.030059	-0.029022
10	-1.2818	0.029797	-0.029155
11	-1.2815	0.029486	-0.029193
12	-1.2817	0.029573	-0.029142
N_2	$F_x^{t,z}$	$F_z^{t,z}$	$T_y^{t,z}$
8	0.030331	-1.6213	-0.020462
9	0.032726	-1.6289	-0.021200
10	0.033099	-1.6328	-0.021424
11	0.034848	-1.6338	-0.022052
12	0.034840	-1.6333	-0.022107
N_2	F_x^r	F_z^r	T_y^r
8	-0.038282	0.0053406	-1.0208
9	-0.039806	0.0067981	-1.0209
10	-0.040494	0.0071884	-1.0209
11	-0.041404	0.0074846	-1.0208
12	-0.041390	0.0074683	-1.0208
N_2	$\tilde{F}_x^s$	$\tilde{F}_z^s$	$\tilde{T}_y^s$
8	0.13261	0.35890	-0.061405
9	0.13203	0.36072	-0.061420
10	0.13183	0.36149	-0.061373
11	0.13151	0.36171	-0.061267
12	0.13159	0.36162	-0.061259

Table 12 The Three-dimensional Solution

(Comparison with axisymmetric solutions)

(a) Values of F_z^t for a=0.1, x_o=0.0

z_o/a	z_o	PR	YN	DG	DV	MI
50	5.00	-1.0189	-1.0227	---	---	-1.0223
20	2.00	-1.0426	-1.0507	---	---	-1.0502
10	1.00	-1.0574	-1.0723	-1.0596	-1.0730	-1.0682
5	0.50	-1.0559	-1.0666	-1.0532	-1.0667	-1.0626
2	0.20	-1.0515	-1.0540	-1.0505	-1.0542	-1.0513
1.1	0.11	-1.0505	-1.0513	-1.0503	-1.0516	-1.0489
0.0	0.00	-1.0503	-1.0501	---	---	-1.0477

(b) Values of $\tilde{F}_z^s$ for a=0.1, x_o=0.0

z_o/a	z_o	PR	YN	DG	DV
50	5.00	0.039167	0.039324	---	---
20	2.00	0.20804	0.20990	---	---
10	1.00	0.52622	0.53439	0.52797	0.53485
5	0.50	0.83991	0.84852	0.83796	0.84824
2	0.20	1.0054	1.0069	1.0036	1.0068
1.1	0.11	1.0322	1.0319	1.0310	1.0321
0.0	0.00	1.0446	1.0431	---	---

Sources: PR -- The present solution using the weighted residual technique (Section 2.4);

YN -- The present solution using the collocation technique (Section 2.3);

DG -- Dagan, Weinbaum and Pfeffer (1982b);

DV -- Davis (1983);

MI -- Miyazaki and Hasimoto (1984).

Table 13 The Three-dimensional Solution

(Comparison with other solutions)

(a) Values of F_z^t for a=0.5, x_o=0.0

z_o/a	PR	YN	DG
5.0	-1.2063	-1.2638	-1.2509
2.0	-1.3768	-1.4264	-1.3919
1.5	-1.3915	-1.4205	-1.3882
1.1	-1.3847	-1.3946	-1.3777

(b) Values of F_z^t for a=1.0, x_o=0.0

z_o/a	PR	YN	DG
5.0	-1.2237	-1.2814	-1.2795
2.0	-1.6494	-1.8654	-1.8058
1.5	-1.8707	-2.1042	-2.0334
1.1	-2.1416	-2.360	-2.2867

(c) Values of F_z^t for a=2.5, x_o=0.0

z_o/a	PR	YN	DG
2.0	-1.8024	-2.0928	-2.0857
1.1	-4.1749	-5.74	-5.89

Sources: PR -- The present solution using the weighted residual technique (Section 2.4);

YN -- The present solution using the collocation technique (Section 2.3);

DG -- Dagan, Weinbaum and Pfeffer (1982b).

Table 14 The Three-dimensional Solution

(Comparison with the far field solution)

Values of $F_z^{t,z}$ for a=0.5, x_o=5.0

z_o/a	z_o	Present Work	Brenner (1961)
10	5.00	-1.1030	-1.1262
1.5	0.75	-1.7918	-3.2053
1.1	0.55	-1.8732	-11.4589

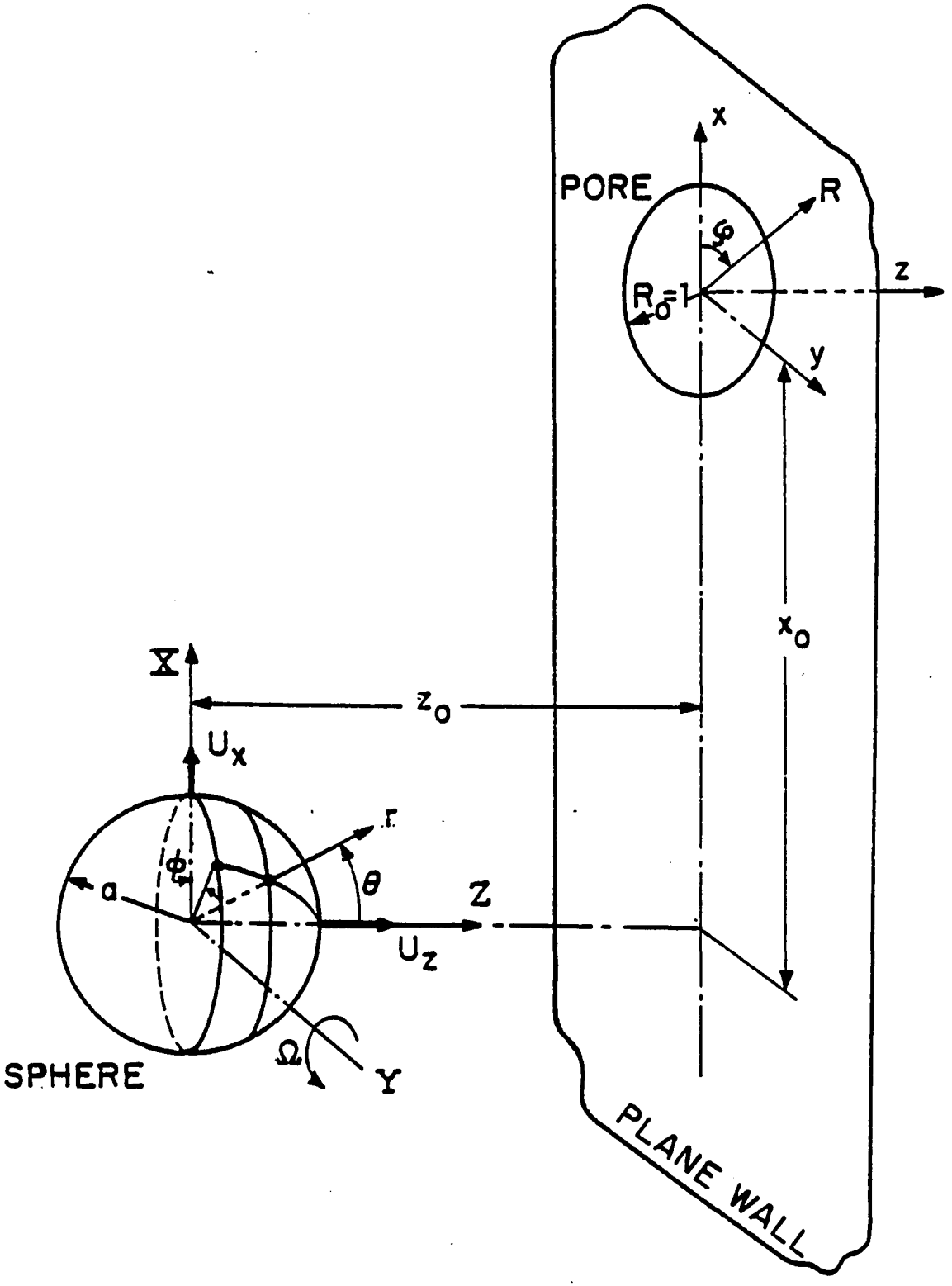

Fig. 1 The entrance geometry

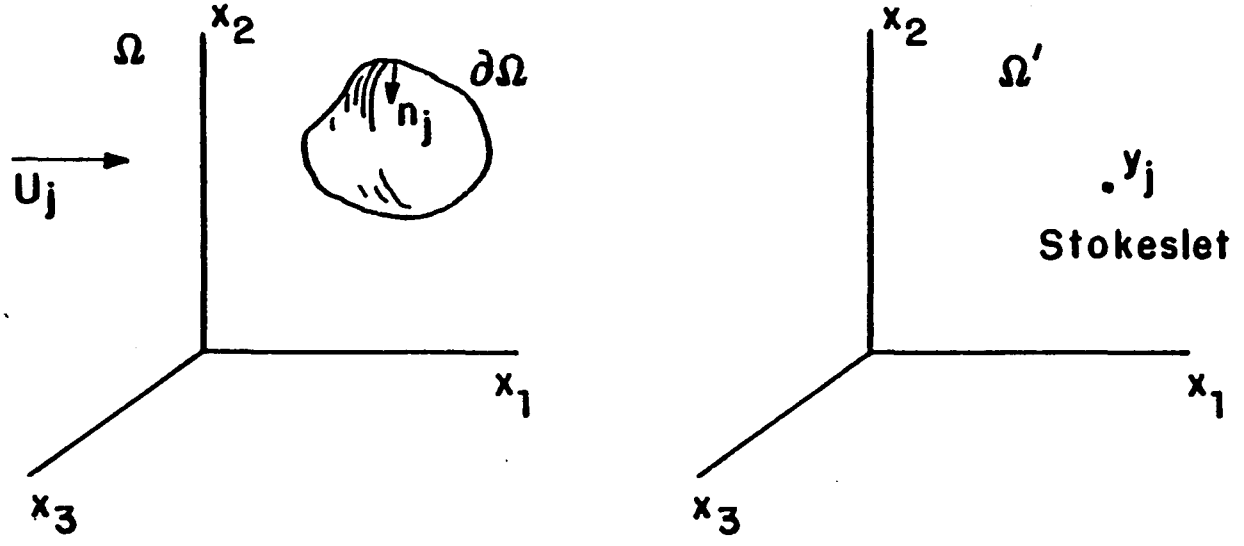

Fig. 2 Two problems of creeping flow

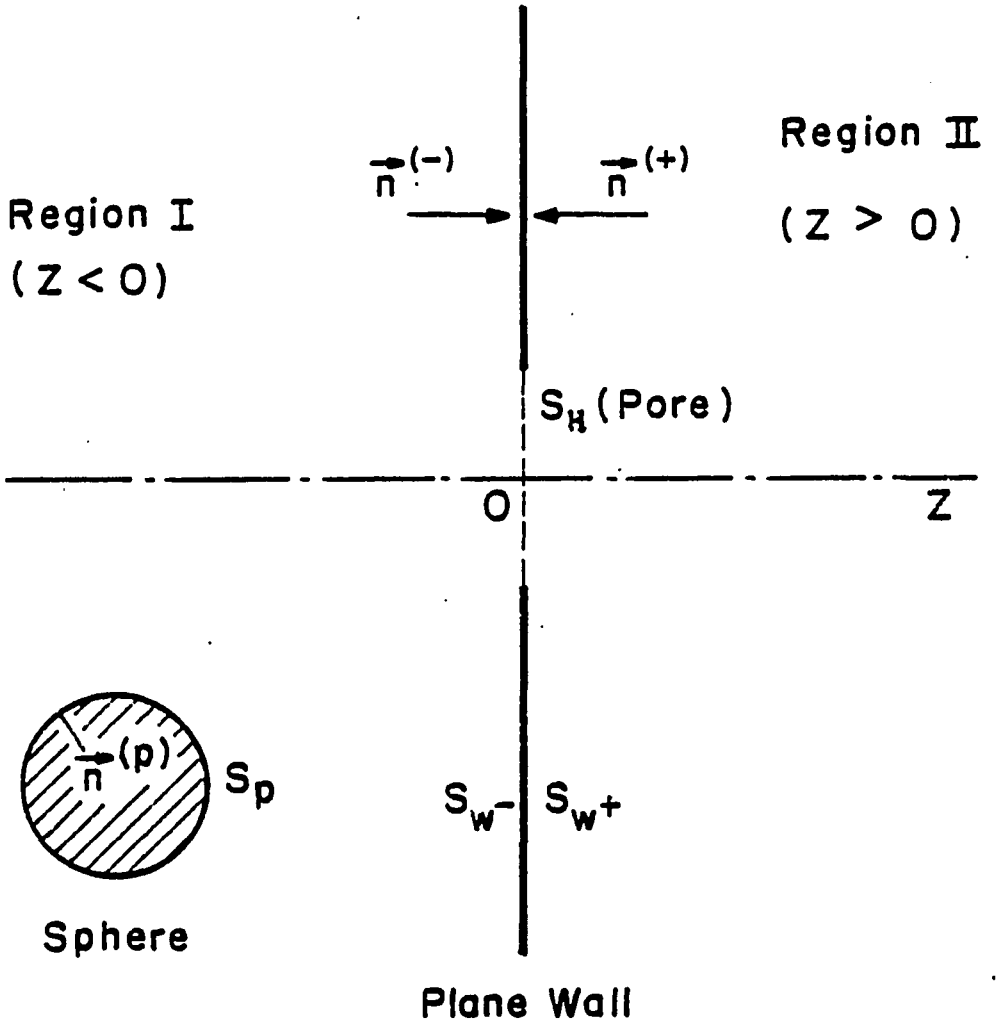

Fig. 3 The division of two regions

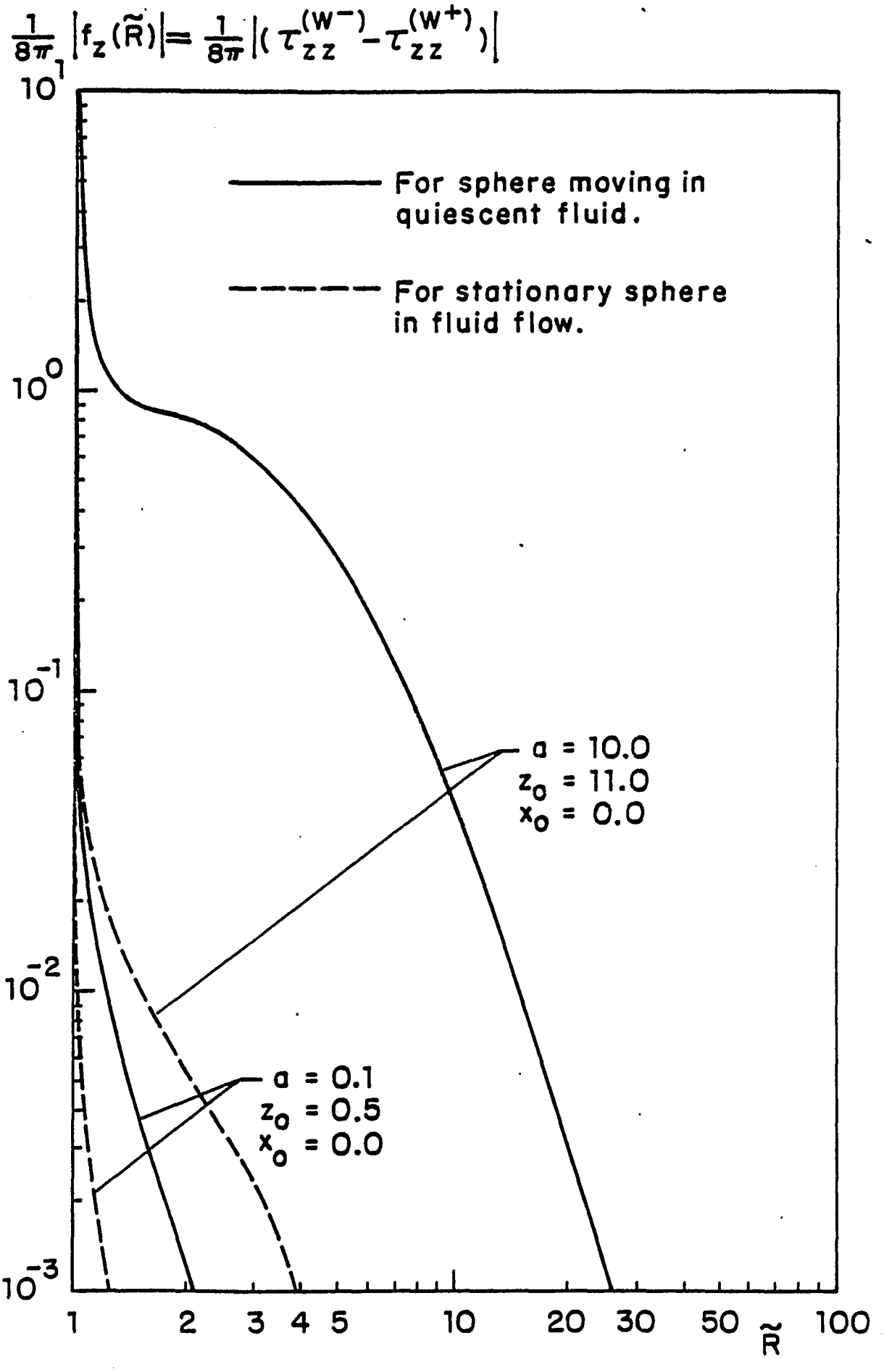

Fig. 4 The typical $f_z(\tilde{R})$ for axisymmetric cases

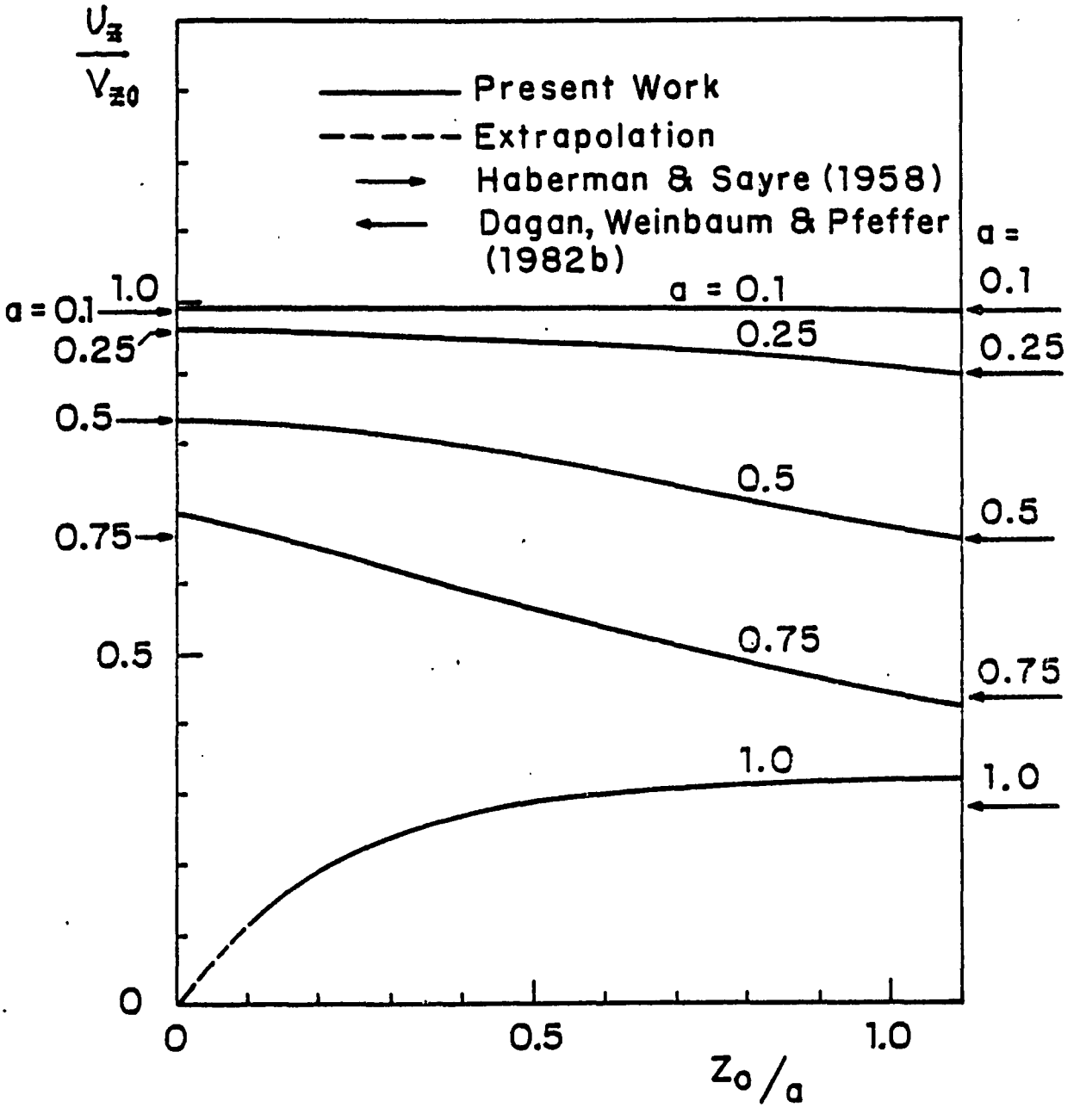

Fig. 5 The neutrally buoyant velocity of the sphere, $0 \leq z_o/a \leq 1.1$, axisymmetric cases

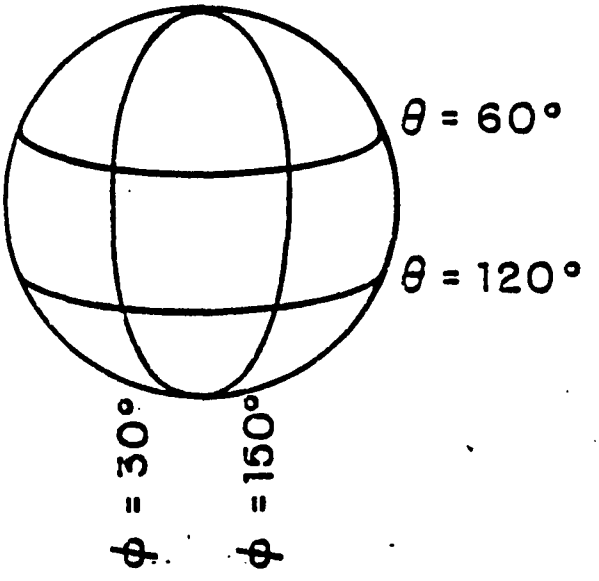

Fig. 6 The collocation points on the sphere surface

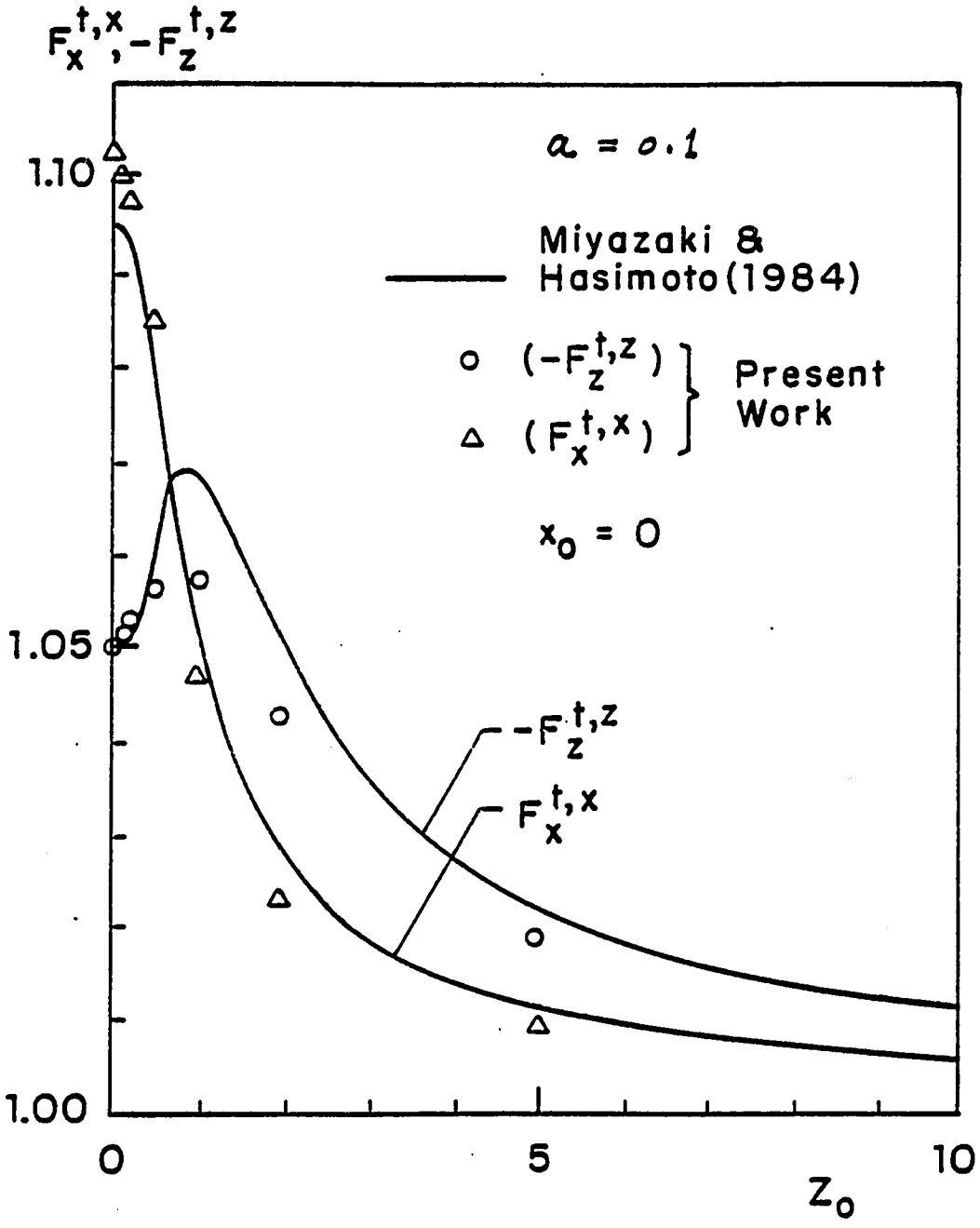

Fig. 7 Comparison of results along the pore axis (x_0=0) between the present solution and Miyazaki and Hasimoto (1984)

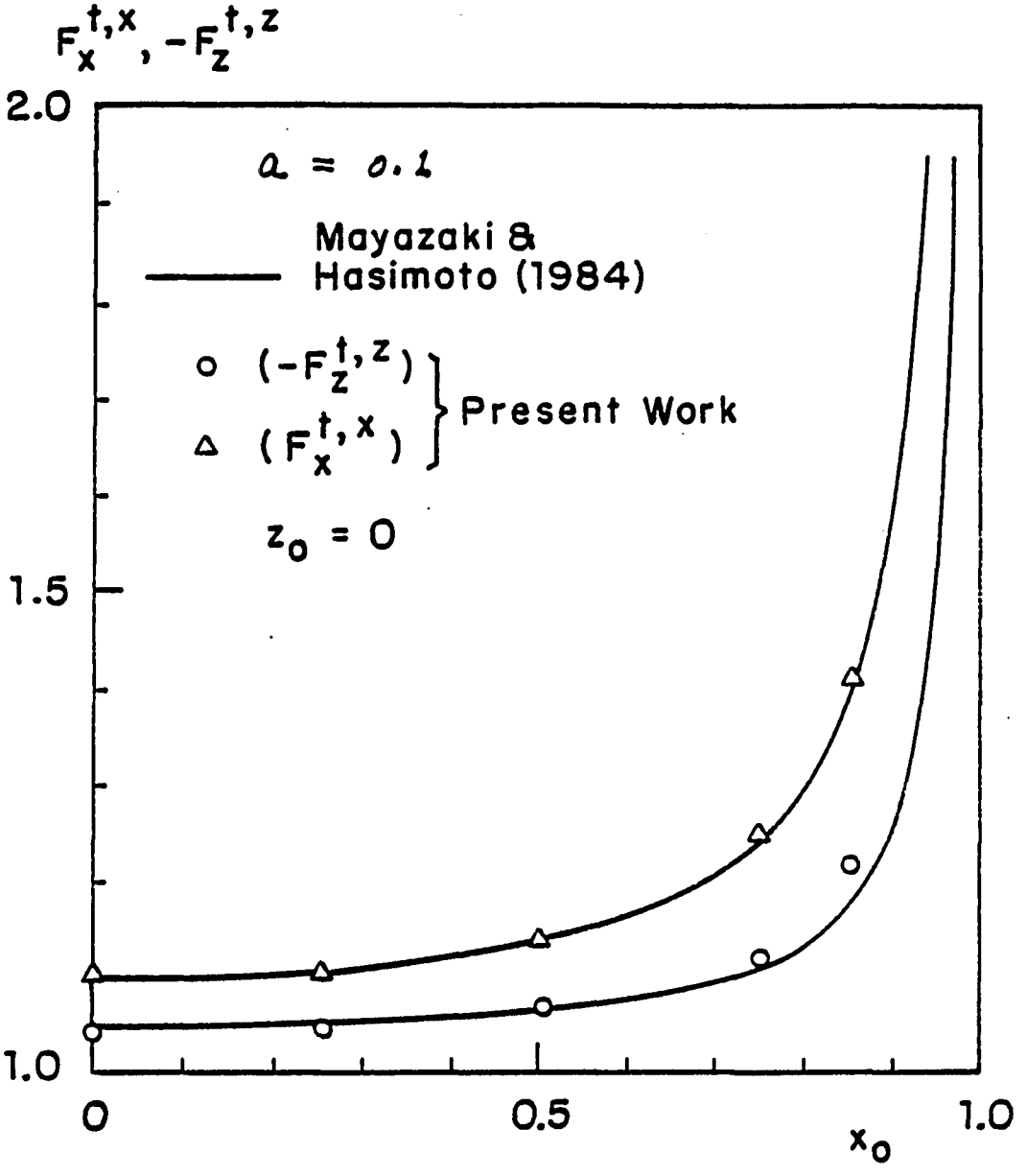

Fig. 8 Comparison of results at the pore opening (z_o=0) between the present solution and Miyazaki and Hasimoto (1984)

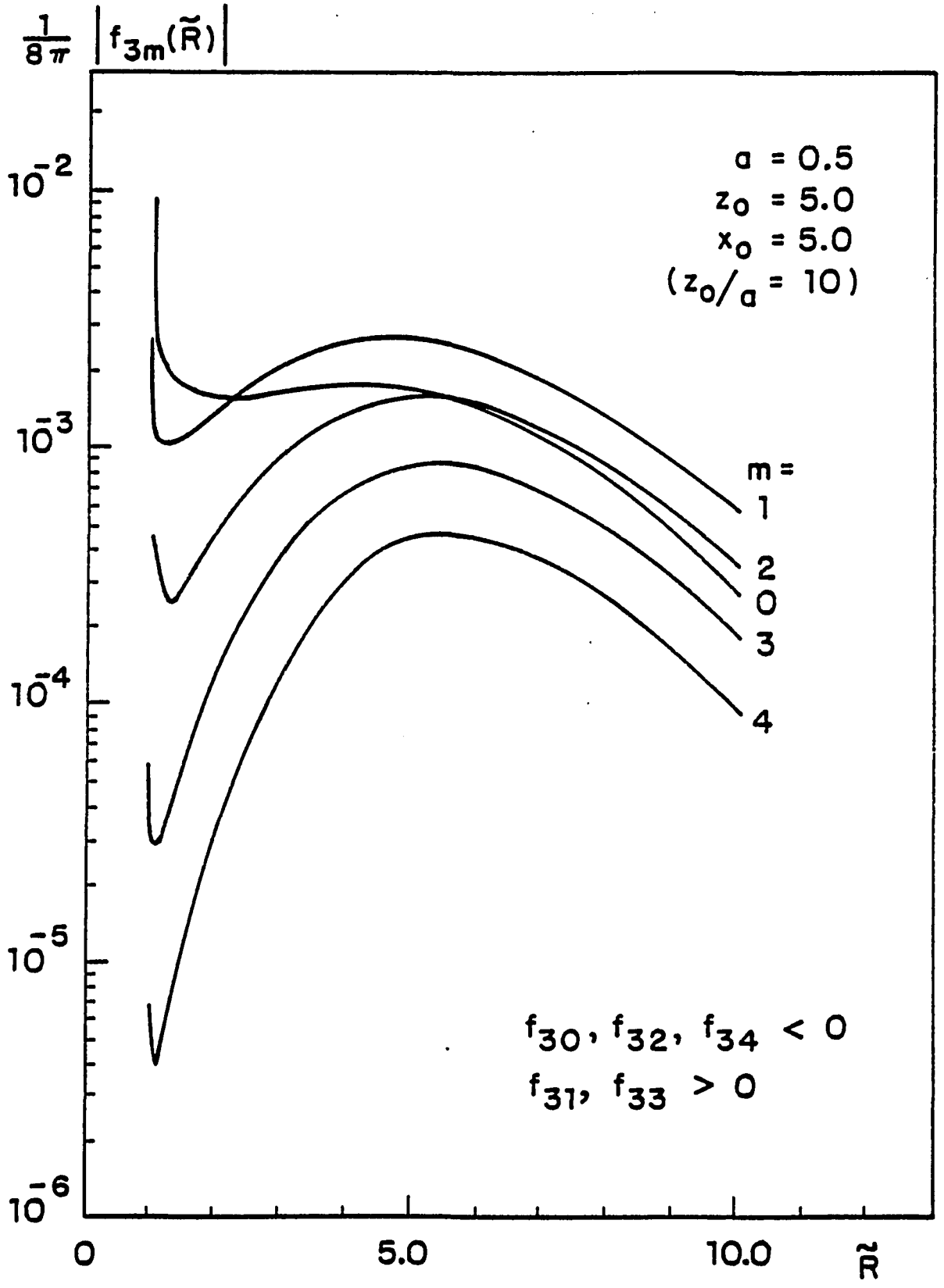

Fig. 9 The values of $f_{3m}(\tilde{R})$ for a=0.5, z_o=5.0, x_o=5.0, the three-dimensional case of a sphere moving perpendicular to the plane of the pore

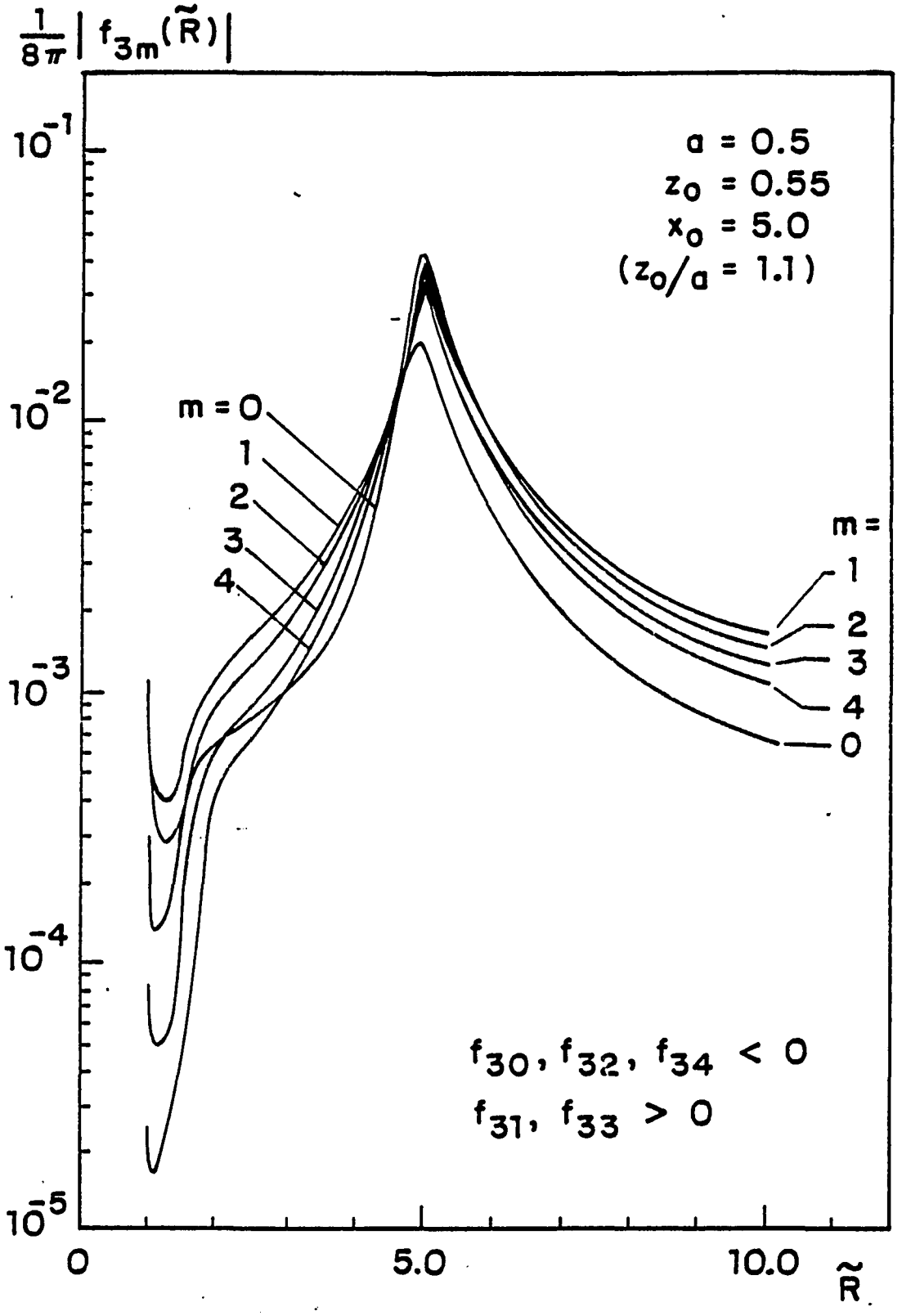

Fig. 10 The values of $f_{3m}(R)$ for a=0.5, z_0=0.55, x_0=5.0, the three-dimensional case of a sphere moving perpendicular to the plane of the pore

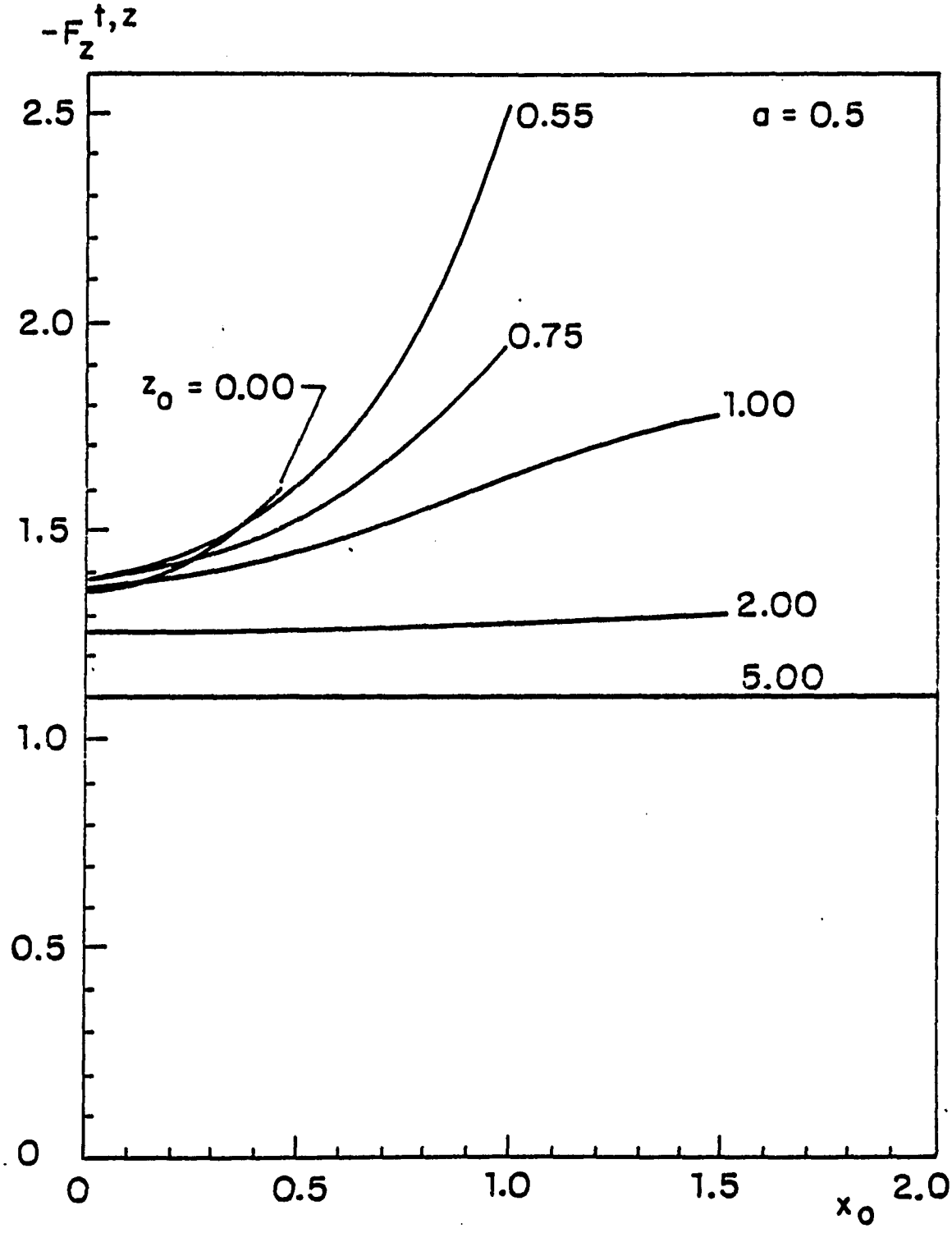

Fig. 11 The results for $F_z^{t,z}$, three-dimensional cases, a=0.5

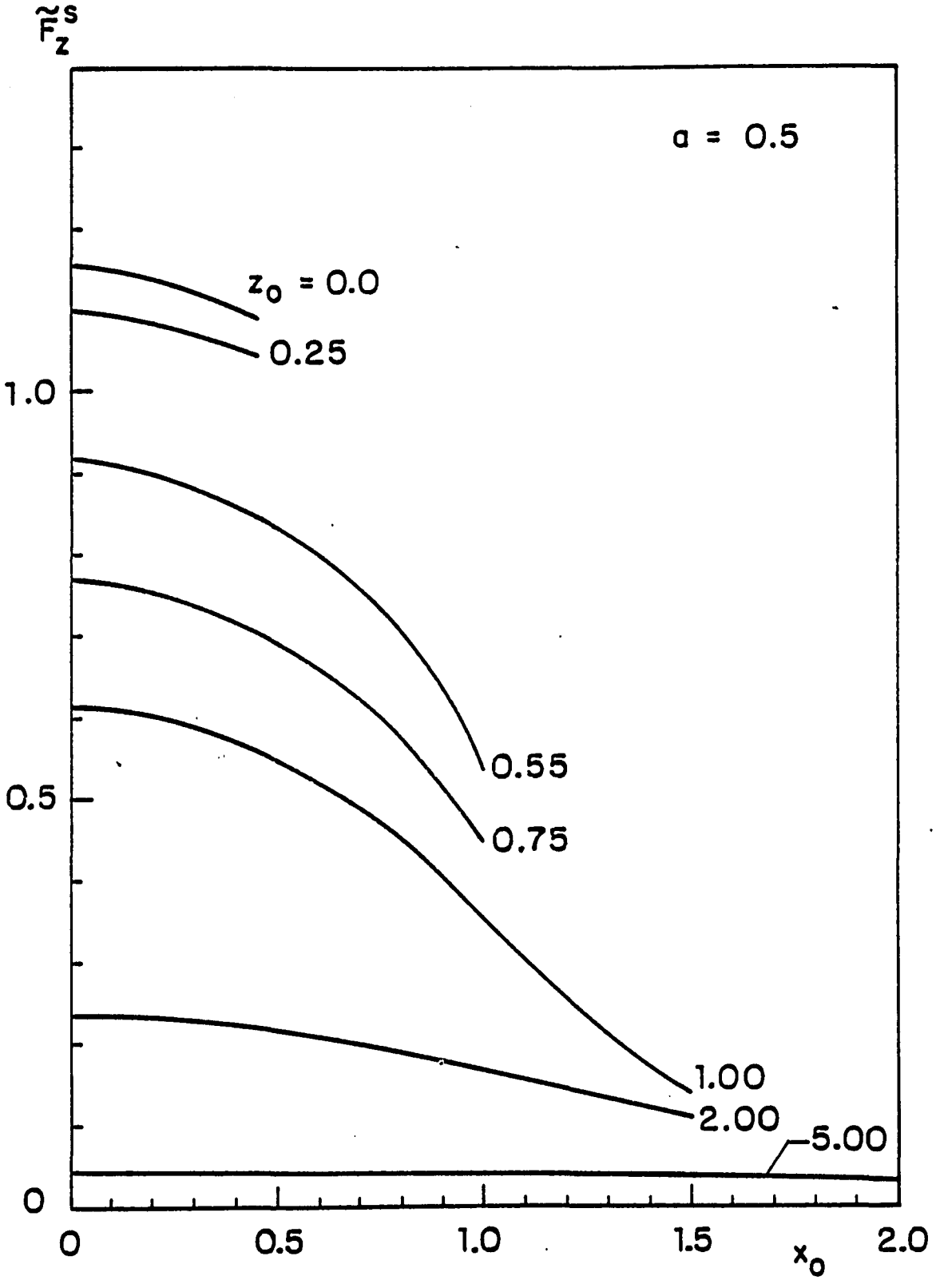

Fig. 12 The results for $\tilde{F}_z^s$, three-dimensional cases, a=0.5

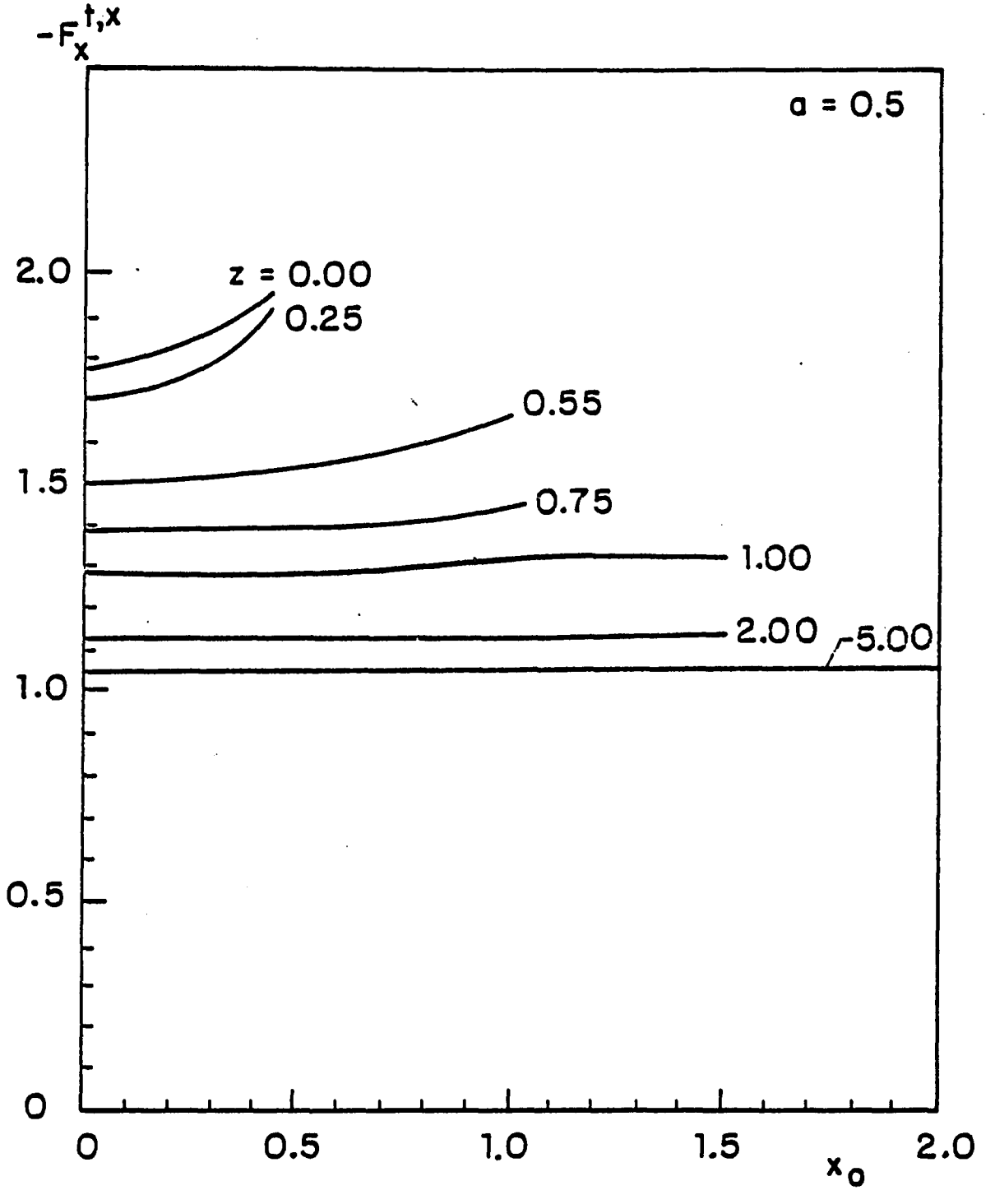

Fig. 13 The results for $F_x^{t,x}$, three-dimensional cases, a=0.5

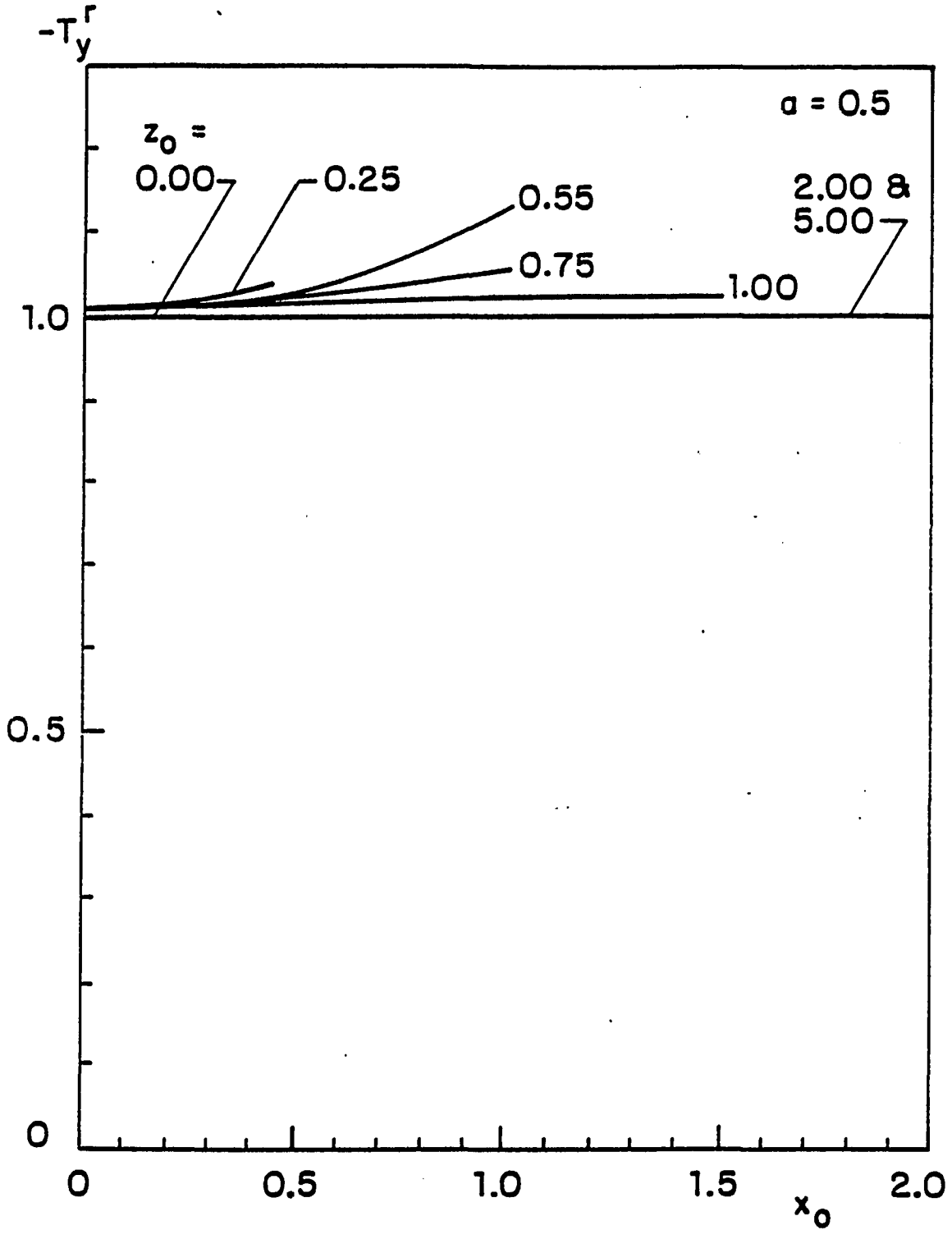

Fig. 14 The results for T_y^r, three-dimensional cases, a=0.5

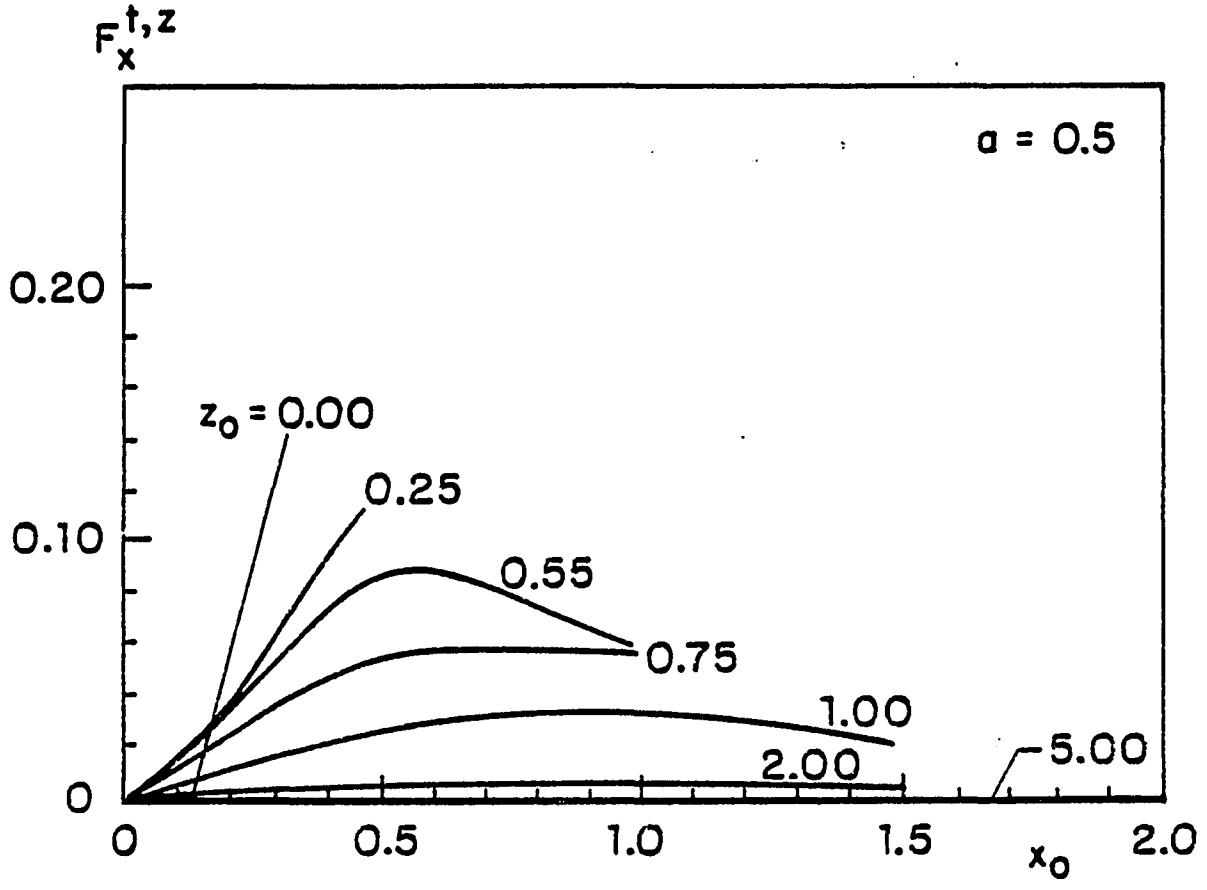

Fig. 15 The results for $F_x^{t,z}$, three-dimensional cases, a=0.5

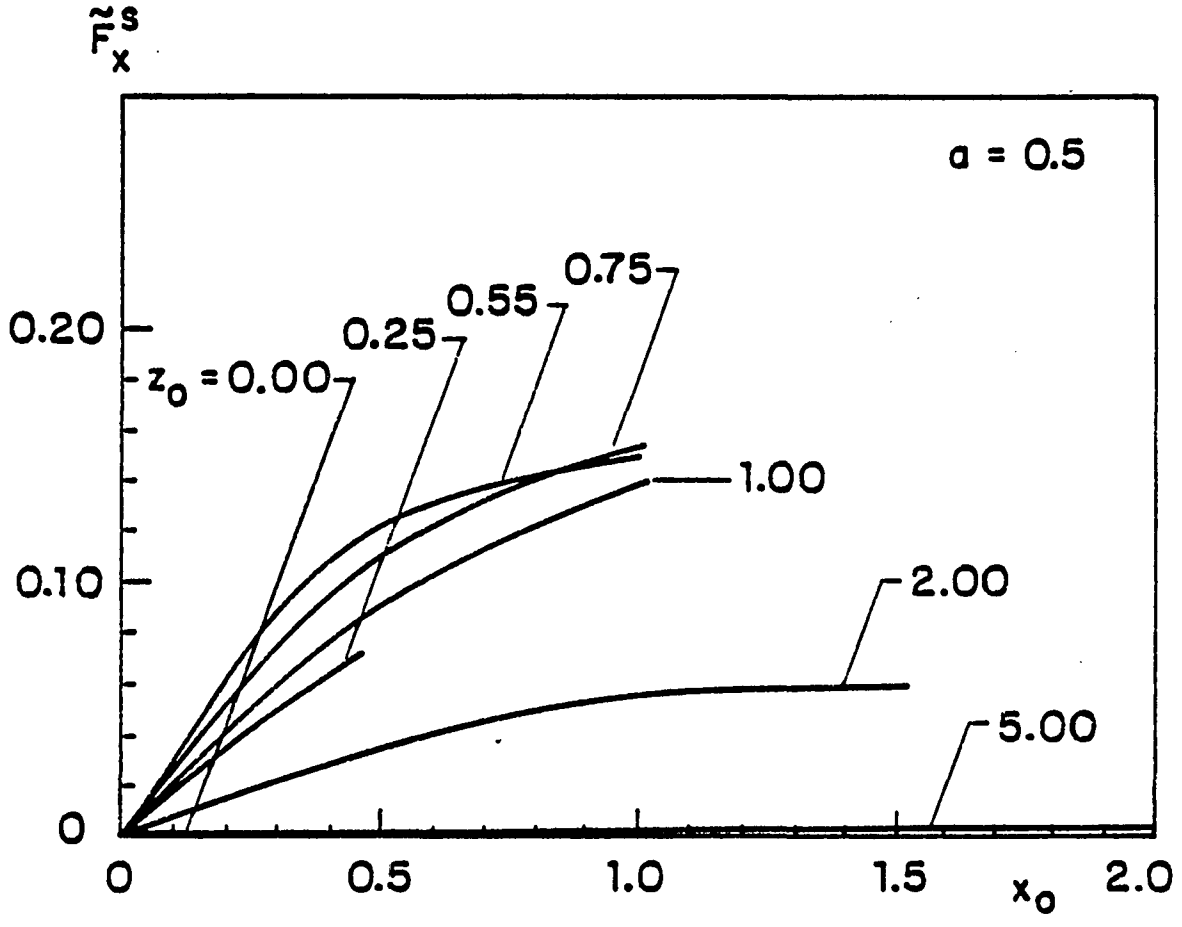

Fig. 16 The results for $\tilde{F}_x^s$, three-dimensional cases, a=0.5

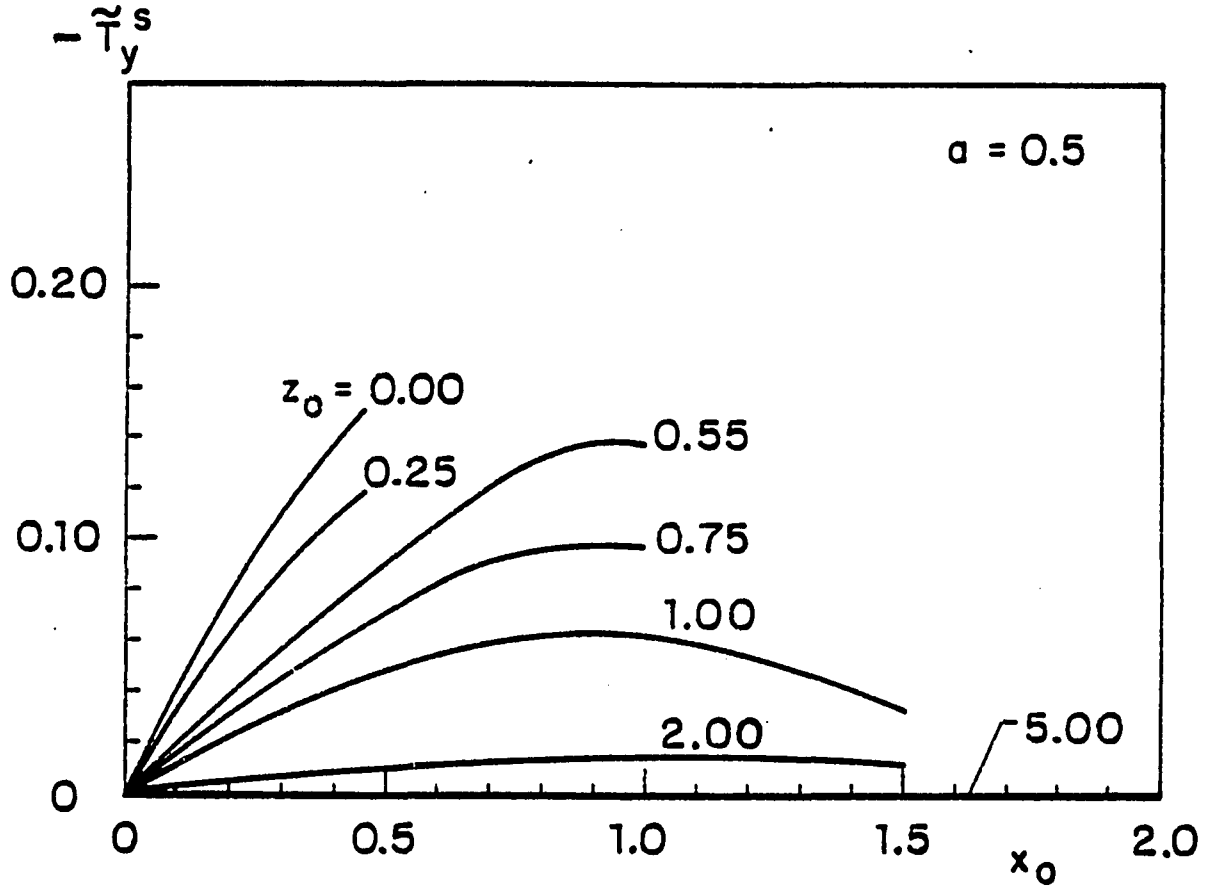

Fig. 17 The results for $\tilde{T}_y^s$, three-dimensional cases, a=0.5

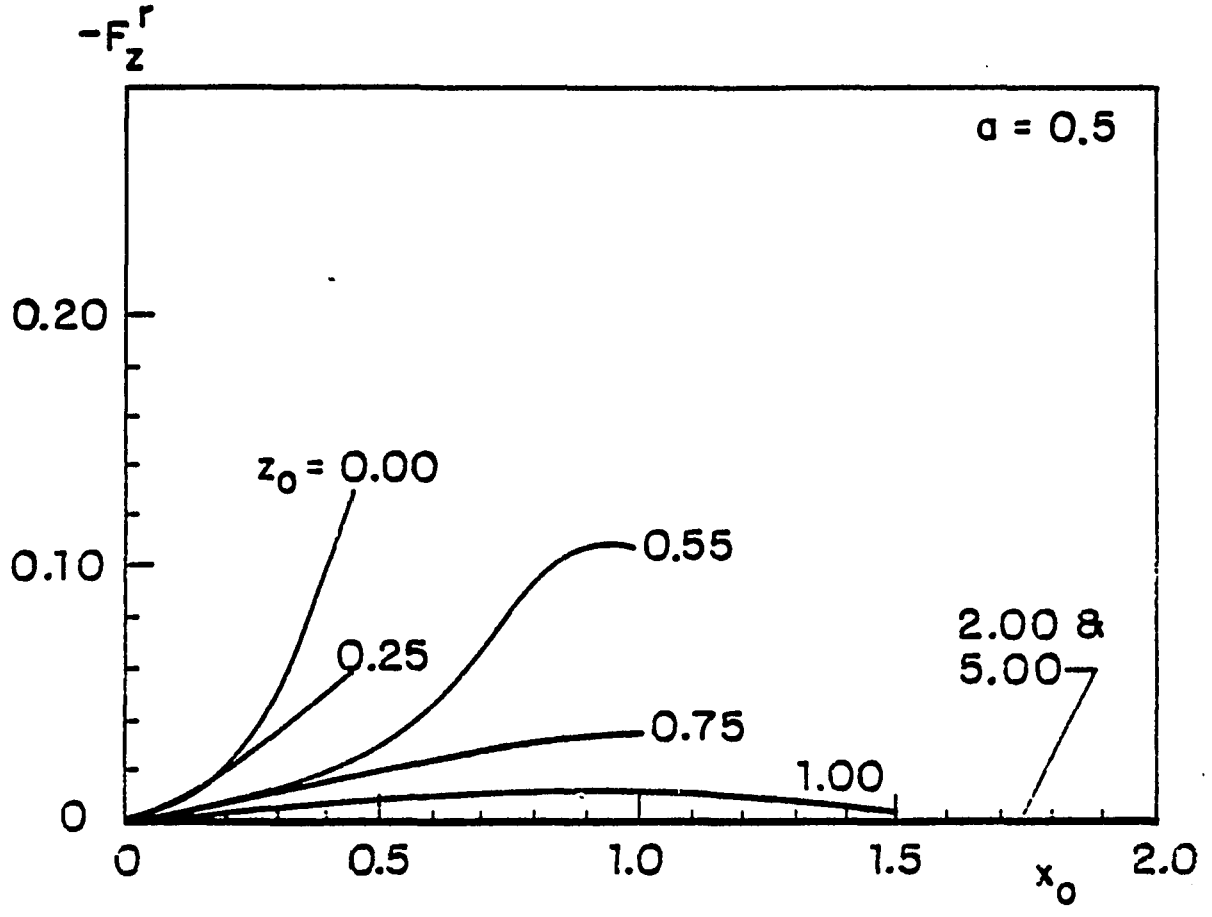

Fig. 18 The results for F_z^r, three-dimensional cases, a=0.5

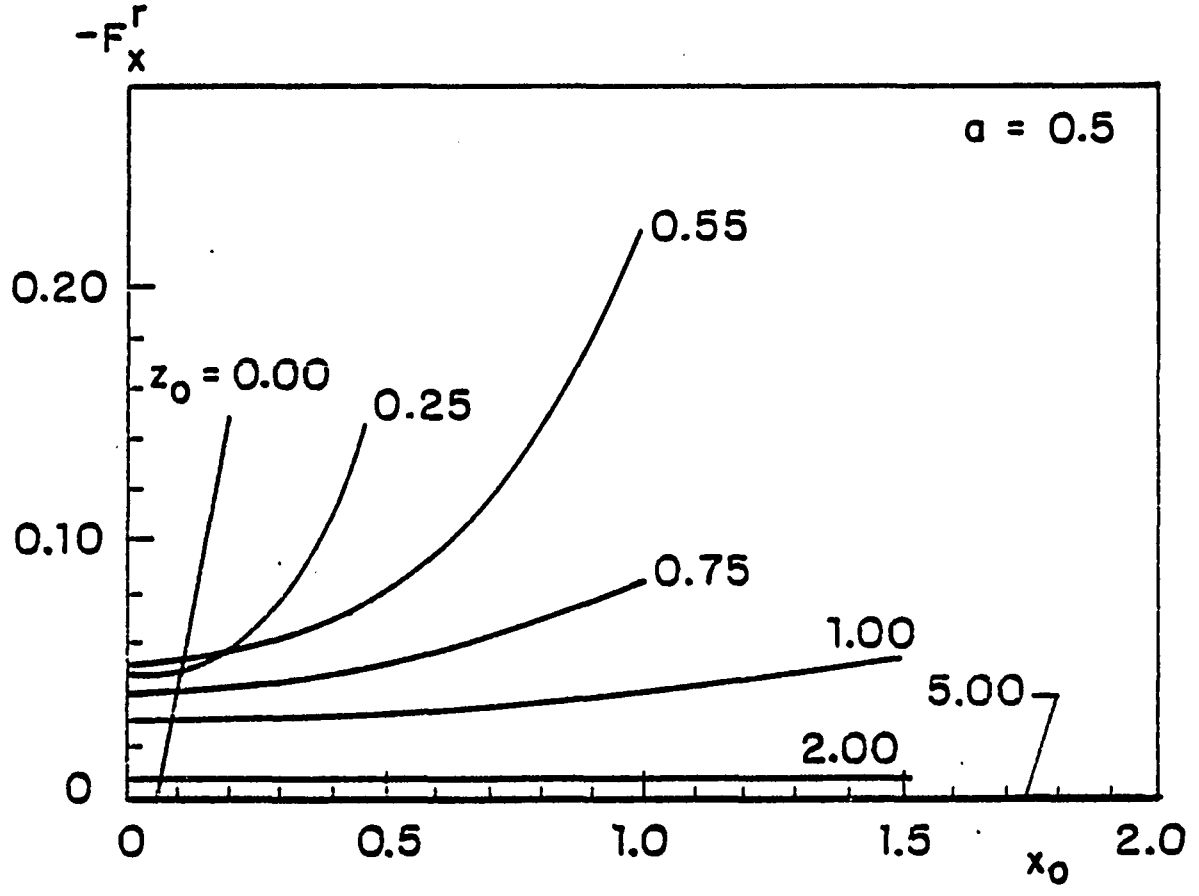

Fig. 19 The results for F_x^r, three-dimensional cases, a=0.5

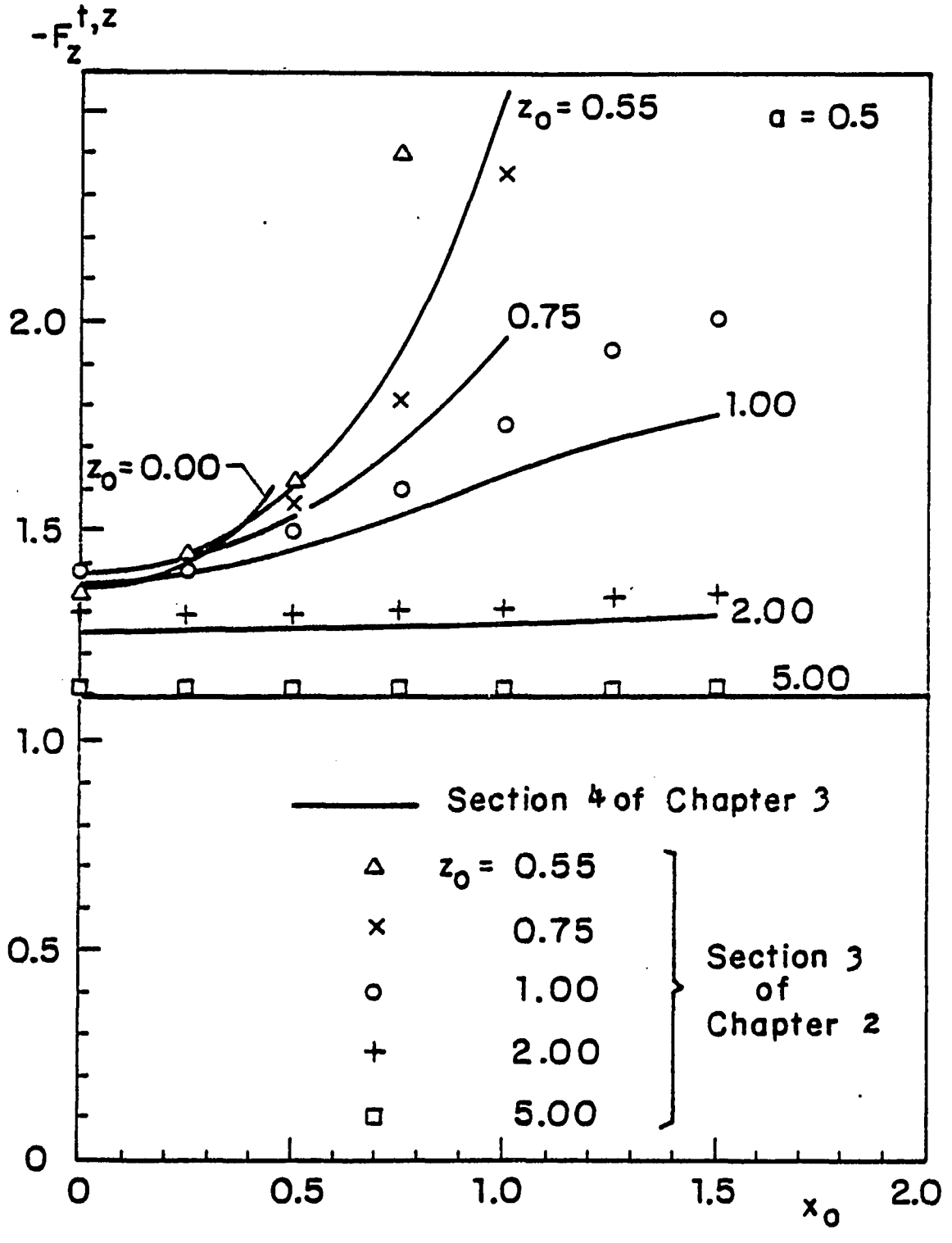

Fig. 20 Comparison of results for $F_z^{t,z}$ between the exact solution in Chapter 3 and the approximate solution in Chapter 2, three-dimensional cases

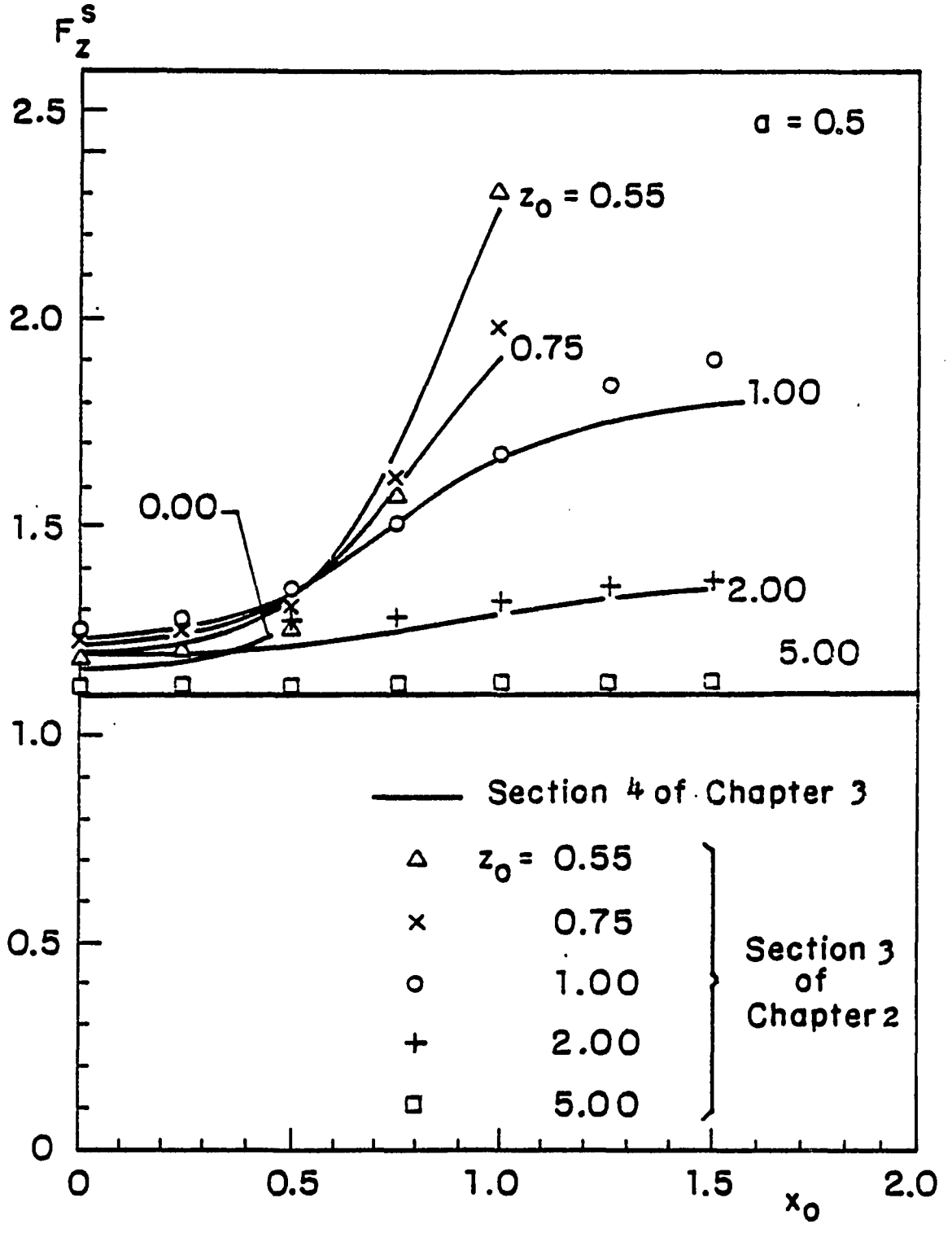

Fig. 21 Comparison of results for F_z^s between the exact solution in Chapter 3 and the approximate solution in Chapter 2, three-dimensional cases

CHAPTER 4

CONCLUDING REMARKS

This thesis has studied two important aspects of the pore entrance phenomena -- the osmotic fine structure and the three-dimensional hydrodynamic interaction near the pore entrance.

Chapter 2 has presented the first complete analysis of the osmotic mechanism, which takes into consideration the flow field both inside the pore itself and in the entrance /exit regions. Detailed concentration and pressure profiles are obtained for both permeable and semi-permeable membranes. The solution for a permeable membrane clearly demonstrates that the local three-dimensional changes in concentration at the pore entrance occur on a length scale of a few pore-radii. The osmotic flow velocity and concentration gradient in this fine-scale region are shown to be far greater than in Pedley's much thicker unstirred layer. The neglect of these entrance/exit effects may lead to a significant error (up to two hundred percent in some extreme case) in estimating the osmotic flow, especially for relatively short pores, small particles and not very dilute solutions. For a permeable membrane with an array of discrete pores, the three-dimensional entrance/exit regions discussed herein form a substructure of Pedley's one-dimensional unstirred layer. When the porosity is low (such as in most biological membranes), the membrane concentration in Pedley's model is the far field concentration of the entrance/exit solutions in the present model.

The model in Chapter 2 is presented for dilute solutions

and for the simplified geometry of a single circular cylindrical pore. To extend it to non-dilute solution, the interactions between solute particles must be taken into account. The consideration of other geometries and various external forces of molecular origin still needs to be investigated. The present model assumes a one-dimensional flow in the pore interior because there is no hydrodynamic theory for determining the off-axis force and torque coefficients for particles in a tube. In principle, a three-dimensional analysis can also be applied to the pore interior once the corresponding hydrodynamic data become available.

Chapter 3 has ddveloped a combined multipole series representation and integral equation method, which is more flexible in treating a complicated geometry than the multipole technique alone and is more accurate and computationally efficient than the integral equation method alone. This combined method has been used to obtain both axisymmetric and three-dimensional solutions for a finite sphere near a zero thickness plane orifice. While the numerical results compare favorably with other solutions in their commonly valid ranges, the present solutions are also valid in the vicinity of the pore opening, including the difficult case where the sphere intersects the plane of the orifice opening, which could not be treated by previous methods. The particle motion in this vicinity is of great concern in many problems involving the pore entrance phenomena. The

range of apllication of the present solutions is limited to a few pore-radii from the pore-axis, except in the neighborhood of the plane wall, due to the excessive computation time involved. With a more powerful computer, the range of validity can be extended.

Because of its flexibility, the combined method proposed herein is a very promising technique for treating more complicated geometries, such as the entrance of a particle into a finite length pore or the entrance problem for a periodic array of pores. The method is especially suited for treating deformable boundaries such as in the entrance problem of a deforming red blood cell, because the stress forces on the boundaries will be given as part of the solution. Two important considerations in any attempt to improve the present method will be how to increase the accuracy and how to reduce the computation time.

BIBLIOGRAPHY

Anderson, J.L. 1981 J. Theoret. Biol. 90, 405.

Anderson, J.L. and Adamski, R.P. 1983 AIChE Symp. Series 222, 79.

Anderson, J.L. and Malone, D.M. 1974 Biophys. J. 14, 957.

Anderson, J.L. and Quinn,J.A. 1974 Biophys. J. 14, 130.

Batchelor, G.K. 1976 J. Fluid Mech. 74, 1.

Bean, C.P. 1972 in "Membrane -- A Series of Advances" (G. Eisenman, Ed.), Vol. 1, 1.

Bird, R.B., Stewart, W.E. and Lightfoot, E.N. 1960 Transport Phenomena, John Wiley and Sons.

Blake, J.R. 1971 Proc. Camb. Phil. Soc. 70, 303.

Brenner, H. 1961 Chem. Eng. Sci. 16, 242.

Brenner, H. and Gaydos, L.J. 1977 J. Colloid and Interface Sci. 58, 312.

Curry, F.E. 1974 Microvasc. Res. 8, 236.

Cox, R.G. and Brenner, H. 1967 Chem. Eng. Sci. 22, 1753.

Dagan, Z., Pfeffer, R. and Weinbaum, S. 1982 J. Fluid Mech. 122, 273.

Dagan, Z., Weinbaum, S. and Pfeffer, R. 1982a J. Fluid Mech. 115, 505.

Dagan, Z,, Weinbaum, S. and Pfeffer, R. 1982b J. Fluid Mech. 117, 143.

Dagan, Z., Weinbaum, S. and Pfeffer, R. 1983 Chem. Eng. Sci. 38, 4.

Dainty, J. 1963 Adv. Bot. Res. 1, 279.

Dainty, J. and Ginzburg, B.Z. 1963 J. Theoret. Biol. 5, 256.

Davis, A.M.J., O'Neill, M.E. and Brenner, H. 1981 J. Fluid Mech. 103, 183.

Davis, A.M.J. 1983 Int. J. Multiphase Flow 9, 575.

Forsythe, G.E. and Wasow, W.R. 1960 Finite-difference Methods for Partial Differential Equations, Wiley.

Ganatos, P., Pfeffer, R. and Weinbaum, S. 1978 J. Fluid Mech. 84, 79.

Ganatos, P., Pfeffer, R. and Weinbaum, S. 1980 J. Fluid Mech. 99, 755.

Ganatos, P., Weinbaum, S., Fischbarg, J. and Liebovitch, L. 1980 Adv. in Bioengineering, ASME, 193.

Ganatos, P., Weinbaum, S. and Pfeffer, R. 1980 J. Fluid Mech. 99, 739.

Gluckman, M.J., Pfeffer, R. and Weinbaum, S. 1971 J. Fluid Mech. 50, 705.

Goldman, A.J., Cox, R.G. and Brenner, H. 1967 Chem. Eng. Sci. 22, 637.

Haberman, W.L. and Sayre, R.M. 1958 David W. Taylor Model Basin Rep. No. 1143, Washington, D.C.

Happel, J. and Brenner, H. 1973 Low Reynolds Number Hydrodynamics, 2nd ed., Noordhoff.

Hsieh, J.S. 1975 Principles of Thermodynamics, McGraw-Hill.

Katchalsky, A. 1960 in "Membrane Transport and Metabolism", (Kleinzeller, A. and Kotyk, A. ed.), Academic Press, 69.

Kedem, O. and Katchalsky, A. 1958 Biochem. Biophys. Acta 27, 229.

Ladyzhenskaya, O.A. 1963 The Mathematical Theory of Viscous Incompressible Flow, Chapter 3, Gordon and Breach.

Leal, L.G. and Lee, S.H. 1982 Adv. in Colloid and Interface Sci. 17, 61.

Lee, S.H. and Leal, L.G. 1982 J. Colloid and Interface Sci. 87, 81.

Leichtberg, S., Pfeffer, R. and Weinbaum, S. 1976 Int. J. Multiphase Flow 3, 147.

Lerche, D. 1976 J. Membrane Biol. 27, 193.

Levitt, D.G. 1975 Biophys. J. 15, 533.

Lewellen, P.C. 1982 Hydrodynamic analysis of microporous mass transport, Ph.D. Dissertation, Univ. of Wisconsin -Madison.

Mauro, A. 1957 Science 126, 252.

Miyazaki, T. and Hasimoto, H. 1984 J. Fluid Mech. 145, 201.

Ogston, A.G. and Michel, C.C. 1978 Proc. Biophys. Molec. Biol. 34, 197.

Pedley, T.J. and Fischbarg, J. 1978 J. Theoret. Biol. 70, 427.

Pedley, T.J. 1980 J. Fluid Mech. 101, 843.

Pedley, T.J. 1981 J. Fluid Mech. 107, 281.

Rallison, J.M. and Acrivos, A. 1978 J. Fluid Mech. 89, 191.

Ray, P.M. 1960 Plant Physiol. 35, 783.

Sampson, R.A. 1891 Phil. Trans. Roy. Soc. A182, 449.

Weinbaum, S. 1981 Lectures on Mathematics in Life Sciences, Amer. Math. Soc. 14, 110.

Wu, W.Y. and Skalak, R. 1984 The creeping motion of a sphere from a half-space to a semi-infinite circular cylindrical pore (to be published).

Youngren, G.K. and Acrivos, A. 1975 J. Fluid Mech. 69, 377.

Youngren, G.K. and Acrivos, A. 1976 J. Fluid Mech. 76, 433.